universität wien

MASTERARBEIT / MASTER'S THESIS

Titel der Masterarbeit / Title of the Master's Thesis

„Cancer associated fibroblast to myeloid cell communication and its impact on differentiation and polarization of macrophages in colorectal cancer."

verfasst von / submitted by

Alexander Biermeier BSc

angestrebter akademischer Grad / in partial fulfilment of the requirements for the degree of

Master of Science (MSc)

Wien, 2019 / Vienna 2019

Studienkennzahl lt. Studienblatt / degree programme code as it appears on the student record sheet:	UA 066 877
Studienrichtung lt. Studienblatt / degree programme as it appears on the student record sheet:	Masterstudium Genetik und Entwicklungsbiologie
Betreut von / Supervisor:	Assoc. Prof. Priv. Doz. Mag. Dr. Helmut Dolznig

Acknowledgments

First of all, I want to express my gratitude to my supervisor Helmut Dolznig for giving me this great opportunity to work in his lab. I really appreciate his way of communication and collaboration – always respectful, kind and patient.

I want to thank Monika, Wolfgang, Erika, Willi and Maria for supporting me throughout my years of study.

I would like to thank Danielka for being my balance.

Finally, I want to thank Isabella, Karin and Heribert for being the greatest support in my life. I cannot express my gratitude in mere words.

Statutory Declaration

I hereby declare that I carried out this Master's thesis with the topic "Cancer associated fibroblast to myeloid cell communication and its impact on differentiation and polarization of macrophages in colorectal cancer " under the direction of Assoc. Prof. Priv. Doz. Mag. Dr. Helmut Dolznig, independently, and without any unauthorized help.

Any assumptions of literal or content quotes are marked in the appropriate places.

I hereby declare that this Master's thesis as not been presented in this or any other form before.

_____

Place, Date

_____

Signature

Eidesstattliche Erklärung

Hiermit versichere ich, dass ich diese Masterarbeit mit dem Thema "Cancer associated fibroblast to myeloid cell communication and its impact on differentiation and polarization of macrophages in colorectal cancer" unter der Leitung von Assoc. Prof. Priv. Doz. Mag. Dr. Helmut Dolznig eigenständig und ohne unerlaubte Hilfe angefertigt habe.

Jegliche Übernahme wörtlicher oder inhaltlicher Zitate wurde an den entsprechenden Stellen gekennzeichnet.

Ich versichere, dass diese Masterarbeit in der jetzigen oder einer ähnlichen Form noch bei keiner anderen Prüfung vorgelegt wurde.

_____

Ort, Datum

_____

Unterschrift

Abstract

Colorectal cancer (CRC) ranks among the top three cancers in terms of incidence and mortality rates worldwide. Numerous environmental factors and mutated genes have been associated with its development and progression over the last few decades. Less understood is the interaction with its tumor microenvironment, which for the most part is infiltrated by cancer-associated fibroblasts (CAFs) and tumor-associated macrophages (TAMs). Blood-circulating monocytes are recruited to the tumor sites by dynamic networks of chemo-attractants and have been shown to differentiate and polarize into a tumor-favoring anti-inflammatory M2-like phenotype. CCL2 – one of the most studied chemokines – is believed as key player in these mechanisms. However, its regulation so far remains controversial.

This thesis was focusing on the roles of CCL2/CCR2 and M-CSF/M-CSFR signaling axis in the communication between CAFs and macrophages. First, we determined CCR2 and M-CSFR expression in 2D cultured CAFs and monocytes. In the past, increased levels of intra-tumoral CCL2 were found and these elevated levels are associated with bad prognosis. We therefore established a multicolor flow cytometry workflow allowing for precise analysis of CCL2/CCR2 and M-CSF/M-CSFR interference-effects on several markers in either mono- or cocultured 3D collagen gel setups. Cocultured CAFs, which displayed no expression of CCR2, did not respond to CCR2 and M-CSFR small molecule inhibitors RS 504393 and BLZ 945, but showed high expression levels of CCL2. We therefore exclude a possible autocrine effect of CCL2 through CCR2 in CAFs and suggest a paracrine effect on macrophages. Moreover, we provide evidence that interference with the M-CSF/M-CSFR pathway by BLZ 945 resulted in loss of CCL2 and CCR2 expression, downregulation of M-CSFR and loss of the M2-like macrophage marker CD163 in the myeloid cells. On the other hand, blockage of CCL2/CCR2 signaling by RS 504393 resulted in a compensatory increase in CCR2 and CCL2 expression in the macrophages indicating a tightly regulate feedback mechanism.

In addition, to demonstrate the *in vivo* relevance of our *in vitro*, we investigated CCL2 expression in colorectal cancer patients. Indeed, confocal laser scanning microscopy confirmed the presence of CCL2 expressing fibroblasts and CCL2 expressing macrophages in both healthy and tumor patient samples. This validated our hypothesis of strictly stromal derived expression of CCL2 in CRC.

In summary, we show that the M-CSF/M-CSFR axis acting via CCL2/CCR2 plays an important role in the communication between cells in the tumor microenvironment and contribute to a better understanding of CRC biology.

Zusammenfassung

Das kolorektale Karzinom gehört mit hohen Inzidenz- und Mortalitätsraten zu den häufigsten Krebserkrankungen der Welt. In den letzten Jahrzenten wurden zahlreiche Umweltfaktoren und mutierte Gene mit dessen Entstehung und Entwicklung assoziiert. Charakteristisch für die Mikroumgebung des Tumors ist eine intensive Einwanderung von sogenannten tumor-assoziierten Fibroblasten (CAFs) und von tumor-assoziierten Makrophagen (TAMs). Deren Interaktionen sind bis heute jedoch nicht vollständig geklärt. Im Blut zirkulierende Monozyten werden durch dynamische Netzwerke von chemotaktischen Faktoren zum Ort des Tumors rekrutiert, differenziert und in einen M2-ähnlichen anti-inflammatorischen Phänotyp umpolarisiert. CCL2 als eines der am häufigsten untersuchten Chemokine wird in diesem Kontext als Schlüsselfaktor angesehen.

Diese Masterarbeit konzentriert sich auf die Rolle des CCL2/CCR2 und des M-CSF/M-CSFR Signalweges in der Kommunikation zwischen CAFs und Makrophagen. Wir haben gezeigt, dass 2D Kulturen mit diesen Zelltypen eine Expression von CCR2 und M-CSFR zeigen. Dies ist insofern relevant, da vergangene Forschungsarbeiten erhöhte intratumorale CCL2 Konzentrationen zeigten. Wir haben deshalb ein Durchflusszytometer-basiertes Arbeitsprotokoll etabliert, welches uns die Effekte von CCL2/CCR2 und M-CSF/M-CSFR auf CAFs und Makrophagen aus 3D Kollagen Typ 1 Gelen untersuchen lässt. Kokultivierte M-CSFR-negative/CCR2-negative/CCL2-positive CAFs zeigten keine von uns wahrnehmbaren Veränderungen durch die Behandlung mit CCR2 (RS 504393) oder M-CSFR (BLZ 945) Inhibitoren. Wir schließen deshalb einen möglichen autokrinen Effekt von CCL2 auf CAFs aus, halten jedoch einen parakrinen Effekt auf Makrophagen für wahrscheinlich. Außerdem konnten wir zeigen, dass die Deregulierung des M-CSF/M-CSFR Signalweges mittels BLZ 945 zum Verlust der CCL2 und CCR2 Expression führt, M-CSFR herunterreguliert wird und myeloische Zellen den M2-ähnlichen Makrophagen Marker CD163 verlieren. Im Gegensatz dazu führte das Blockieren des CCL2/CCR2 Signalweges mittels RS 504393 in Makrophagen zu einem kompensatorischen Anstieg der CCR2 und CCL2 Expression, was auf einen streng regulierten Rückkopplungsmechanismus hindeutet.

Um die *in vivo* Relevanz unsere *in vitro* Experimente zu demonstrieren, überprüften wir die CCL2 Expression im kolorektalem Karzinom. Tatsächlich bestätigte eine Konfokal-Laser-Mikroskopie-basierte *in vivo* Analyse das Vorkommen CCL2 exprimierender Fibroblasten und CCL2 exprimierender Makrophagen in gesunden als auch erkrankten Patienten. Dies bekräftigt

wiederum unsere Hypothese, laut welcher im kolorektalen Karzinom CCL2 grundsätzlich im Stroma exprimiert wird.

Zusammenfassend konnten wir zeigen, dass im kolorektalen Karzinom der durch CCL2/CCR2 wirkende M-CSF/M-CSFR Signalweg eine wichtige Rolle bei der Kommunikation in der Tumorumgebung spielt.

Table of Contents

List of Figures

List of Supplementary Figures

List of Tables

List of Supplementary Tables

Abbreviations

APC	Adenomatous polyposis coli
BSA	Serum Albumin Fraction
CAC	Cancer-Associated Colitis
CAF	Cancer-Associated Macrophage
CCL	Chemokine Ligand
CCR	Chemokine Receptor
CD	Crohn’s Disease
CLSM	Confocal Laser Scanning Microscopy
CRC	Colorectal Cancer
DMEM	Dulbecco's Modified Eagle Medium
DMSO	Dimethyl sulfoxide
DPBS	Dulbecco's Phosphate-Buffered Saline
ECM	Extracellular Matrix
EDTA	Ethylendiaminetetraacedic acid
EGM	Endothelaial Growth Medium
EMT	Epithelial-Mesenchymal Transition
EtOH	Ethanol absolute
FCS	Heat Inactivated Fetal Bovine Serum
FFPE	Formalin-Fixed Paraffin-Embedded
GM-CSF	Granulocyte-Macrophage Colony-Stimulating Factor
IBD	Inflammatory Bowel Disease
IL	Interleukin
kDa	Kilo Dalton
LPS	Lipopolysaccharide
MCP	Monocyte Chemotactic Protein
M-CSF	Macrophage Colony-Stimulating Factor
MFI	Mean Fluorescence Intensity
min	Minutes
M-MDSC	Monocyte-related Myeloid-Derived Suppressor Cell
MMP	Matrix Metalloproteinase
NaOH	Sodium Hydroxide
PBMCs	Peripheral Blood Mononuclear Cells

PDGF	Platelet-Derived Growth Factor
PET	Polyethylene terephthalate
QC	Quality Control
ROI	Region of Interest
rpm	Rotations per minute
RPMI	Roswell Park Memorial Institute Media
RT	Room Temperature
SEM	Standard Error of Mean
TAM	Tumor-Associated Macrophage
TE	Trypsin EDTA
TNF-α	Tumor-Necrosis-Factor α
UC	Ulcerative Colitis
xg	G-force

1. Introduction

1.1. Colorectal cancer

1.1.1. Epidemiology

The worldwide incidence and mortality of cancer in general are rapidly growing. According to GLOBOCAN Global Cancer Statistics, 18.1 million new cases and 9.6 million cancer deaths were estimated worldwide in 2018. Colorectal cancer (CRC) ranks third most for incidence with more than 1.8 million new cases and second most for mortality with 881.000 deaths (**Figure 1**), accounting for about 1 in 10 cancer cases and deaths (Bray *et al.*, 2018).

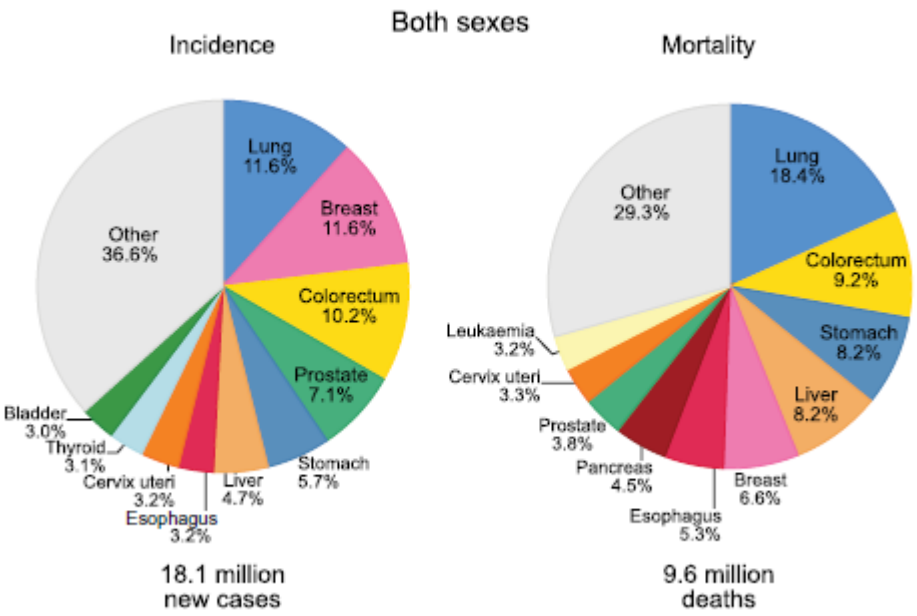

Figure 1: Percentage distribution of new cases and deaths for the 10 most common cancers in 2018 for both sexes.
Colorectal cancer ranks third most for incidence and second most for mortality in all cancers (data obtained from (Bray *et al.*, 2018)).

Depending on the world region, colorectal cancer incidence rates show high variance. Still, incidence rates of countries undergoing major development transition tend to rise uniformly with increasing Human Development Indices, suggesting it as a marker for socioeconomic development (Bray, 2014; Fidler, Soerjomataram and Bray, 2016). Transitioned countries show about 3-fold higher colorectal cancer incidence rates compared to transitioning countries. While

rates of both colon and rectal cancer incidence tend to be low in most regions of Africa and Southern Asia, highest rates are found in parts of Europe, Australia/New Zealand, Northern America and Eastern Asia with Hungary and Norway ranking first among males and females **(Figure 2)** (Bray *et al.*, 2018).

Dietary patterns, obesity and lifestyle factors are linked to rising incidence, while improved cancer treatment and management in more developed countries lead to declines in mortality (Arnold *et al.*, 2017). In their Cancer Statistics Report, Siegel et al also state, that changing risk factors and more advanced screening methods contribute to the reductions of incidence since the turn of this millennium. Colonoscopy as pre-dominant screening method e.g. facilitates removal of premalignant lesions. Among adults aged 50 years or older its use tripled from 21% to more than 60% since 2000 (Siegel, Ward and Jemal, 2012). In the US, CRC incidence patterns are similar between men and women. Still a decrease of 3% in the last 5 years for men is observed while for women rates stabilized (Siegel, Miller and Jemal, 2019). According to Kuipers et al., age-standardized incidence rate of colorectal cancer is higher in men (20.6 per 100000 individuals) than in women (14.3 per 100.000) (Kuipers *et al*., 2015).

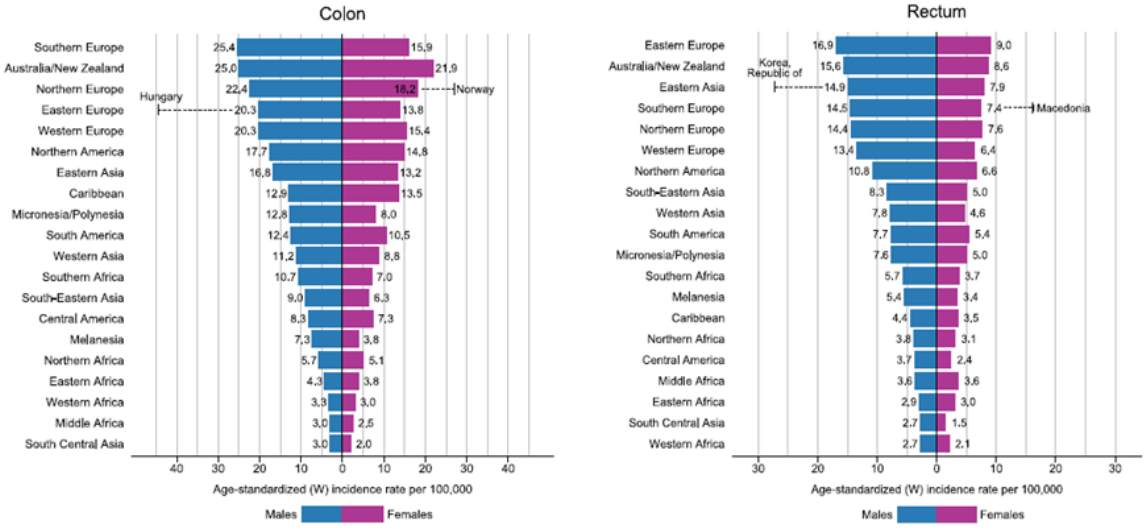

Figure 2: Region-specific incidence rates by sex; age-standardized for colon and rectum.
Highest age-standardized incidence rates in developed western world regions. Europe, Australia, New Zealand and Korea show highest rates for colon or rectum cancer incidence per 100.000. Incongruity between males and females. Inclination of incidence towards males in both colon and rectal cancer (data obtained from (Bray *et al.*, 2018)).

Until 2035 colon and rectal cancer mortality rates are predicted to drop by 8.4% and 5.1%. This decline will be observed in most countries, with exception of Latin American and Caribbean

countries, where availability of screening, public awareness, therapeutic procedures and patient management are not advanced enough yet (Araghi *et al.*, 2019).

1.1.2. Development

CRC is a slow stepwise process usually beginning as noncancerous polyp developing from the inner colon or rectum epithelial lining (Stryker *et al.*, 1987; Winawer and Zauber, 2002). Mostly it further is classified as from glandular cells arising adenoma, whereof less than 10% are estimated to progress to invasive cancer (Levine and Ahnen, 2006; Risio, 2010). Given that a larger adenoma is more likely to become cancerous, they usually are removed after colonoscopy screenings as preventive action (Pickhardt *et al.*, 2013). About 96% of all CRCs are adenocarcinomas (Stewart *et al.*, 2006). Apart from preponderant adenocarcinoma, rare types such as neuroendocrine, squamous cell, adenosquamous, spindle cell and undifferentiated carcinomas are found (Fleming *et al.*, 2012).

The classic model for CRC formation describes a vast majority of cancers arising from polyps beginning with an aberrant crypt further turning into an early adenoma of less than 1 cm in size. The next stage is an advanced adenoma of more than 1 cm in size before progressing to colorectal cancer. Although histology of conventional adenomas is homogeneous, polyps show heterogeneous molecular biology. This might be an explanation for only about 10% of adenomas progressing to CRC (Kuipers *et al*., 2015).

Glandular formation often characterizes conventional adenocarcinomas. Well-differentiated adenocarcinomas show gland forming tumors at more than 95%, while only 50-95% account for moderately differentiated adenocarcinomas. However, about 70% of all in practice diagnosed colorectal adenocarcinomas are moderately differentiated (Fleming *et al.*, 2012).

1.1.3. Risk factors

CRC results from complex interactions between inherited susceptibility and environmental factors. Still, about 75% of CRC cases are sporadic with no apparent evidence of having inherited disorder (PDQ® Screening and Prevention Editorial Board, 2019). The average lifetime risk for colorectal cancer is in the range of 3-5% in most western populations (Kuipers

et al., 2015). Environmental lifestyle factors like alcohol consumption, smoking, physical inactivity and overweight/obesity play important roles in the development of CRC. Most of them are largely modifiable.

Alcohol intake shows a relative risk of 1.41 for 45 g/day consumption compared to nondrinkers (PDQ® Screening and Prevention Editorial Board, 2019; Cho *et al.*, 2004) resulting in a 20% higher risk of CRC for people who have a lifetime average of 2 to 3 drinks per day and 40% increased risk with 3 drinks or more (Bagnardi *et al.*, 2015).

Smoking also is associated with an increased risk of CRC and lower survival (American Cancer Society, 2017). The Nurses' Health Study found a minimum induction period for cancer of at least 35 years (Giovannucci *et al.*, 1994), while in the Cancer Prevention Study 2 multivariate-adjusted CRC mortality rates were highest among current smokers, intermediate for former smokers and lowest in nonsmokers. Thereby increased risk became relevant after a period of 20 or more years of smoking in both sexes (Chao, 2000).

Overweight and obesity prevalence has been constantly increasing over the last decades. The CRC risk is stronger for colon than for rectal tumors in men compared to women. In contrast to normal weight men, colon cancer risk in overweighed men rises by 50% and rectal cancer risk by 20% – in women 20% or 10%, respectively (American Cancer Society, 2017).

The American Cancer Society and Centers for Disease Control and Prevention recommend physical activity of moderate-intensity for at least 150 minutes or of vigorous-intensity for 75 minutes a week to aim for preventive effects towards CRC. Several studies show in a line that physically active people tend to have a 25% lower risk of developing tumors. Additionally, in case of CRC diagnosis, they are less likely to die from the disease (American Cancer Society, 2017).

Red meat and processed meat increase CRC risk by 1.16-fold per 100 g daily intake. By contrast, a diet with regular intake of milk, whole grains, fresh fruits and vegetables containing certain amounts of calcium, fiber, multivitamins and vitamin D have been reported to decrease risk. Approximately 10% per daily intake of every 10 g fiber, 300 mg calcium or 200 ml milk (Kuipers *et al.*, 2015).

Chronic diseases of the gut with high levels of inflammation have been demonstrated to be jointly associated with CRC development. The two major forms of Inflammatory Bowel Disease (IBD), Ulcerative Colitis (UC) and Crohn's Disease (CD), were object of research for some decades. In this context, the specific form of colon cancer is termed Colitis-Associated Cancer (CAC), which increases cancer incidence up to 20% depending on the disease duration

(Grivennikov, 2013). Compared to the general population, risk of CAC development is increased by 8.3% in CD patients and up to 33.2% in UC patients (Kim and Chang, 2014). In total, CAC represents about 2% of all CRC cases (Francescone, Hou and Grivennikov, 2015).

1.1.4. Genetics of CRC

Genetic and environmental factors can lead to progressive accumulation of genetic and epigenetic alterations causing oncogene activation and tumor suppressor gene inactivation. Thereby genomic and/or epigenomic stability is lost. This was often observed in early neoplastic lesions of aberrant crypt foci, adenomas or serrated polyps (Kuipers *et al.*, 2015).

10% to 30% of CRC patients have a family history. Polyposis and the Lynch syndrome are the two best described forms of hereditary CRC. Pathogenic variants in the adenomatous polyposis coli (APC) gene were identified as causing familial adenomatous polyposis and attenuated familial adenomatous polyposis, while MUTYH-associated polyposis is caused by variants in the MUTYH gene. In contrast, responsible variants for hereditary nonpolyposis colorectal cancer – or Lynch syndrome – were observed in DNA mismatch repair genes MLH1, MSH2, MSH6 and EPCAM (PDQ® Screening and Prevention Editorial Board, 2019).

Fearon and Vogelstein first identified three mutated genes among sporadic CRCs in 1990 (Fearon and Vogelstein, 1990). Their findings are presumed as classical CRC tumor model, which describes APC mutations involved in adenoma formation followed by an oncogenic KRAS mutation promoting the transition from intermediate adenomas to carcinomas with TP53 inactivation (Yu *et al.*, 2015). Nowadays, APC, CTNNB1, KRAS, BRAF, SMAD4, TGFBR2, TP53, PIK3CA, ARID1A, SRY are seen as most common alterations. Especially deregulation of the Wnt signaling pathway has lately been reported as initiating CRC by progressing neoplastic cells upon deregulation of other signaling pathways including RAS-RAF-MAPK, TGF-β and the PI3K-AKT pathways (Kuipers *et al.*, 2015).

Similarly, common genetic and signaling pathways, involving Wnt, CTNNB1, KRAS, TGF-β or DNA mismatch repair proteins are altered in CAC (**Figure 3**). The timing of TP53 or APC inactivation as well as KRAS activation differs between CAC and CRC (Terzić *et al.*, 2010).

Genetic mutations are often accompanied by epigenetic alterations driving polyps to progress to cancer. CpG islands are often located in 5’ regions of genes for transcriptional regulation or

changing chromatin structure. In CRC, CpG islands of tumor suppressor gene promoters are often hypermethylated while the opposite occurs in oncogenes (Kuipers *et al.*, 2015).

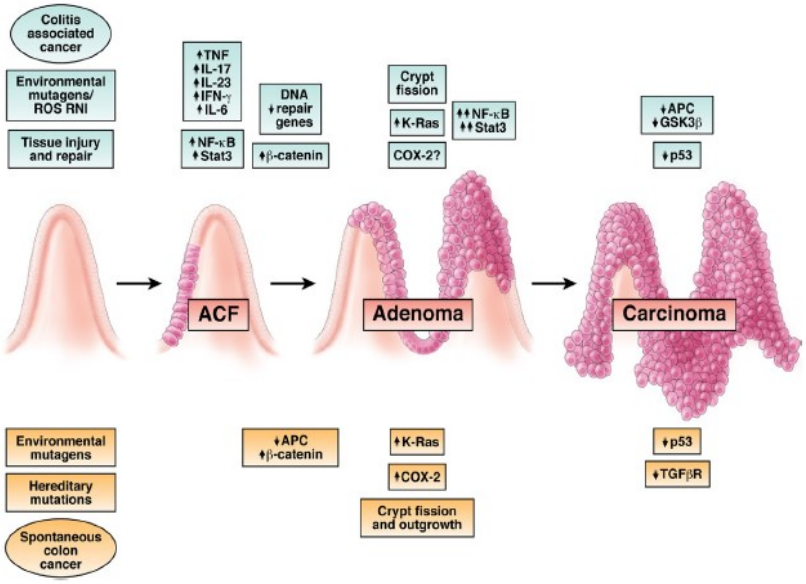

Figure 3: Altered genetics and signaling pathways in CRC and CAC development.
Stages of colorectal carcinoma development are illustrated with common belonging alterations. The stepwise process begins with formation of aberrant crypt foci (ACF) further turning into adenoma and consequently carcinoma. Deregulation of Wnt/β-catenin, KRAS, TGF-β signaling or loss of DNA mismatch repair occur as major alterations in both CRC and CAC orchestrated by deregulation of APC and TP53 at different time points. (data obtained from (Terzić *et al.*, 2010)).

1.2. Tumor microenvironment

The promotion of tumor growth is linked to the accumulation of a variety of cells caused by local inflammation at the side of solid malignancies (Peddareddigari, Wang and Dubois, 2010). Like most solid tumors, colon carcinomas are infiltrated (

Figure 4) by mesenchymal cells, such as tumor-associated macrophages (TAMs), cancer-associated fibroblasts (CAFs), monocytes, myeloid-derived suppressor cells, mast cells, neutrophils, CD8 and CD4 T-cells, dendritic cells, natural killer cells, endothelial cells, endothelial progenitor cells, platelets and mesenchymal stem cells (Murdoch *et al.*, 2008). The activation and/or recruitment of these cell types is achieved by soluble chemo-attractants which are secreted by tumor cells as well as stromal cells (Peddareddigari, Wang and Dubois, 2010).

The first phase is critical for the developing tumor, as infiltrating stromal cells are not exclusively beneficial for its promotion. With time, cells with antitumor properties seem to decrease due to dynamic interactions between stromal and tumor cells and tumor progression

favoring changes enhancing proliferation, survival and metastasis occur (De Visser, Eichten and Coussens, 2006).

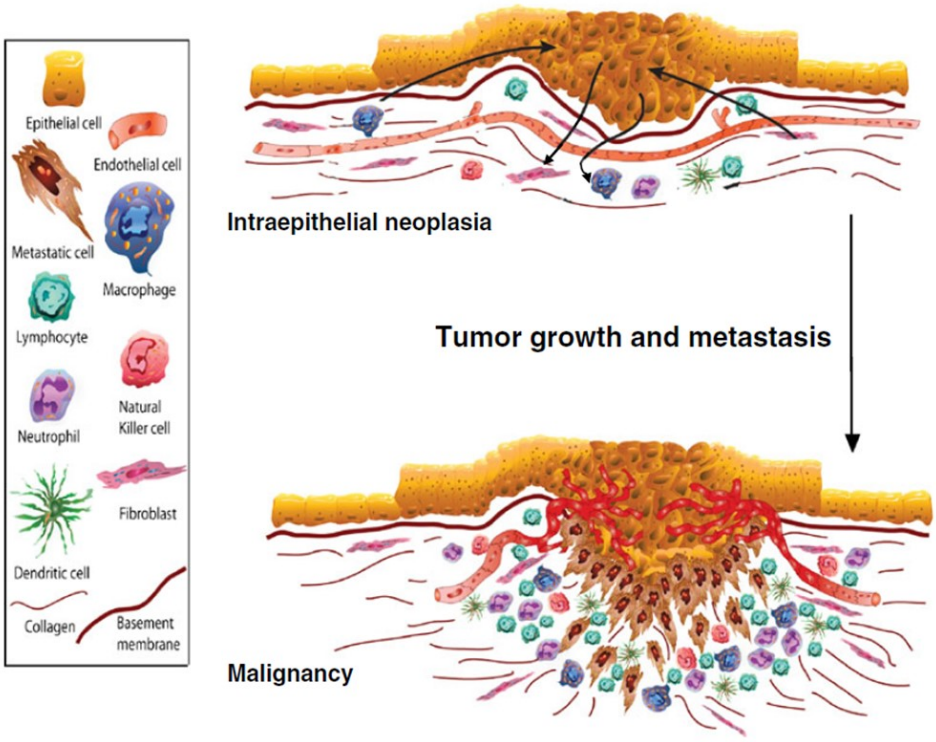

Figure 4: Model of tumor-stroma interaction in cancer progression.
Tumor microenvironment is increasingly infiltrated by several cell types, predominantly by CAFs or TAMs and other immune cells (data obtained from (Peddareddigari, Wang and Dubois, 2010)).

1.2.1. Cancer-associated fibroblasts

Fibroblasts are a major key component in the tumor stroma. First they are described in the 19th century as non-vascular, non-epithelial and non-inflammatory cells of the connective tissue, where they are embedded within the fibrillar matrix (Tarin and Croft, 1969). Fibroblasts are involved in the regulation of epithelial differentiation, the regulation of inflammation, wound healing, but most importantly, they are to a large extent responsible for the synthesis of extracellular matrix (ECM) (Tomasek *et al.*, 2002; Parsonage *et al.*, 2005). Moreover, they are also capable of degrading the ECM by producing matrix metalloproteinases (MMPs) (Kalluri and Zeisberg, 2006).

Fibroblasts of the tumor stroma are called cancer-associated fibroblasts (CAFs) – or also often referred to as myofibroblasts or activated fibroblasts, and are the main cellular stromal component in CRC (Herrera *et al.*, 2013). Numerous times α-SMA, fibroblast activation protein-alpha (FAP-α), fibroblast-specific-protein-1 (FSP-1/S100A4), or platelet-derived growth factor receptor-b (PDGFR-b) were reported as CAF markers. They are also positive for Vimentin and CD90 and generally maintain their phenotype in culture also in absence of cancer cells (Herrera *et al.*, 2013; Tommelein *et al.*, 2015).

CAFs mostly originate from either differentiating resident fibroblasts or from bone marrow residing mesenchymal stem cells (MSCs). The former are believed to be differentiated by cancer cells secreting CAF-promoting cytokines and growth factors including TGF-β, platelet-derived growth factor (PDGF), IL-4, IL-6, insulin-like growth factor (IGF)-II, and prostaglandin E (PGE) (Tommelein *et al.*, 2015).

De Wever *et al.* show how CAFs contribute to a tumor-friendly environment according to Hanahan and Weinberg's hallmarks of cancer (Hanahan and Weinberg, 2011; Tommelein *et al.*, 2015). Colon CAFs secrete growth factors that act through MAPK and PI3K/AKT pathway activation and consequently regulate cell proliferation, anti-apoptotic signaling, cytoskeletal rearrangements or invasion. Furthermore, proliferation is boosted through Smad2/Smad4 activation by TGF-β. Moreover, colony size and number of HCT116 cells were increased by CAFs producing ECM protein periostin in 3D co-culture systems (Kikuchi *et al.*, 2008). A plethora of factors are additionally described to contribute to tumor progression.

Vascularization of tumor tissue is crucial for its growth and development. Colon CAFs are known for producing substantial amounts of IL-6 and thereby up-regulating VEGF secretion (Nagasaki *et al.*, 2014). This has been demonstrated in co-cultures with CRC cells and CAFs where expression of VEGF mRNA in CAFs increased (Koshida, Kuranami and Watanabe, 2006).

CAFs are able to recruit monocytes, which are transformed into tumor-associated macrophages (TAMs) by tumor derived factors. Macrophages can be present in many different populations with two phenotypical extremes: M1 macrophages displaying anti-tumor response by producing inflammatory molecules like IL-6, IL-12, IL-23, TNF-α or ROS and NO, and CD163-positive M2 macrophages producing immunosuppressive cytokines like IL-10 and TGF-β to promote tumor progression, angiogenesis and degradation of ECM (Tommelein *et al.*, 2015).

1.2.2. Monocytes and macrophages

Macrophages belong to the innate immune system and play major roles in host defense and tissue homeostasis (Gordon and Martinez, 2010). Circulating bone marrow-derived monocytes are precursors of tissue-resident and inflammatory macrophages, which are capable of extravasating into target tissues and further polarizing into diverse subsets with different phenotypes depending on microenvironmental cues (Murray and Wynn, 2011; Davies *et al.*, 2013). However, bone marrow-derived monocytes are not the only source. Experiments in mice have shown, that macrophages in certain tissues like the brain microglia originate from precursors seeded during fetal and embryonic development (Geissmann *et al.*, 2010; Ginhoux *et al.*, 2016).

Macrophages infiltrate tumors in high numbers and are the most abundant immune cell type of the tumor microenvironment (Komohara *et al.*, 2016).

Depending on the tumor microenvironment, macrophages will polarize towards different phenotypes. As shortly depicted above two major extremes with many possible intermediates can be distinguished: classical M1- or alternative M2-like macrophages. M1-like macrophages are driven by the Th1 cytokine interferon-γ, lipopolysaccharide (LPS) and other Toll-like receptor agonists. M1-like macrophages produce pro-inflammatory factors (IL-6, IL-12, IL-23 and TNF-α) and express high levels of histocompatibility complex molecules (class 1 and 2) required for presentation of tumor specific antigens (Chanmee *et al.*, 2014). On the other hand, M2-like macrophages are, other than inflammatory and anti-tumorigenic response driving M1s, exerting anti-inflammatory and pro-tumorigenic activities. They are characterized by expression of Th2 cytokines such as IL-4 and IL-13. M2 macrophages can further be subdivided into four subgroups: M2a, M2b, M2c and M2d. Their conversion is stimulated by specific combinations of cytokines. More importantly, TAMs are usually described as M2d phenotype (Chanmee *et al.*, 2014). A tumor adjusts its microenvironment with time - hence, classical M1 polarized macrophages impeding its progression continuously skewed towards an anti-inflammatory, pro-angiogenic and pro-tumorigenic M2 phenotype. Secretion of angiogenic factors by TAMs depends on the tumor progression stage (Zaynagetdinov *et al.*, 2011): in early stages the M1-like macrophages inhibit angiogenesis in conjunction with the activation of tumor immunity, in advanced stages M2-like macrophages secret pro-angiogenic factors to enhance tumor angiogenesis (Gordon and Mantovani, 2011).

In 2016 Kumar *et al.* showed that circulating monocyte-related myeloid-derived suppressor cells (M-MDSCs), which are recruited into tumor tissues, can also differentiate into mature TAMs, which is mediated by downregulation of transcription factor STAT3 (Kumar *et al.*, 2016). M-MDSCs are known for their direct promoting effect of tumor metastasis (Bronte *et al.*, 2016).

1.2.3. Tumor-associated macrophages in colorectal cancer

The adult gastrointestinal tract is host to a microbe-mucosal ecosystem that contains more than a hundred trillion bacteria (Round and Mazmanian, 2009). For innate host responses it is substantially challenging to distinguish non-harmful commensal organisms from dangerous ones. Macrophages play a major role in the first-line defense. Due to ongoing confrontation with microbes and pathogens and the high self-renewal rate of the colon, tissue resident macrophages become apoptotic and need to be replaced by continuous recruitment of monocytes (Smith *et al.*, 2011; Peterson and Artis, 2014).

As described in the previous section, in case of CRC circulating monocytic precursors are recruited to the tumor site. This is mediated by chemokines like CCL2 and CCL5, VEGF, TGF-β or colony stimulating factors GM-CSF and M-CSF (Balmain *et al.*, 1993; Negus *et al.*, 1995; Yaal-Hahoshen *et al.*, 2006; Allavena *et al.*, 2008). In the tumor context, monocytes are thought to be mainly polarized into M2 macrophages by factors such as M-CSF, PGGE2, TGF-beta, IL-6 and IL-10 (Erreni, Mantovani and Allavena, 2011). In 2013, Edin *et al* differentiated purified monocytes to adherent macrophages by M-CSF stimulation for one week *in vitro* and further differentiation into M1 macrophages was achieved by addition of LPS and IFN-γ. M2 macrophages were generated by addition of IL4 and IL-10. The outcome was a higher expression of pro-inflammatory cytokines (IL-1, IL-6, IL-12, IL-23 and TNF-α) in M1 macrophages – which were not expressed in M2.

Cytokine expression profiling showed that secreted factors from CRC cells induce TAMs of a "mixed" M1/M2 phenotype, which are characterized by higher expression levels of pro-inflammatory cytokines than M2 macrophages, but still much lower than in M1 macrophages. The authors of this study describe TNF-α as the only exception being expressed at similar levels by TAMs and M1 macrophages. Of note, monocyte attracting chemotactic factor CCL2 was found to be highly expressed in TAM populations (Edin *et al.*, 2013). Vinnakota et al.

demonstrated that M2-conditioned medium enriched in TNF-α and leukotriene D4 promotes colon cancer cell invasion via MMP-9 expression and activation, and the induction of epithelial-to-mesenchymal transition (EMT) (Vinnakota *et al.*, 2017). Only recently, Xiong *et al.* identified NOTCH2 activation as enhancer of CRC EMT in HCT116 cells. Moreover, induction of NOTCH2/GATA3-mediated secretion of IL-4 promotes M2-like TAM polarization. Concordantly, CRC EMT and M2-like TAM polarization was inhibited by downregulation of NOTCH2 expression with miR-195-5p, which has previously been widely explored in various cancers as proliferation inhibiting tumor suppressor (Lin *et al.*, 2019).

In opposition to these findings, it has been shown that TAMs have no significant correlation with patient survival (Bacman *et al.*, 2007) or that TAMs are even associated with good prognosis (Khorana *et al.*, 2003; Tan *et al.*, 2005; Zhou *et al.*, 2010; Kim *et al.*, 2018). Thus, both TAM polarization and its impact on CRC progression remain controversial.

1.3. The roles of chemokine ligand/receptor interactions in colorectal cancer

Previous sections underlined the importance of the communication between tumor cells and their microenvironment, which is often achieved by chemokines. Chemokines or chemotactic cytokines are small heparin-binding proteins that constitute a large family of peptides regulating cell trafficking. With an average size of 8-12 kDa, chemokines are built of three major domains: a highly flexible N-terminal domain; the long loop leading into three antiparallel ß-pleated sheets; and an alpha-helix overlaying the sheets (Baggiolini and Loetscher, 2000). Based on the location of the first two cysteine residues, chemokines can be divided into four groups: C-chemokines, CC-chemokines, CXC-chemokines and CX3C-chemokines (Deshmane *et al.*, 2009; Karin, 2018). During inflammation, proinflammatory cytokines are released leading to a chemokine secretion as response. These chemokines are key players in the selective recruitment of several cell types, such as monocytes. They interact with seven transmembrane G-protein-coupled receptors expressed on their target cells. These cells follow a directed migration path along the chemical ligand gradient – known as chemokine gradient. Hence, for example cells expressing the respective chemokine receptor CCR2 move towards high local concentrations of chemokines like CCL2 (Callewaere *et al.*, 2007; Deshmane *et al.*, 2009).

1.3.1. CCL2/CCR2 axis in colorectal cancer

Deshmane *et al.* showed CCL2 expression of a wide range of cells including endothelial, epithelial, myeloid and smooth muscle cells and fibroblasts (Deshmane *et al.*, 2009). It has structural similarities with other monocyte chemotactic proteins and hence was categorized as monocyte chemotactic protein 1 (MCP-1). It shares high sequence homologies and highly conserved secondary structures of two adjacent N-terminal cysteine residues with MCP-2 (CCL8), MCP-3 (CCL7), MCP-4 (CCL13) and MCP-5 (CCL12) (Francoise Bachelerie *et al.*, 2014; Lim *et al.*, 2016). The appropriate receptor that CCL2 preferentially binds to is CCR2, which is present in two isoforms differing by 50 base pairs in the C-terminal domain: CCR2A and CCR2B (Charo *et al.*, 1994). Highly expressed in monocytes, CCR2B is the predominant isoform accounting for 90% of all expressed CCR2s (Lim *et al.*, 2016). CCR2A is expressed by small subsets of mononuclear and smooth muscle cells and induces different biological responses (Sanders *et al.*, 2000; Bartoli *et al.*, 2001). CCL2 seems to be a promiscuous ligand when it comes to binding specificity, as it has also been shown to bind to other receptors like CCR4 or to the even more distinct receptors ACKR1 and ACKR2 (Zhang *et al.*, 2006; Françoise Bachelerie *et al.*, 2014). On the other hand, CCR2 also binds other chemokines, e.g. MCP-2 (CCL8), MCP-3 (CCL7), MCP-4 (CCL13).

Torres *et al.* demonstrated that the colon cancer cell lines KM12C and KM12SM express CCR2 and show enhanced migration and invasion ability by addition of CAF-derived CCL8 or CCL2 (Torres *et al.*, 2013). Also, MDSCs can be modulated by CCL2 during colon cancer development. Chun *et al.* found that patients with colitis-associated CRC, adenocarcinomas and adenomas had increased intratumoral CCL2 levels, while in mouse models the deletion of CCL2 prevented progression from dysplasia to adenocarcinoma. Additionally, the number of colonic MDSCs was reduced in a spontaneous mouse model of CAC deleted for CCL2. Xenografted mice with adenocarcinoma and APC-driven adenoma had accumulated levels of CCL2-induced MDSCs in evolving colonic tumors and thereby enhanced polymorphonuclear MDSC's immunosuppressive features. In case of antibody-mediated CCL2 neutralization, decreased tumor numbers and reduced MDSC accumulation and function were observed (Chun *et al.*, 2015). Wolf *et al.* used both *in vivo* and *in vitro* models to demonstrate that colon carcinoma-derived CCL2 activates endothelial cells through CCR2 and is dependent on JAK2-Sat5 and p38MAPK phosphorylation. Thereby, endothelial vascular permeability was increased which consequently enabled efficient tumor cell extravasation (Wolf *et al.*, 2012).

Only recently Lopez and others investigated the relation between plasma chemokine levels involved in macrophage recruitment (CCL2, CCL3 and CCL4) with tumor-associated macrophage profile markers and clinicopathological features such as tumor-node-metastases stage, desmoplasia, TNF-α and VEGF plasma content. In comparison to healthy tissue, all three chemokines showed higher levels in patients with colon cancer. They also analyzed correlations between TAM populations and the different chemokine levels. A positive correlation was observed for M2 macrophages, which were identified by CD68 and the M2 marker CD163, and CCL4, but not for CCL2 or CCL3 (De la Fuente López *et al.*, 2018). Another recent publication by Grossman *et al.* investigated the recruitment of $CCR2^+$ TAMs to sites of liver metastasis in human CRC. Worse clinical outcome is connected to increased pre-operative monocyte prevalence in peripheral blood of metastatic CRC patients. Most of these peripheral monocytes are $CCR2^+$ inflammatory monocytes, which are recruited to the tumor sites through CCL2/CCR2 chemotaxis. Lastly, these tumor sites show increased expression of CCL2 and are heavily infiltrated by immunosuppressive TAMs (Grossman *et al.*, 2018).

Lifestyle factors and their possible effects on CRC development were already mentioned above. This year, Guo *et al.* investigated the effects of high-fat-diet-induced gut microbiota dysbiosis on the CCL2/CCR2 axis. They found that participants with high-fat-diet are more likely to develop advanced colorectal neoplasia, especially invasive carcinoma. In more detail, CRC patients with high-fat-diet displayed bacterial dysbiosis leading to an up-regulation of CCL2 and CCR2, and an increased M2 TAM infiltration as demonstrated by significantly increased CD163 (Guo Z, Liu T, Jiang K, *et al.*, 2019). Back in 2016 Xu *et al.* analyzed effect of alcohol on migration/invasion and metastasis of CRC. Migration and invasion were increased by alcohol in CRC cells in a concentration-dependent manner, especially in the cell line HCT116, which also displayed the highest up-regulation of CCL2/CCR2. The alcohol-stimulated migration could be blocked by CCR2 antagonist or CCL2/CCR2 knock-down (Xu *et al.*, 2016).

So far it seems that high levels of CCL2 promote a tumor-friendly and immunosuppressive environment by enhancing invasion and migration of cancer cells and accumulation of M2 macrophages.

1.3.2. Targeting CCL2/CCR2 axis

The previously described roles of the CCL2/CCR2 axis rather supporting the notion for a promoting role of CCL2/CCR2 in cancer development, suggest it as a promising target for therapeutic interventions.

In several experimental models of cancer a reduction of tumor growth and metastasis by CCL2 inhibition has been reported. However, the use of the anti CCL2 human IgG1 monoclonal antibody (CNTO888) or CCR2 inhibiting IgG1 antibody (MLN1202) in patients showed only little, none or adverse effects. Patients responded with augmented CCL2 expression, suggesting a homeostatic feedback mechanism or other compensatory mechanisms being involved, e.g. upregulation of its receptor CCR2 (Galdiero, Marone and Mantovani, 2018). Even in animal models Bonoapace *et al.* observed unexpected adverse effects in syngeneic metastatic breast cancer in terms of overshooting metastases and accelerated death when CCL2 was inhibited (Bonapace *et al.*, 2014).

Apart from blocking or inhibiting the axis, also enhancing it by overexpression was tested. Sun *et al.* showed in 2017, that overexpressing CCL2 in mammary epithelium leads to an increased number of macrophages, increased stroma density and elevated mRNA expression of MMP tissue inhibitor, which in all induced low level chronic inflammation (Sun *et al.*, 2017).

According to Sierra-Filardi *et al.*, the CCL2/CCR2 expression profile differs between M1- and M2-like macrophages. They differentiated and polarized PBMC derived monocytes ($CD14^+/CD16^+$) towards M1- or M2-like phenotype by addition of required factors. M2-like macrophages expressed higher levels of CCL2, CCL7 and CCL8. Furthermore, they also release higher levels of CCL2. On the other hand, less CCR2A and CCR2B receptors are expressed in these cells. Interestingly, $CCR2^+$ monocytes showed a pro-inflammatory M1-like expression pattern after polarization with M-CSF and simultaneous continuous presence of CCL2 inhibitory antibody (Sierra-Filardi *et al.*, 2014).

Thus, the biology of the CCL2/CCR2 axis is obviously not fully understood in cancer and additional experiments are needed to delineate under which circumstances high/low CCL2 levels are desirable.

1.3.3. M-CSF/M-CSFR axis in colorectal cancer

The macrophage colony-stimulating factor (M-CSF/CSF-1) is an essential regulator of macrophage homeostasis *in vivo*. It is produced constitutively by a wide variety of cells and its circulation level is increased during chronic inflammatory diseases and cancer (Hume and MacDonald, 2012). Circulating M-CSF has been reported to increase in colorectal cancer patients compared to the control group (Mroczko, Szmitkowski and Okulczyk, 2002; Mroczko *et al.*, 2007). M-CSFR (CSF-1R), a member of the type III RTK family, is exclusively expressed by cells of the monocyte lineage (Mantovani *et al.*, 2017). M-CSF competes for colony-stimulating factor-1 receptor (M-CSFR/CSF-1R) with IL-34, another cytokine that promotes the differentiation and viability of monocytes and macrophages (Lin *et al.*, 2008).

It is believed that the oncogenic potential of M-CSF/M-CSFR axis rather results from ligand-receptor co-expression than mutations that render the receptor constitutively active (Sapi, 2004). This means that M-CSFR can be activated either in an autocrine manner (co-expressed with M-CSF by tumor cells or in a paracrine manner (M-CSF secreted by CAFs) (Achkova and Maher, 2016).

M-CSF is commonly used to generate monocyte-derived macrophages in vitro (Irvine *et al.*, 2009). These macrophages have been described as rather immunosuppressive alternatively activated M2-like macrophages (Martinez *et al.*, 2006; Svensson *et al.*, 2011).

By all accounts M-CSF might act tumor-promoting as it has been numerously reported in cancer contexts and rather polarizes macrophages towards an immunosuppressive phenotype.

1.3.4. Targeting M-CSF/M-CSFR axis

M-CSF as the major growth and differentiation factor for cells of the monocyte/macrophage lineage, and, as previously addressed, as a key player in TAM-cancer interaction, is an obvious target for enabling interference.

Xenografted colon cancer mouse models showed lower macrophage infiltration in tumors by inhibiting the expression of M-CSF by antisense oligonucleotides and consequently decreased tumor growth and prolonged life span. (Kruse *et al.*, 2013)

To investigate the effects of M-CSF/M-CSFR inhibition on macrophage differentiation, polarization and survival, Pyonteck *et al.* used the M-CSFR small molecule inhibitor BLZ 945 to target TAMs in a mouse pro-neural glioblastoma multiforme model. BLZ 945 treatment increased animal survival and led to regression of established tumors. Moreover, M2-like marker expression decreased in TAMs of treated animals (Pyonteck *et al.*, 2013; Pathria, Louis and Varner, 2019). Yan *et al.* used the same tumor model and found that another M-CSFR inhibitor, PLX3397, blocked glioma progression, suppressed tumor cell proliferation and reduced tumor grade (Yan *et al.*, 2017). Another group showed that M-CSFR inhibition delayed growth of orthotopically transplanted mammary cancer cells lines derived from the breast cancer mouse model MMTV-PyMT. However, resistance emerged within a subset of mice (Strachan *et al.*, 2013; Quail and Joyce, 2017).

Ries and associates generated their own M-CSFR inhibitory antibody (RG7155) and treated mice that were inoculated with syngeneic MC-38 cells. Flow cytometry analysis revealed significant reduction of TAMs, while other types of immune cells such as neutrophils, natural killer cells and $CD4^+$ and $CD8^+$ T cells increased in the tumor-microenvironment (Ries *et al.*, 2014).

Taken together, inhibition of M-CSF/M-CSFR axis seems to rather favor a preferable clinical outcome. However, further research needs to clarify dose-resistance relation and effects on immune cells other than TAMs.

1.4. Aims of this Master's Thesis

Previous experiments in the Dolznig lab showed that PBMC-derived monocytes differentiate to macrophages and display induction of M2-like markers in 3D collagen gels by CAF derived mechanisms. Cytokine profiling revealed four promising factors that might be crucially involved: CCL2, M-CSF, IL-6 and IL-8 (Stadler, 2016).

CCL2 was fortyfold induced in macrophages and twofold in CAFs by co-culture of CAFs with macrophages but not with tumor cells. Interfering with the CCL2/CCR2 axis showed manifold results. The human monocytic cell line THP-1 treated with the CCR2 inhibitor RS 504393 showed decreased recruitment ability towards CAF conditioned medium This was less pronounced by inhibition with a CCL2 neutralizing antibody. Macrophages, co-cultured with CCL2 siRNA-knockdown-CAFs, decreased their CCL2 production but did not change their

polarization profile. Interestingly, however, the knockdown-CAFs displayed a reduction in cell number indicating a proliferative and/or cell survival phenotype (Pudelko, 2016). Hence, many questions regarding CCL2 function in CAF-myeloid cell interaction remain to be solved.

Our current hypothesis is that CAFs instruct recruited monocytes to differentiate and polarize into M2-like macrophages. The signaling is not clear yet, but CCL2 and M-CSF are the two most promising candidates. Therefore, the focus of this thesis was to further investigate the signaling between CAFs, macrophages and tumor cells with a special focus on CCL2 and M-CSF. Moreover, we also aimed to demonstrate that the *in vitro* findings of high CCL2 expression in both TAMs and CAFs can be found *in vivo* in human tumor as well.

The experiments of this thesis can be divided into two categories: *in vitro* experiments and *in vivo* analysis. The first approach of the *in vitro* part was to identify if CAFs, tumor cells, monocytes or M1- and M2-like macrophages express the required receptors (CCR2 and/or M-CSFR) to respond to CCL2 or M-CSF. Thus, I monocultured each cell type in 2D before analyzing cells by flow cytometry. For proper differentiability of polarized macrophage phenotypes M1-like or M2-like, I analyzed the expression of several monocyte/macrophage specific markers and compared them to each other. In the second approach, I aimed to better delineate CCL2 regulation, how CCL2 or M-CSF signaling is involved and what role M2-like macrophages play in this context. Hence, I used CCR2 as well as M-SCFR small molecule inhibitors to disrupt the signaling. To more closely mimic the *in vivo* situation of cell-cell and cell-ECM interaction, I performed 3D collagen gel assays in presence of above described inhibitors in mono- and co-culture setups. The outcome of each treatment was evaluated by multicolor flow cytometry. For this the establishment of a flow cytometry protocol and workflow in this context was essential and another major goal of this thesis.

In the second part, I intended to find out if our hypothesis generally applies *in vivo*. I therefore stained healthy and tumor tissue FFPE samples of colorectal cancer patients for CCL2 and macrophage marker CD68 to evaluate CCL2 expression in CAFs and macrophages by confocal laser scanning microscopy.

2. Material and methods

2.1. Cell culture

Table 1: Reagents and solutions (1.1.)

Product Name	Company	Article no.
Accutase® StemPro®, Cell Dissociation Reagent	Life Technologies, Carlsbad, CA, USA	A1110501
Dulbecco's Modified Eagle Medium (DMEM) 1x (4.5g/l D-Glucose, 0.11g/l Sodium Pyruvate)	Gibco, Thermo Fisher Scientific, Waltham Massachusetts, USA	21969-035
Dimethyl sulfoxide (DMSO)	Sigma-Aldrich, St. Louis, MO, USA	D5879
Dulbecco's Phosphate-Buffered Saline (DPBS) 1x	Lonza, Basel, Switzerland	17-512F
Ethylendiaminetetraacedic acid (EDTA)	Sigma-Aldrich, St. Louis, MO, USA	E7889
Endothelaial Growth Medium (EGM2-MV)	PromoCell GmbH, Heidelberg, Germany	C-22022
EGM2-MV Supplement Mix	PromoCell GmbH, Heidelberg, Germany	C-39226
Ethanol absolute (EtOH)	VWR, West Chester, PA, USA	20821.310
Heat Inactivated Fetal Bovine Serum (FCS)	Gibco, Thermo Fisher Scientific, Waltham Massachusetts, USA	10082-147
L-glutamine	Gibco, Thermo Fisher Scientific, Waltham Massachusetts, USA	25030-024
Roswell Park Memorial Institute Media 1640 (RPMI)	Gibco, Thermo Fisher Scientific, Waltham Massachusetts, USA	52400-025

Trypsin	Serva, Heidelberg, Germany	37289.02

Trypsin-EDTA (TE)	*DMEM/10% FCS*	*RPMI/10% FCS*	*EGM2-MV*
- 1x PBS *- 2200 U Trypsin* *- 2% NaEDTA (pH 7.4)*	*- DMEM* *- 10% FCS* *- 1% L-glutamine*	*- RPMI* *- 10% FCS* *- 1% L-glutamine*	*- EGM2-MV* *- EGM2-MV Supplement Mix*

Table 2: Equipment (1.1.)

Product Name	**Company**	**Article no.**
12-Well-Plate	STARLAB INTERNATIONAL GmbH, Hamburg, Germany	CC 7682-7512
Analog Vortex Mixer	VWR International, Radnor, Pennsylvania, USA	444-2790
Bright-Line Hematocytometer	Hausser Scientific, Horsham, PA, USA	513135
Cell Scraper	STARLAB INTERNATIONAL GmbH, Hamburg, Germany	CC 7600-0250
Centrifuge 5810R	Eppendorf AG, Hamburg, Germany	5611YP444820
Cryo Tubes (2 ml)	VWR International, Radnor, Pennsylvania, USA	10018-754
Falcon Tube	Sarstedt AG & Co. KG, Nümbrecht, Germany	62.554.502 (25ml) 62.559.001 (50ml)
Graduated Tips	STARLAB INTERNATIONAL GmbH, Hamburg, Germany	S1111-3000 (10µl) S1111-1006 (200µl) S1111-6001 (1000µl)

Heraeus BBD 6226 Incubator	Thermo Fisher Scientific, Waltham Massachusetts, USA	41062283
Micro-Centrifuge Tubes for High G-Force (1.5ml)	VWR International, Radnor, Pennsylvania, USA	211-0015
MSC-Advantage 1.8	Thermo Fisher Scientific, Waltham Massachusetts, USA	41066846
Olympus IX51 Microscope	Olympus Corp., Tokyo, Japan	9708340
Pipette	Eppendorf AG, Hamburg, Germany	4402049 (0,5-10µl) 3373392 (10-100µl) 4004955 (100-1000µl)
Serological Pipette	Sarstedt AG & Co. KG, Nümbrecht, Germany	86.1253.601 (5ml) 86.1254.001 (10ml) 86.1685.001 (25ml) 86.1256.001 (50ml)
Tissue Culture Dishes Sterile (10cm)	STARLAB INTERNATIONAL GmbH, Hamburg, Germany	CC7682-3394

2.1.1. Cell types and cultivation

Three cell types were used to closely mimic the *in vivo* situation of cell-cell and cell-ECM interaction in a human colon cancer: HCT116 colon carcinoma cells, CAF3 cancer associated fibroblasts and monocytes/macrophages. HCT116 cells, obtained from the American Type Culture Collection (ATCC® CCL-247™, Rockville, MD, USA), were cultured in Dulbecco's Modified Eagle Medium with 10% FCS and 1% L-glutamine. The primary cancer associated fibroblasts CAF3 (17790) were previously isolated from colon carcinomas (Dolznig *et al.*, 2011) and cultured in Endothelial Growth Medium 2-MV. Monocytes were isolated from Peripheral Blood Mononuclear Cells (PBMCs) from healthy male donor and further differentiated into macrophages. For the latter, Roswell Park Memorial Institute (RPMI) Media with 10% FCS and 1% L-glutamine was used for cultivation.

Cultivation was carried out in Heraeus BBD 6226 incubator at 37°C, 5% CO2 and 95% relative humidity. Cells were handled under sterile conditions in an MSC-Advantage Biological Safety Cabinet and mainly cultivated in a 10 cm petri dish with a working volume of 8 ml.

2.1.2. Cell thawing

Long-term storage of cells at -190°C in liquid nitrogen tank. Cryo Tube taken out and thawed at room temperature. Liquid cell suspension was transferred to 15 ml falcon tube with 8ml of DMEM/10% FCS/1% L-Glu immediately after thawing to prevent toxic effects of DMSO by diluting it out. Cells were now centrifuged at 1000 rpm/3 min/24 °C. Supernatant was discarded before cells were resuspended in belonging media and split onto petri dishes in desired ratio. Further cultivation as described above.

2.1.3. Cell passaging

Cell-type specific media, 1x DPBS, TE and accutase were prepared and left at RT. Meanwhile, media was discarded and cells were washed with 6ml of DPBS per 10 cm dish by carefully moving the plate back and forth several times before again removing it. Except from macrophages, all cell types were then treated with 1.2 ml of TE and incubated at 37°C for 2 min – macrophages with accutase for 5 min. Cells should easily detach after TE treatment, if not, soft finger tapping helped. Macrophages attach much better to dish surface and do not detach by accutase treatment only. They require additional cell scraping. Subsequently, at least 5x volume DMEM/10% FCS/1% L-Glu were added to inactivate TE immediately. Cells were resuspended by pipetting up and down several times, then transferred to 15ml falcon tube and centrifuged at 1000 rpm/3 min/24° C. Supernatant was again discarded and cells were resuspended in the belonging media. Split factors usually were 1:3 for CAFs and 1:6 – 1:10 for HCTs. A Hematocytometer counting chamber was used to determine cell count/vol for further experiments. At 10x magnification, alive cells in each of the four quadrants were counted. The average value times 10^4 equals the number of cells per milliliter.

2.1.4. Cell cryopreservation

Cells were washed with DPBS, trypsinized with TE and centrifuged as described in previous topic. Discarding of supernatant was followed by resuspending cells in 900 µl of FCS. Then, 100 µl (ratio 1:10) of DMSO were added drop by drop under shaking softly. The final volume of 1 ml was transferred to a 2 ml Cryo Tube. Next, they were put on ice for about 15 min followed by 24 h at -80°C in a styrofoam box and finally long-term stored in a nitrogen liquid tank at -196°C.

2.2. Isolation and culture of monocytes and macrophages

Table 3: Reagents and solutions (1.2.)

Product Name	Company	Article no.
Ciprofloxacin Kabi 100 mg/50 ml	Fresenius Kabi Austria CmbH, Graz, Austria	1-26637
Ficoll Paque™ PLUS 1.077 +/- 0.001 g/ml (20°C)	GE Healthcare, Uppsala Sweden	17-1440-02
Human M-CSF	PeproTech, Rocky Hill USA	300-25
Human GM-CSF	PeproTech, Rocky Hill USA	300-03
LPS	Sigma-Aldrich, St. Louis, Missouri, USA	-
IFN-γ	Sigma-Aldrich, St. Louis, Missouri, USA	-

Serum-free DMEM	*PBS/EDTA Buffer*
- DMEM *- Ciprofloxacin (1:40)* *- 1% L-glutamine*	*- 1x PBS* *- 2 mM EDTA*

2.2.1. Isolation of peripheral blood mononuclear cells by density gradient centrifugation

Peripheral Blood Mononuclear Cells (PBMCs) were taken from healthy male donor. Each cannula contained ~9ml of EDTA/blood and was transferred into a 50 ml falcon tube and diluted with 31.5 ml (3.5x vol) of freshly prepared and sterile filtrated PBS/EDTA buffer. Additionally, another 50 ml falcon tube was filled with 7 ml of Ficoll Paque^{TM} PLUS (density 1.077 +/- 0.001 g/ml), which was carefully overlayed with the EDTA/blood mix. Pipetboy pump was turned off to prevent interspersing of the two phases.

Next, centrifugation at 400x g for 35 min at 20°C without break (deceleration = 0; acceleration = 6). The density gradient leads to five separate phases, whereof the phase below the plasma contains the PBMCs (**Figure 5**). This "Buffy Coat" was carefully transferred to a 15ml falcon tube after removing most of the plasma and finally mixed 1:2 with PBS/EDTA buffer. After centrifugation at 300x g/20°C/10 min, supernatant was completely removed, and pellet was resuspended in 15 ml of PBS/EDTA buffer. This washing step was repeated three times at 200x g.

2.2.2. Isolation of monocytes from PBMCs

Isolated and washed PBMC pellet was resuspended in 1ml of DMEM/Ciprofloxacin (1:40)/1% L-Glu and pooled with another pellet. Two pellets make the optimum amount of cells for seeding on a 10 cm petri dish. The pooled pellets were filled up with media to a final volume of 8 ml, seeded on an untreated 10 cm cell culture dish and incubated at 37°C for 1.5-2 hours.

Afterwards, supernatant was discarded leaving monocytes as only attached cell type behind in the culture dish. Those were washed with plain DMEM. In case of direct use of monocytes for further experiments, media was discarded, and monocytes were incubated with 1.2 ml of accutase per 10 cm culture dish for 5 min at 37°C after washing with PBS. 7 ml of DMEM/10% FCS/1% L-Glu were added and monocytes were detached by using a cell scraper.

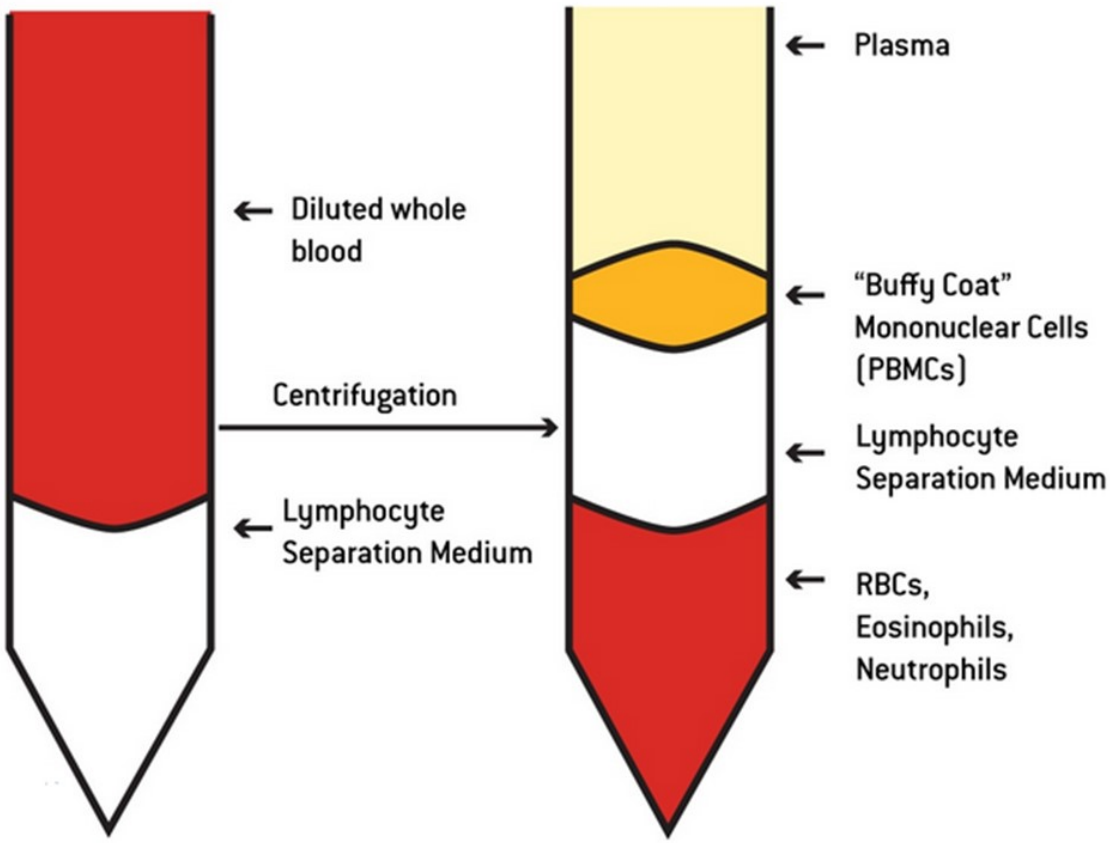

Figure 5: Density gradient centrifugation of peripheral blood mononuclear cells (PBMCs).
PBMCs can be separated from red blood cells (RBCs) and granulocytes (eosinophils, neutrophils and basophils) by density gradient centrifugation with Ficoll-Paque™ lymphocyte separation medium. Centrifugation makes erythrocytes (density ~ 1.100 g/ml) sink through pre-overlayed Ficoll Paque™ (density 1.077 g/ml) down to the bottom. Granulocytes (density 1.090 - 1.080 g/ml) remain between RBCs and Ficoll Paque™. PBMCs (density 1.060 - 1.070 g/ml) appear as "Buffy Coat" and localize between Ficoll Paque™ and plasma (density >1.025 g/ml). Figure obtained from Lonza Pharma and Biotech (Lonza, 2019).

2.2.3. Monocyte differentiation and macrophage polarization

Monocytes were from now on supplied with RPMI/10%FCS/1%L-Glu and treated with 20 ng/ml Macrophage-Colony Stimulating Factor (M-CSF) for the next 6 days (refresh all 48 hours) to differentiate them into macrophages (**Figure 6**). These could have been further pushed into M2-like polarization by 20 ng/ml IL-4 treatment for another 6 days (refresh all 48 hours). For M1-like polarization monocytes were first treated with GM-CSF (20 ng/ml) instead and then with a combination of LPS (100 ng/ml) and IFN-gamma (100 ng/ml).
Macrophages were collected for further experiments as described in previous topic.

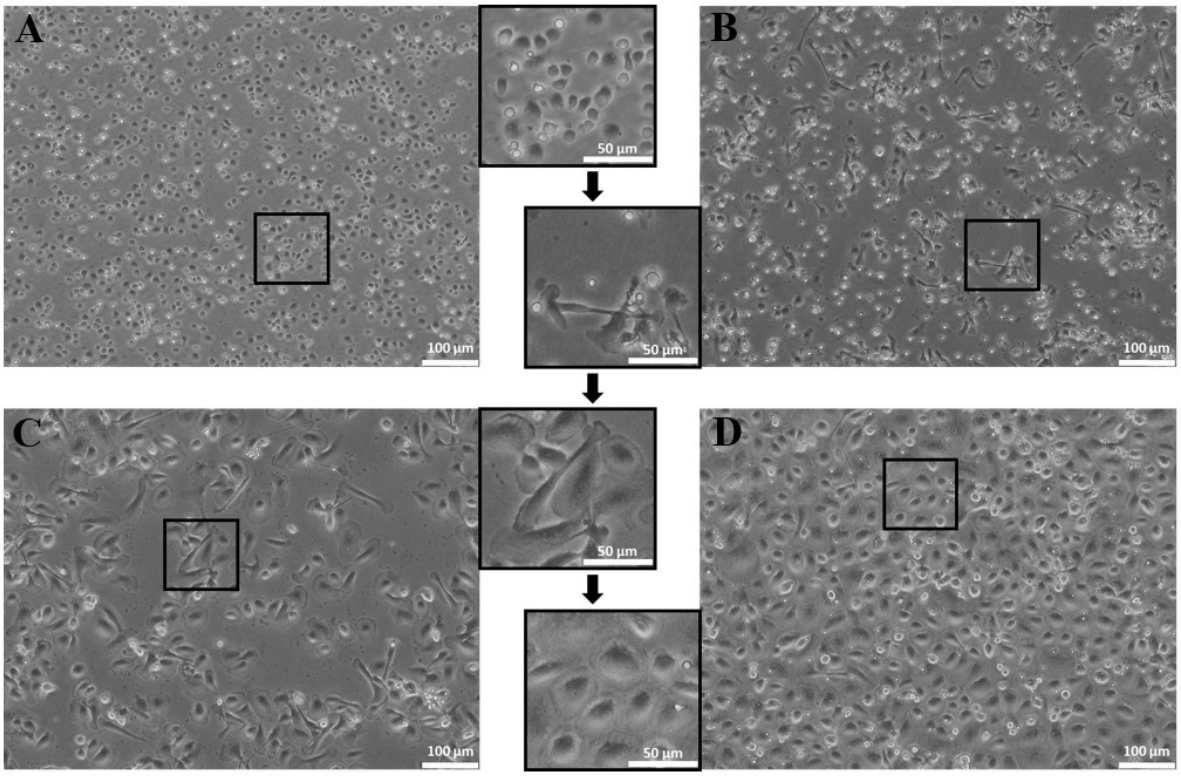

Figure 6: Monocyte to macrophage differentiation.
A,B,C,D show gradual differentiation of monocytes into macrophages. **A** Monocytes freshly isolated from PBMCs were incubated for 6 days with 20 ng/ml of M-CSF. Light-microscopy images were taken with Olympus IX51 at 10x magnification every 48 hours (**A** = 0h; **B** = 48h; **C** = 96h; **D** = 144h) before media- and M-CSF-refresh. Black-framed images show zoomed in regions for each time point. Differentiation is characterized by gradual changes in morphology from round-shaped smaller monocytes to larger outstretching macrophages.

2.3. 3D collagen-gel coculture

Table 4: Reagents and solutions (1.3.)

Product Name	Company	Article no.
Collagen Type I Rat Tail (3.52 mg/ml)	Corning Incorporated, New York, USA	354236
Collagenase B	Roche, Mannheim Germany	11088815001
Dulbecco's Phosphate-Buffered Saline (DPBS) 10x	Bio Whittaker® Lonza, Basel, Switzerland	BE-17-515F
Sodium Hydroxide (NaOH)	MERCK, Darmstadt, Germany	1.06498.1000

DMEM/2% FCS	*Collagen Gel*	*Collagenase Digest Buffer*
- DMEM *- 2% FCS* *- 1% L-glutamine*	*- DMEM/2% FCS/1% L-glutamine* *- 10% (v/v) 10x PBS* *- 2 mg/ml Collagen Type 1* *- ~1% 1M NaOH*	*- 1x DPBS* *- Collagenase B (1:8)*

Table 5: Equipment (1.3.)

Product Name	Company	Article no.
Polyester mesh (mesh size: 100 µm; fiber diameter: 77 µm)	Bückmann GmbH & Co., Mönchengladbach, Germany	20000194
Polystyrene Round-Bottom Tube (5 ml)	Corning Incorporated, New York, USA	352054
Thermomixer Comfort	Eppendorf AG, Hamburg, Germany	5355

2.3.1. Preparation and culture of 3D gels

3D collagen gel coculture assays are a tool to closely mimic the in vivo situation of cell-cell and cell-Extracellular Mass (ECM) interactions in human colon cancer. For further investigations HCT116 cancer cells, CAF3 fibroblasts and macrophages were either mono-, co- or triplecultured. Cells were cultured, harvested and counted as described in previous chapter. The desired amount of cells (HCT116: 3.000 cells; CAF3: 300.000 cells; macrophages: 300.000 cells) was transferred into 1.5 ml Eppendorf Tubes, centrifuged at 1000 rpm/3 min/24°C, and kept on ice after discarding supernatant. Cells were pooled in case of co- or tripleculture. Meanwhile – it is important to perform all steps on ice invariably – 1.2 ml of Collagen Gel were prepared. A 2 ml FACS tube was first filled with ice-cold PBS, DMEM and Collagen according to protocol to a final volume of 1.2 ml. NaOH was added and titrated until the color switched from yellow to mellow pink after vigorous shaking. Despite short spinning of the tube, bubbles remain on top of collagen mix. Therefore a final volume of 1.2ml was chosen to provide enough bubble-free collagen mix for three gels (time-maximum usability: 30 min). For each gel, cells were resuspended carefully and bubble-free in 300 µl of collagen mix by pipetting up and down for at least 15 times. Beforehand, three 300 µl silicon casting forms were adhered to the inside of a 10 cm culture dish lid with a 10 µl drop of 1x PBS and prewarmed in the incubator. Forms were then filled with gel/cell suspension and a ring-shaped PET mesh was submerged in the gel to provide stability for later gel transfer and prevent mechanical tightening of the gel by fibroblasts. Gels were then incubated for 15 min at 37°C and transferred into 12-well-plate well, which was filled with 2 ml of DMEM/2% FCS/1% L-Glu and appropriate dilutions of treatment factors. Cells were cultivated for 6 days (refresh all 48h).

2.3.2. Collagenase digest of 3D gels

Further FACS analysis requires cells in suspension, which was achieved by Collagenase B digest. For each gel one Eppendorf tube was prepared with 1ml of Collagenase Digest Buffer. Gels were carefully transferred to tubes with sterile (Bunsen Burner) tweezers and subsequently incubated at 37°C on a Thermomixer at 300 rpm for 15 min. Collagenase digest was then stopped by addition of 0.5M EDTA pH 8. Centrifugation at 1000 rpm/3 min/24°C, removal of the PET mesh and another round of washing with PBS set the cells up for further experiments.

2.4. Fluorescence Activated Cell Sorting Analysis (FACS)

Table 6: Reagents and solutions (1.4.)

Product Name	Company	Article no.
CytoFLEX Daily QC Fluorospheres	Beckman Coulter, Brea, USA	B53230
Fix and Perm® Cell Fixation and Permeabilization Kit	Nordic MUbio, Susteren, Netherlands	GAS-002
Human TruStain FcX™	Biolegend, San Diego, California, USA	422302
Serum Albumin Fraction V (pH 7.0) (BSA)	AppliChem GmbH, Darmstadt, Germany	A1391.0100
UltraComp eBeads™ Compensation Beads	Invitrogen Thermo Fisher Scientific, Waltham Massachusetts, USA	01-2222
Zombie NIR Fixable Viability Kit	Biolegend, San Diego, California, USA	423106

FACS Buffer

- *1x DPBS*
- *2% BSA*

Table 7: Equipment (1.4.)

Product Name	Company	Article no.
CytoFLEXS Flow Cytometer	Beckman Coulter, Brea, USA	AS38034
Polystyrene Round-Bottom Tube with Cell-Strainer Cap	Corning Incorporated, New York, USA	352235

Table 8: Conjugated antibodies and belonging IgG controls for flow cytometry analysis.

Target	Conjugated Dye	Species Reactivity	Concentration [µg/ml]	Dilution	Final Conc [µg/ml]	Company	Catalog No	Clone	Lot	Isotype Control	Binding
CCL2/MCP-1	PE	human	50	1:50	1	BioLegend	502604	5D3-F7	B192074	mIgG1	Intracellular
CCR2	APC	human	100	1:20	5	BioLegend	357208	K036C2	B262805	mIgG2a	Extracellular
CCR2	APC	human	10	1:10	1	R&D Systems	FAB151A	48607	LDA0714042	mIgG1	Extracellular
CD14	APC	human	100	1:20	5	BD Pharmingen	561383	M5E2	4045977	mIgG2a	Extracellular
CD45	Brilliant Violet 421	human	25	1:50	0.5	BioLegend	304032	HI30	B258229	mIgG1	Extracellular
CD68	Alexa Fluor 488	human	200	1:100	2	BioLegend	556059	Y1/82A	4267934	mIgG2b	Intracellular
CD86	Alexa Fluor 488	human	400	1:20	20	BioLegend	305414	IT2.2	B243405	mIgG2b	Extracellular
CD86	PE	human	100	1:50	2	BioLegend	305406	IT2.2	B210795	mIgG2b	Extracellular
CD90/Thy1	Alexa Fluor 647	human	80	1:20	4	BioLegend	328116	5,00E+10	B196394	mIgG1	Extracellular
CD115/M-CSFR	PE	human	50	1:10	5	R&D Systems	FAB329P	61708	KFD0618022	mIgG1	Extracellular
CD140b/PDGFRß	PE	human	400	1:100	4	BioLegend	323606	18A2	B214318	mIgG1	Extracellular
CD163	Alexa Fluor 647	human	200	1:100	2	BD Pharmingen	562669	GH/61	8276870	mIgG1	Extracellular
CD163	PerCP/Cy5.5	human	200	1:20	10	BioLegend	333608	GHI/61	B263021	mIgG1	Extracellular
Vimentin	Alexa Fluor 405	human	500	1:300	1,67	abcam	ab210152	EPR3776	/	rIgG	Intracellular
Vimentin	Alexa Fluor 594	human	500	1:5000	0.1	abcam	ab154207	EPR3776	GR3173742-5	rIgG	Intracellular
Vimentin	Alexa Fluor 647	human	500	1:5000	0.1	abcam	ab195878	V9	/	mIgG1	Intracellular

Target	Conjugated Dye	Concentration [µg/ml]	Company	Catalog No	Clone	Lot	Binding
mIgG1 (FC)	Alexa 647	100	BioLegend	400130	MOPC-21	B205347	Extracellular
mIgG1 (FC)	APC	200	BioLegend	400122	MOPC-21	B271888	Extracellular
mIgG1 (FC)	Violet 421	100	BioLegend	400158	MOPC-21	B265345	Extracellular
mIgG1 (FC)	PE	200	BioLegend	400114	MOPC-21	B245983	Extracellular
mIgG1 (ICFC)	PE	40	BioLegend	400140	MOPC-21	B200983	Intracellular
mIgG1 (FC)	PerCP/Cy5.5	200	BioLegend	400150	MOPC-21	B272764	Extracellular
mIgG2a (FC)	APC	100	BioLegend	400222	MOPC-173	B269399	Extracellular
mIgG2b (ICFC)	Alexa 488	200	BioLegend	400329	MPC-11	B196616	Intracellular
mIgG2b (FC)	PE	200	BioLegend	400314	MPC-11	B246305	Extracellular
rIgG (ICFC)	Alexa 405	50	R&D Systems	IC1051V	60024B	AESA0119011	Intracellular
rIgG (ICFC)	Alexa 594	500	abcam	ab208568	EPR25A	GR3186329-4	Intracellular

2.4.1. Staining procedure

For FACS analysis cells were either taken directly from 2D culture or digested out of the gels from 3D culture as described in the previous section. $1x10^6$ cells were transferred into Eppendorf tube, centrifuged at 1000 rpm/3 min/24°C and supernatant taken off. Another round of washing with 1 ml of 1x DPBS to remove media residua. Henceforth all steps were performed with $1x10^6$ cells in a final volume of 100 µl.

2.4.1.1. Staining of cell surface markers for FACS analysis

To discriminate between dead and alive cells, 15 min of incubation in 100 µl PBS with 1:1000 Zombie NIR in the dark were undertaken and cells were again centrifuged afterwards. Given that a variety of cells expresses Fc receptors and can hence lead to false positive or false negative results, we blocked them by incubating cells for 15 min in 100 µl of FACS buffer with TrueStainFcX (1:50). After centrifugation and supernatant removal, staining was performed in 100 µl FACS buffer and the appropriate dilutions of antibodies (**Table 8**) for cell surface markers were added at 4°C in the dark for 30 min. In case of staining for surface markers only, cells were now resuspended and washed in 1 ml FACS buffer, centrifuged, supernatant taken off and resuspended in 500 µl buffer for FACS measurement.

2.4.1.2. Staining of intracellular proteins for FACS analysis

Intracellular proteins were stained in a second step after cell surface marker staining. After finished incubation of antibodies against surface markers and washing them out, pellet was resuspended and kept in 50 µl of 1x DPBS and 100 µl of Fix and Perm Medium A for 15 min in the dark before centrifuging and removing supernatant again. Another round of washing and pellet was resuspended and kept in 100 µl of Fix and Perm Medium B plus appropriate dilutions of antibodies (**Table 8**) against intracellular proteins for 20 min in the dark. Two further steps of washing and centrifugation before giving them in suspension with 500 µl of FACS buffer for FACS measurement.

1.4.1.3. IgG controls

Staining with fluorescently labeled antibodies always bears risk of false positive results by unspecific binding. To minimize that, every sample was verified with an unstained control and an IgG control (**Table 8**). Unstained usually means, Fc receptor block and Zombie stain as described above but no labeled antibody or fixation. IgG controls were prepared the same way as described above. Also, it is essential to distinguish between intracellular and extracellular staining procedure depending on the target.

2.4.2. CytoflexS setup and gating strategy

Before starting with actual analysis of samples, daily start up program including QC-standardization had to be passed to make sure operating soft- and hardware configuration, measuring laser powers, verifying laser delays and calibrating the gains correctly (**Figure 7**).

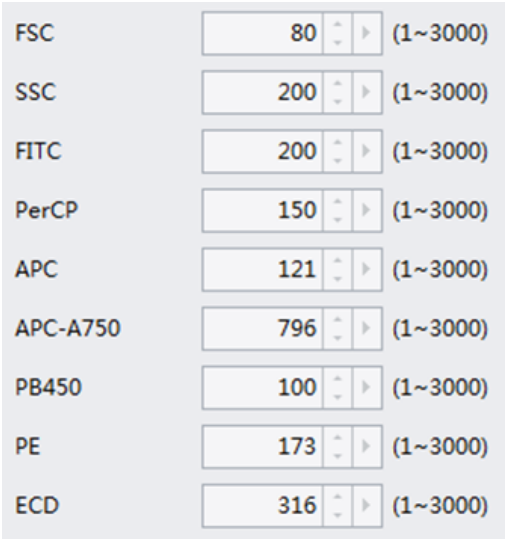

Figure 7: Gain setup after QC-standardization.

Sample flow rate was adjusted to ~800 events per second. For each sample 20000 events were recorded in the singlets gate. With the CytoflexS software only raw singlet selection was performed as FlowJo software was used for precise analysis afterwards. The first three plots were supposed to discriminate against debris, dead cells and doublets or triplets. FSC-A x SSC-A shows cells plotted by their size and granularity (**Figure 8 A**). This usually results in a linear

correlation between those two parameters inside of each cell population as cells scatter more granularity-caused laser light with increasing size. Debris and dead cells cluster in a separate linear cloud upwards left of the target populations.

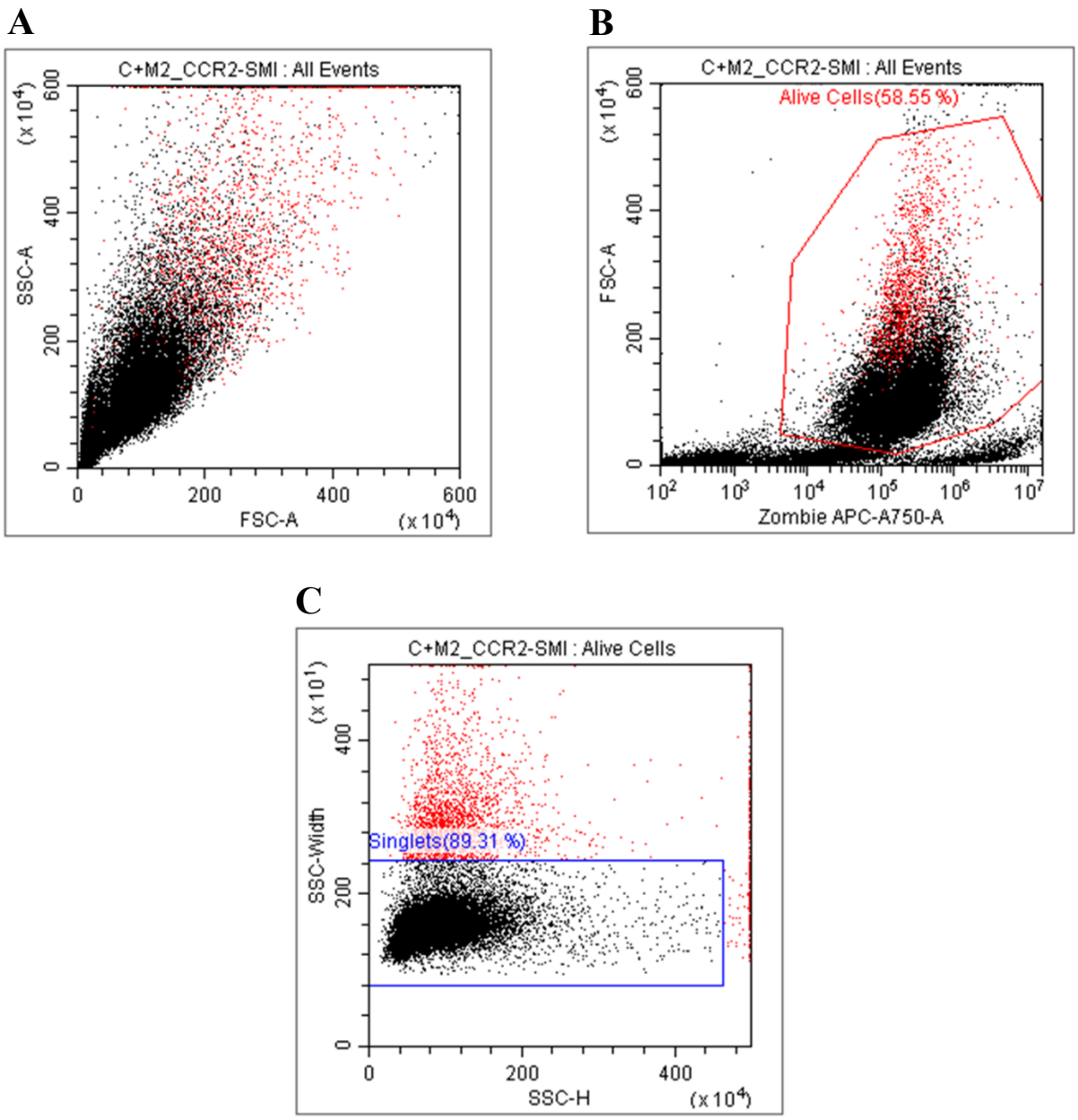

Figure 8: Singlet gating strategy with Cytoflex S flow cytometer software.
A,B,C Representative illustration of stepwise gating strategy of collagen digested 3D cocultured CAF and M2-like macrophage singlets with Cytoflex S flow cytometer. **A** All events plotted by size-reporting forward-scatter area (FSC-A) times granularity-reporting sideward-scatter area (SSC-A). **B** Cells plotted by dead cell marker Zombie NIR™ versus FSC-A. Separation of alive cells (inclusive red gate) from dead/Zombie NIR™-positive cells (cloud at lower right) and debris (clouds at lower left). **C** Discrimination against singlets (inclusive blue gate) by SSC-height versus SSC-width. Red marked dots represent backgated cells from **C** backwards. Each dot represents one event plotted on X- times Y-axis depending on its signal intensity.

The upper right plot clusters cells by size and signal intensity in the APC-A750-A channel. Dead cells are more permeant to Zombie NIR™ and make their own distinguishable population at the lower far right end (**Figure 8 B**). The Singlets Gate is the third and last for pre-sorting the cells (**Figure 8 C**). Several strategies for doublet exclusion exist and often rather unprecise options like width vs. area plotting are chosen. We decided to use SSC-Height vs. SSC-Width as height is independent of width, making this strategy more accurate since it is not affected by area scaling. This singlet gate was then further applied among the channels for features of interest.

2.4.3. Establishment of a compatible dye-panel

Several Dye-Panels were used for the experiments included in this thesis. The course of action is illustrated by our widest panel with a simultaneous staining of 7 different targets (CCR2-APC; MCSFR-PE; CD163-PerCP Cy5.5; CD86-Alexa Fluor 488; CD45-Brilliant Violet 421; Vimentin-Alexa Fluor 594) in the following sections.

2.4.3.1. Spectra analysis for compatibility and spillover check

The simultaneous use of several fluorescent dies in Flow Cytometry is not trivial. Each conjugated dye has specific and varying characteristics concerning excitation and emission. The emission spectrum of some dyes can be of wider ranges than others and hence cause unwanted signals at PMTs of other channels – known as spillover. Bio Rad's Spectra Viewer Tool was used for determination of compatible conjugated dyes (**Figure 9)**. Resulting filter coverage shows substantial spillover for Alexa Fluor 594, PerCP-Cy5.5 and APC requiring compensation to avoid false positive signals (**Figure 10**).

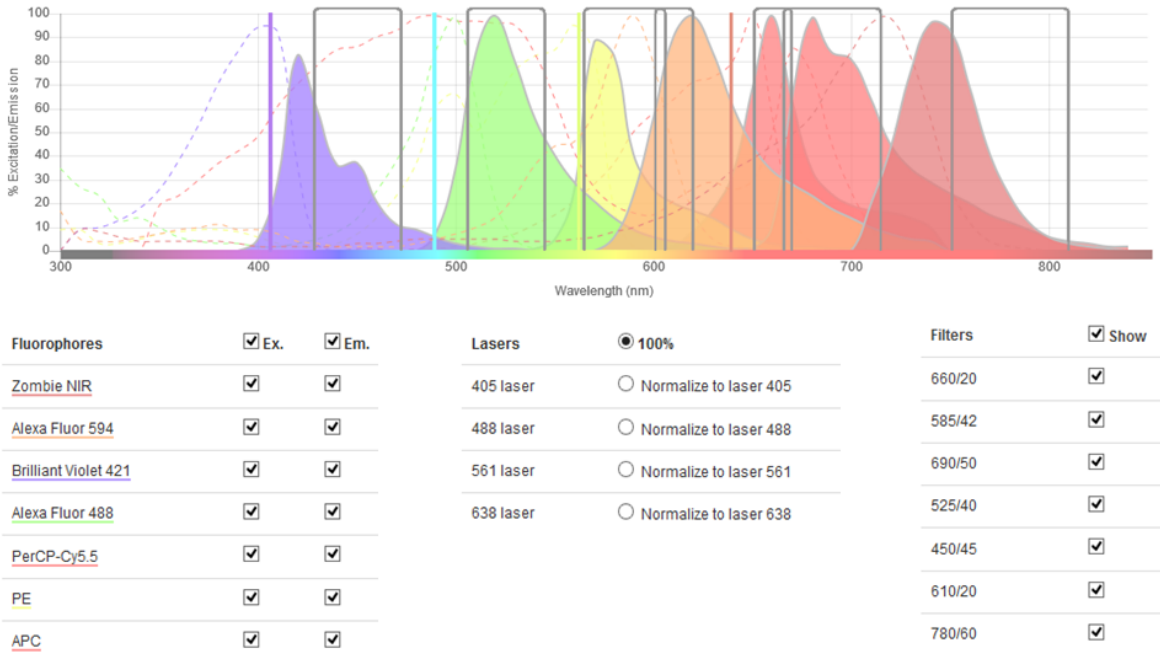

Figure 9: Compatibility and spillover check of dyes for flow cytometry.
Seven antibodies with different conjugated dyes were used simultaneously for flow cytometry analysis. Befor usage, the online tool of Bio Rad (*https://www.bio-rad-antibodies.com/spectraviewer.html*) was used fo compatibility check and potential spillover. The four required excitation lasers are illustrated as vertical lines Emission spectra are color coded for each conjugated dye. Filter settings according to Cytoflex S flow cytometer Gray frames depict recorded emission light by photon multipliers (PMTs).

Fluorophores / Filters	660/20	585/42	690/50	525/40	450/45	610/20	780/60
Zombie NIR	0%	0%	4%	0%	0%	0%	25%
Alexa Fluor 594	**31%**	21%	18%	0%	0%	**94%**	0%
Brilliant Violet 421	0%	0%	0%	1%	**33%**	0%	0%
Alexa Fluor 488	0%	12%	0%	**79%**	0%	3%	0%
PerCP-Cy5.5	**37%**	0%	**78%**	0%	0%	0%	11%
PE	2%	**59%**	1%	0%	0%	18%	0%
APC	**81%**	0%	**31%**	0%	0%	5%	0%

Figure 10: Pre-calculated filter coverage with potential spillover.
Filter coverage calculation with the online tool of Bio Rad (*https://www.bio-rad-antibodies.com/spectraviewer.html*) for each conjugated dye. First band-pass filter belongs to last fluorescent dye, order of columns and lines are inverted. The matrix additionally shows spillover signals recorded by unwanted fluorescent channels. The highest signals are detected by the belonging channels for every dye. Alexa Fluor 549 shows substantial spillover in APC, PE and PerCP-Cy5.5 channels; PerCP-Cy5.5 with substantial spillover in the APC channel; PE generates unwanted signal in Alexa Fluor 594 channel; and APC comes with unwanted high signal for PerCP-Cy5.5.

2.4.3.2. Creation of compensation matrix (CytoflexS)

To compensate spillover, a compensation matrix was created with UltraComp eBeads™ of Invitrogen. One drop of beads contains a positive and a negative population of beads, meaning, only positive population will react with fluorochrome-conjugated antibody. Still both populations lead to results making this bimodal distribution suitable for single-color compensation.

A 1.5 ml Eppendorf tube was prepared for each conjugated antibody and filled with 1 drop of UltraComp eBeads™ after several times pulse-vortexing. A drop was about 40 µl and was filled up to a final volume of 100 µl with FACS buffer and appropriate dilutions of antibodies. Again pulse-vortexing followed by 20 min incubation in the dark at 4°C. Unbound antibodies were washed out by addition of 1 ml FACS buffer and centrifugation at 500x g for 3 minutes. Supernatant was taken off prior to pellet-resuspension in 500 µl of FACS buffer. 10.000 events per vial were recorded and compensation matrix was calculated (**Figure 11**) and exported as *.comp* file for later application in FlowJo.

Autofl.	Channel	-FITC%	-PerCP...	-APC%	-APC-A700%	-APC-A750%	-PB450%	-KO525%	-Violet610%	-Violet660%	-PE%	-ECD%	-PC5.5%	-PC7%
0.13	FITC		0.08	0.04	0.00	0.12	0.02	0.00	0.00	0.00	1.30	2.54	0.00	0.00
0.02	PerCP	0.57		5.53	0.00	1.45	0.00	0.00	0.00	0.00	5.48	3.75	0.00	0.00
0.33	APC	0.00	0.85		0.00	0.09	0.00	0.00	0.00	0.00	0.02	0.58	0.00	0.00
0.00	APC-A700	0.00	44.73	135.55		8.61	0.00	0.00	0.00	0.00	0.05	1.39	0.00	0.00
0.01	APC-A750	0.00	45.08	140.02	0.00		0.00	0.00	0.00	0.00	0.05	0.58	0.00	0.00
2.71	PB450	0.01	0.06	0.07	0.00	0.23		0.00	0.00	0.00	0.00	3.78	0.00	0.00
0.00	KO525	0.31	0.05	0.06	0.00	0.21	8.63		0.00	0.00	0.03	2.90	0.00	0.00
0.00	Violet610	0.03	0.04	0.41	0.00	0.07	0.36	0.00		0.00	2.61	10.12	0.00	0.00
0.00	Violet660	0.00	2.72	11.10	0.00	0.02	0.04	0.00	0.00		0.32	2.11	0.00	0.00
0.18	PE	0.00	0.01	0.16	0.00	0.00	0.00	0.00	0.00	0.00		10.12	0.00	0.00
0.21	ECD	0.00	0.05	4.06	0.00	0.04	0.00	0.00	0.00	0.00	68.12		0.00	0.00
0.00	PC5.5	0.00	83.66	133.07	0.00	0.95	0.00	0.00	0.00	0.00	13.21	42.50		0.00
0.00	PC7	0.00	40.91	36.97	0.00	9.54	0.00	0.00	0.00	0.00	2.72	11.24	0.00	

Figure 11: Generated compensation matrix with UltraComp eBeads™.
UltraComp eBeads™ were stained with each of the 7 dyes according to protocol and recorded via Cytoflex S flow cytometer. Compensation matrix is automatically calculated for all available channels, irrelevant ones are lined out. FITC records signal of conjugated dye Alexa Fluor 488; PerCP records PerCP-Cy5.5; APC records APC; APC-A750 records Zombie NIR™; PB450 records Brilliant Violet 421; PE records PE; and ECD records Alexa Fluor 594. First column shows marginal values for bead autofluorescence. The matrix clusters calculated compensation values for each channel in an end-by-end table.

Figure 12 shows results of 10.000 recorded uncompensated beads stained with PE-conjugated antibody with spillover in several unwanted channels. Application of previously calculated compensation matrix allows successful reduction of spillover (**Figure 13**).

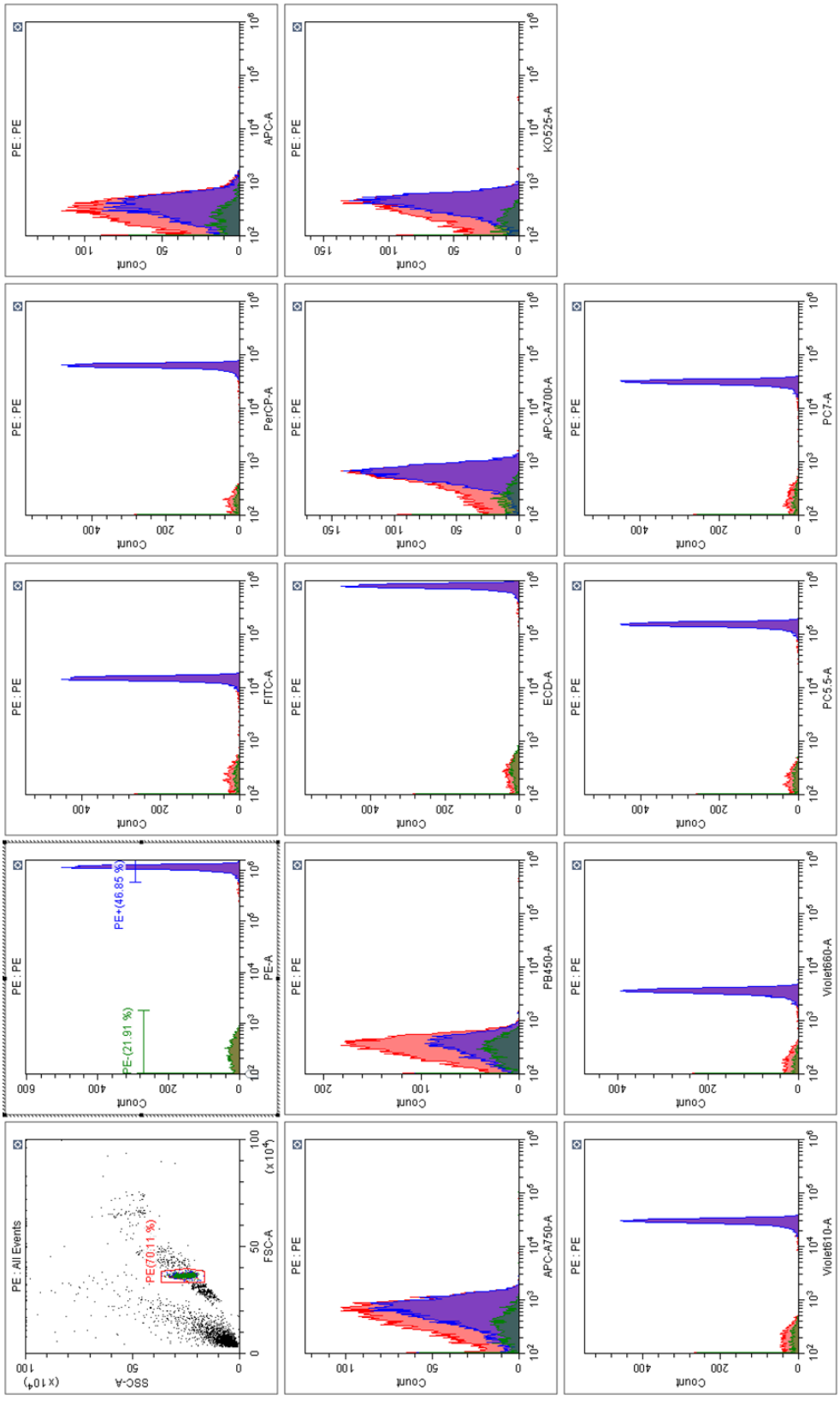

Figure 12: Spillover resulting from uncompensated UltraComp eBeads™ stained with PE-conjugated antibody.

UltraComp eBeads™ were stained with PE-conjugated antibody and gated (red population). Histograms of available channels of Cytoflex S are depicted: PE-negative bead populations in green, PE-positive populations in blue. Spillover observed in FITC, PerCP, ECD and others.

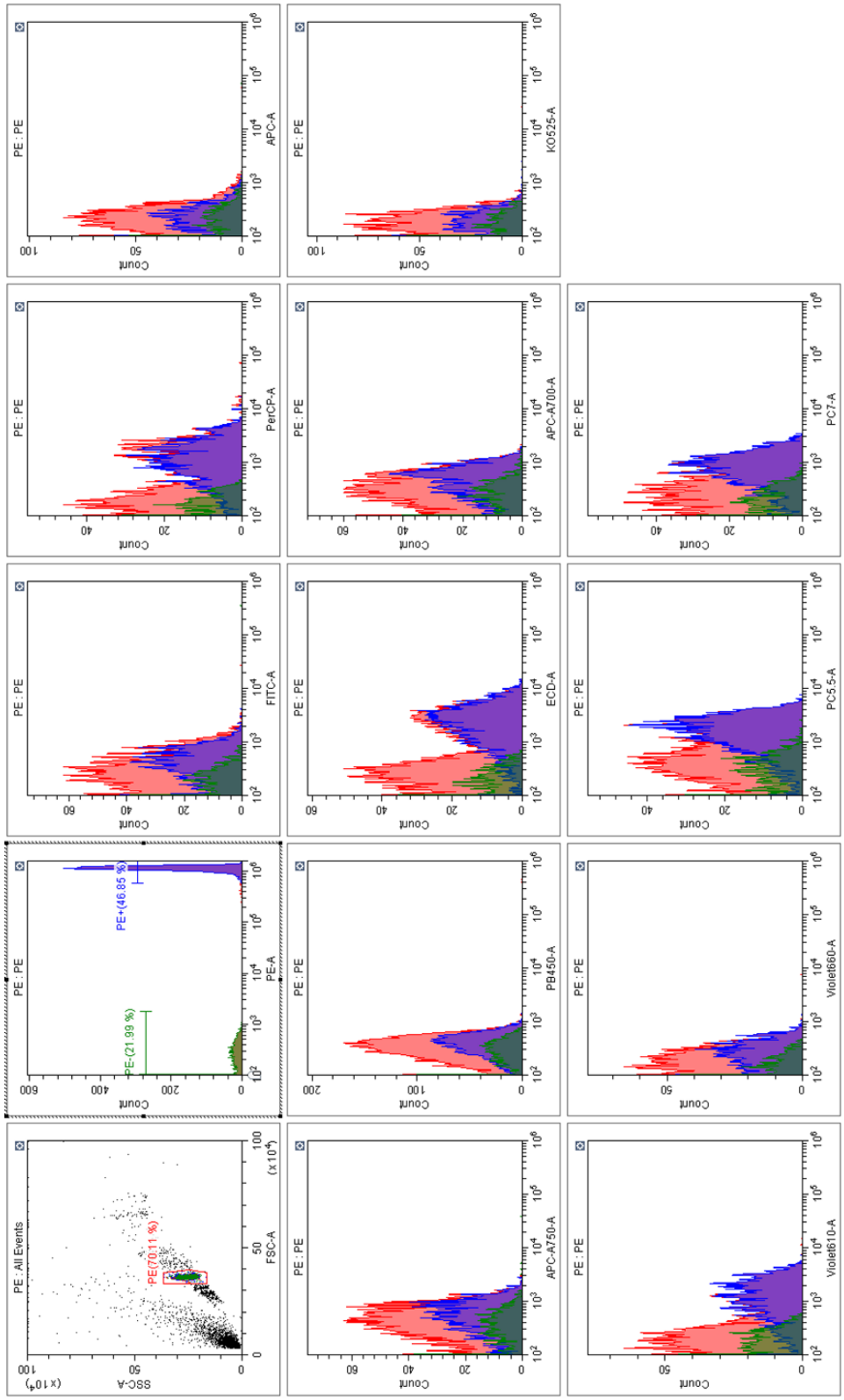

Figure 13: Compensated UltraComp eBeads™ stained with PE-conjugated antibody without spillover. Results of
Figure 12 are illustrated with applied compensation matrix (
Figure 11). Original bead population (10000 events), whereof half is negative unbinding control, are shown in red; PE-negative bead populations in green; PE-positive populations in blue. Signal only observed in PE-channel. Spillover compensated in all other channels.

2.4.4. Data processing with FlowJo software

CytoflexS data was saved as *.fcs* file and exported to FlowJo version 10. First, sample quality check was performed and if required, samples were adjusted with time gate function. Next, Compensation Matrix was applied. Unfortunately, FlowJo does not automatically align parameters with positive and negative samples correctly. Most of them are mixed up and Matrix Calculation Error occurs until it gets corrected manually (**Figure 14**). Once bead populations are adjusted in histogram mode (**Figure 15**) and all slots match, compensation matrix can be calculated and finalized.

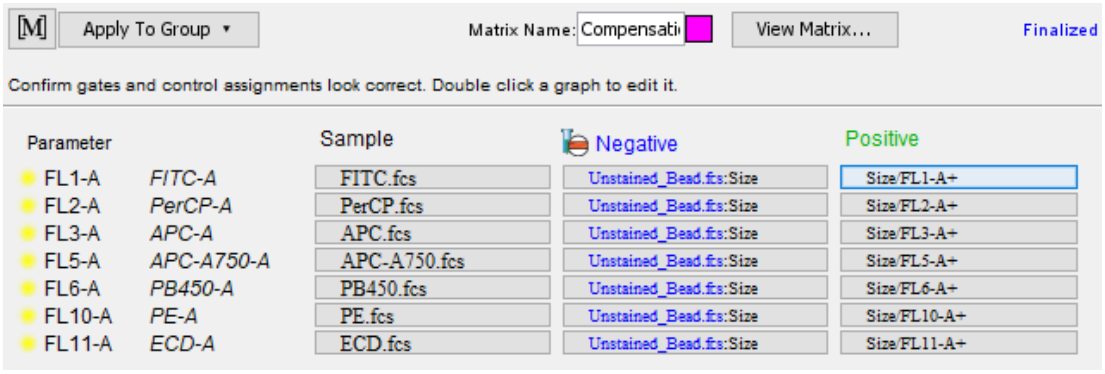

Figure 14: Screenshot of correct parameter adjustment and successful compensation matrix calculation in FlowJo.
Parameters selected for all 7 dyes: FL1-A/FITC-A for conjugated dye Alexa Fluor 488; FL2-A/PerCP-A for conjugated dye PerCP-Cy5.5; FL3-A/APC-A for conjugated dye APC; FL5-A/APC-A750-A for Zombie NIR™; FL6-A/PB450-A for conjugated dye Brilliant Violet 421; FL10-A/PE-A for conjugated dye PE; and FL11-A/ECD-A for conjugated dye Alexa Fluor 59.

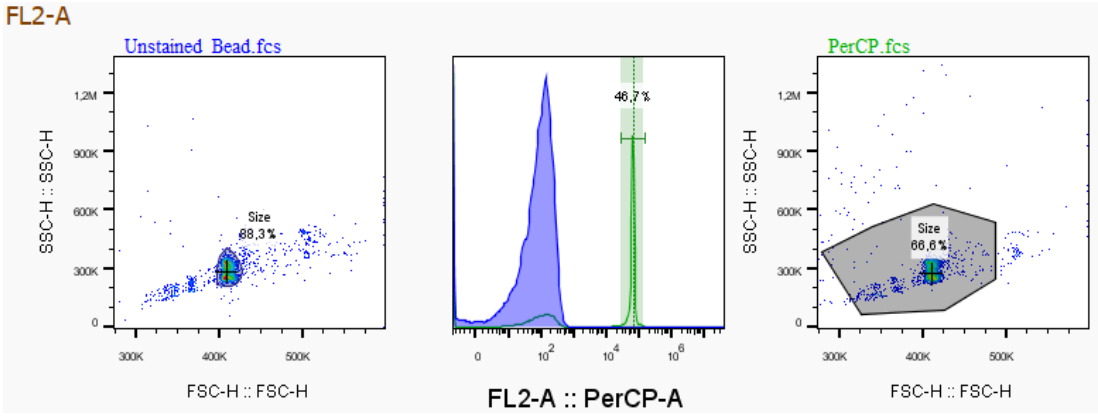

Figure 15: Screenshot of manual bead population selection and distinguishing positive beads in histogram mode.
Illustration of FL2-A/PerCP channel as representative example. Positive bead population defined in histogram mode (green).

The gating strategy is similar to previous pre-gating with CytoflexS software. Dead cells were gated out by plotting Zombie/APC-A750-A vs. FSC-A. Alive cells were then discriminated from debris in FSC-A vs. SSC-A and singlets by plotting SSC-H vs. SSC-W. In co-culture samples, macrophages and fibroblasts were separated by either CD45, CD68, CD163 or combinations (**Figure 16**).

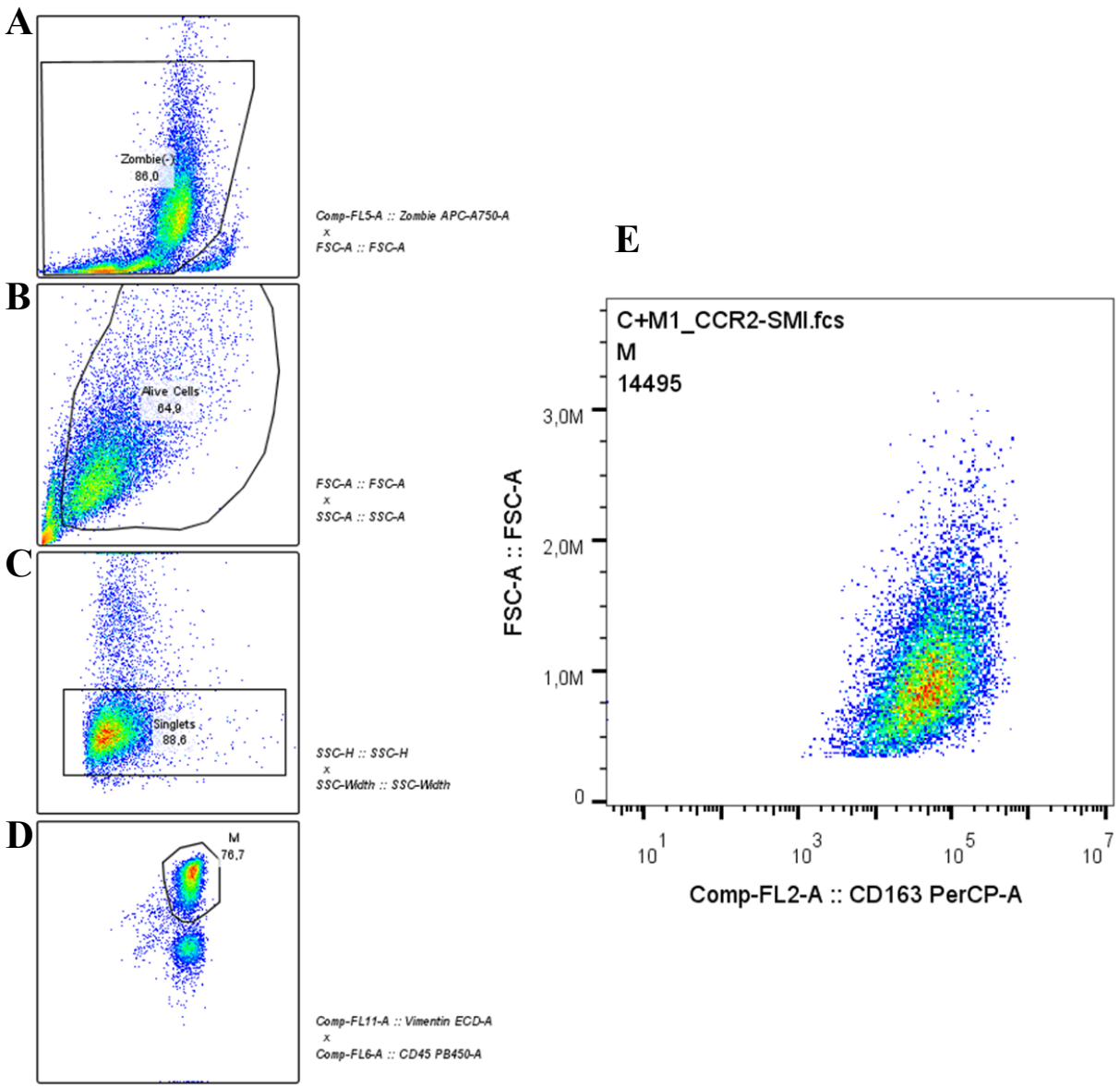

Figure 16: Representative singlet-gating strategy of a specific cell type for a specific marker.
3D co-cultured (CAFs and macrophages) collagen type 1 gels were digested and set up for flow cytometry. **A,B,C,D** illustrate typical gating strategy of CAF- or macrophage singlets. **A** Zombie NIR™ was used for dead cell discrimination. **B** Size plotted against granularity allows for debris exclusion. **C** Doublet exclusion was achieved by SSC-H times SSC-width plotting. **D** Macrophages and fibroblasts are positive for Vimentin; macrophages identified by specific CD45 marker. **E** Gated macrophages are positive for M2-like macrophage marker CD163.

2.4.5. Statistical analysis of flow cytometry data

Flow cytometry data was obtained from Cytoflex S and further processed with FlowJo version 10. Subsequent to proper gating of cells with markers of interest, quantitative data (mean, standard deviation, count) was created by FlowJo table tool, exported to MS Excel 2016 and further evaluated with GraphPad Prism 6. Depending on the experimental setup, significance was tested for by either one-way ANOVA (column analysis, multiple column mean-comparison) or unpaired t-test (Holm-Sidak method for multiple comparison correction). Resulting P values (alpha: 0.05) are indicated according to following classification:

ns	$P > 0.05$
★	$P \leq 0.05$
★★	$P \leq 0.01$
★★★	$P \leq 0.001$
★★★★	$P \leq 0.0001$

2.5. Immunofluorescence of Formalin-Fixed Paraffin-Embedded (FFPE) patient material

Table 9: Reagents and solutions (1.5.)

Product Name	Company	Article no.
DAPI	Sigma-Aldrich, St. Louis, Missouri, USA	D9542
Eosin Y Solution Alcoholic	Sigma-Aldrich, St. Louis, Missouri, USA	HT110116
Eukitt Quick Hardening Mounting Medium	Sigma-Aldrich, St. Louis, Missouri, USA	03989
Haematoxylin Mayers Hemalum Solution	MERCK, Darmstadt, Germany	HX87717149

Citrate Working Solution	*Blocking Solution*	*Staining Buffer*
- 0.1 M citric acid solution in H_2O (Solution A) *- 0.1 M sodium citrate solution in H_2O (Solution B)*	*- 1x DPBS* *- 10% FCS* *- 2% BSA* *- TruStain (1:50)*	*- 1x DPBS* *- 2% BSA*

Table 10: Equipment (1.5.)

Product Name	Company	Article no.
Confocal Laser Scanning Microscope Leica TCS SP8	Leica Microsystems, Wetzlar, Germany	-
Inverted Microscope Olympus IX51	Olympus Shinjuku, Tokio, Japan	-
Liquid Repellent Slide Marker Wax Pen for Staining Procedure	Daido Sangyo, Tokyo, Japan	-
Magnetic Immuno Staining Humid Chamber	Cellpath Ltd., Newtown, UK	-
Menzel Coverslips	VWR International, Radnor, Pennsylvania, USA	631-1340
Microtome Type Razor	MICROS Austria Produktions- und Handelsges.m.b.H, St. Veit/Glan, Austria	100133
Plate Cooler Type MPS/C	SLEE medical GmbH, Mainz, Germany	I1140054
Superfrost® PLUS Object slides (poly-L-Lysine)	Thermo Fisher Scientific, Waltham Massachusetts, USA	J1800AMNZ

Table 11: Primary and secondary antibodies with belonging IgG controls for immunofluorescence analysis.

Primary antibodies

Target	Species Reactivity	Concentration [µg/ml]	Dilution	Final Conc [µg/ml]	Company	Catalog Number	Clone	Lot	Isotype Control
CCL2/MCP1	human	500	1:200	2.5	abcam	ab9669	Polyclonal	GR4808-60	rbIgG
CD68	human	500	1:250	2	BioLegend	916104	KP1	B283618	mIgG1

Secondary antibodies

Target	Conjugated Dye	Species Reactivity	Concentration [µg/ml]	Dilution	Final Conc [µg/ml]	Company	Catalog Number	Clone	Lot
Primary AB to CCL2/MCP1	Alexa Fluor 546	rabbit	2000	1:500	4	ThermoFisher Scientific	A11035	Polyclonal	1120111
Primary AB to CD68	Alexa Fluor 647	mouse	2000	1:500	4	ThermoFisher Scientific	A31571	Polyclonal	1757130

IgG controls

Target	Concentration [µg/ml]	Company	Catalog No	Lot
mIgG	200	Santa Cruz Biotechnology	sc-3877	E1110
rIgG	200	Santa Cruz Biotechnology	sc-3888	H2410

2.5.1. Microtome sectioning

FFPE samples of colorectal cancer patients – one healthy and tumor sample each per patient – were obtained from the Pathology institute of the Medical University of Vienna. FFPE-blocks were pre-cooled for 20 min on plate cooler at -8°C. Then samples were cut in 4 µm slices and carefully transferred into cold water-bath with marten-hair brushes. From here swimming slices were picked up with object slides, shortly submerged in 45°C water-bath to stretch them out and air dried afterwards.

2.5.2. Haematoxylin and Eosin staining (H&E)

H&E staining was performed to check sample quality in terms of uniform cutting and depth. Air-dried sections were incubated in drying cabinet at 60°C for 45min to melt the paraffin and afterwards washed in Xylene 1 (5 min) and Xylene 2 (10 min) to remove paraffin. For rehydration they were put 2 min each in EtOH 96%, EtOH 70%, EtOH 50% and washed in dH2O. Nuclei were stained for 30 sec with Haematoxlyin and immediately washed twice with H2O for 5 min. For dehydration they were kept in EtOH 50% and EtOH 70% for 2 min each. Extracellular matrix and cytoplasm were finally counterstained with Eosin for 1 min and washed out with H_2O sufficiently before mounting them in Eukitt mounting media under coverslips. Samples were then evaluated with Olympus IX51 Inverted Microscope.

2.5.3. Immunofluorescence on FFPE tissues

Slides were incubated in drying cabinet at 60°C for 1 hour. Sections were deparaffinized 15min each in Xylene 1 and 2 followed by 5min each in graded ethanol 100%, 96% and 70% for dehydration. Afterwards they were washed in dH2O and 1x PBS. Antigen retrieval was enabled by boiling them in citrate working solution at 100°C for 20 min. Sample tissue was then, after two washing steps in PBS, encircled with Wax Pen and blocked by incubation in 100 µl of blocking solution for 30 min in a humid chamber. Sections were washed in PBS and incubated in 100 µl staining buffer with appropriate dilution of primary antibody (**Table 11**) overnight in humid chamber. The next day they were washed twice in PBS before being incubated in staining

buffer with fluorescently labeled secondary antibody (1:500) (**Table 11**) for 45 minutes. Again, washing in PBS and finally staining in DAPI solution for 10min. Same protocol was performed with belonging IgG controls (**Table 11**) for each sample. Slides were washed and kept at 4°C in PBS until Confocal Laser Scanning Microscope analysis.

2.5.4. Confocal Laser Scanning Microscopy (CLSM) setup and acquisition

For CLSM a Leica TCS SP8 with Leica Application Suite X (software version 3.5.2.18963) was used. Each slide was covered with a coverslip and basted with a drop of immersion oil type G for 20x magnification. Samples were scanned at a format of 1024x1024, a speed of 400 Hz, line average of 4 and a frame average of 1. For further analysis, the maximum projection of several z-stacks (ten optical sections in 3 µm stack size) was exported as *Tif.* file.

2.5.5. Colocalization analysis with ImageJ-Fiji

For each patient, several maximum projection snapshots were imported to ImageJ as *Tif*. files. 15 Regions of Interest (ROIs) were defined with ROI-Manager-Tool per snapshot (**Figure 17**). Each ROI represents one single cell, which was visually identified by nuclear DAPI stain and further distinguished by cell-specific markers. CD68 antibody served as macrophage marker, while CCL2 antibody shows expression levels of CCL2.

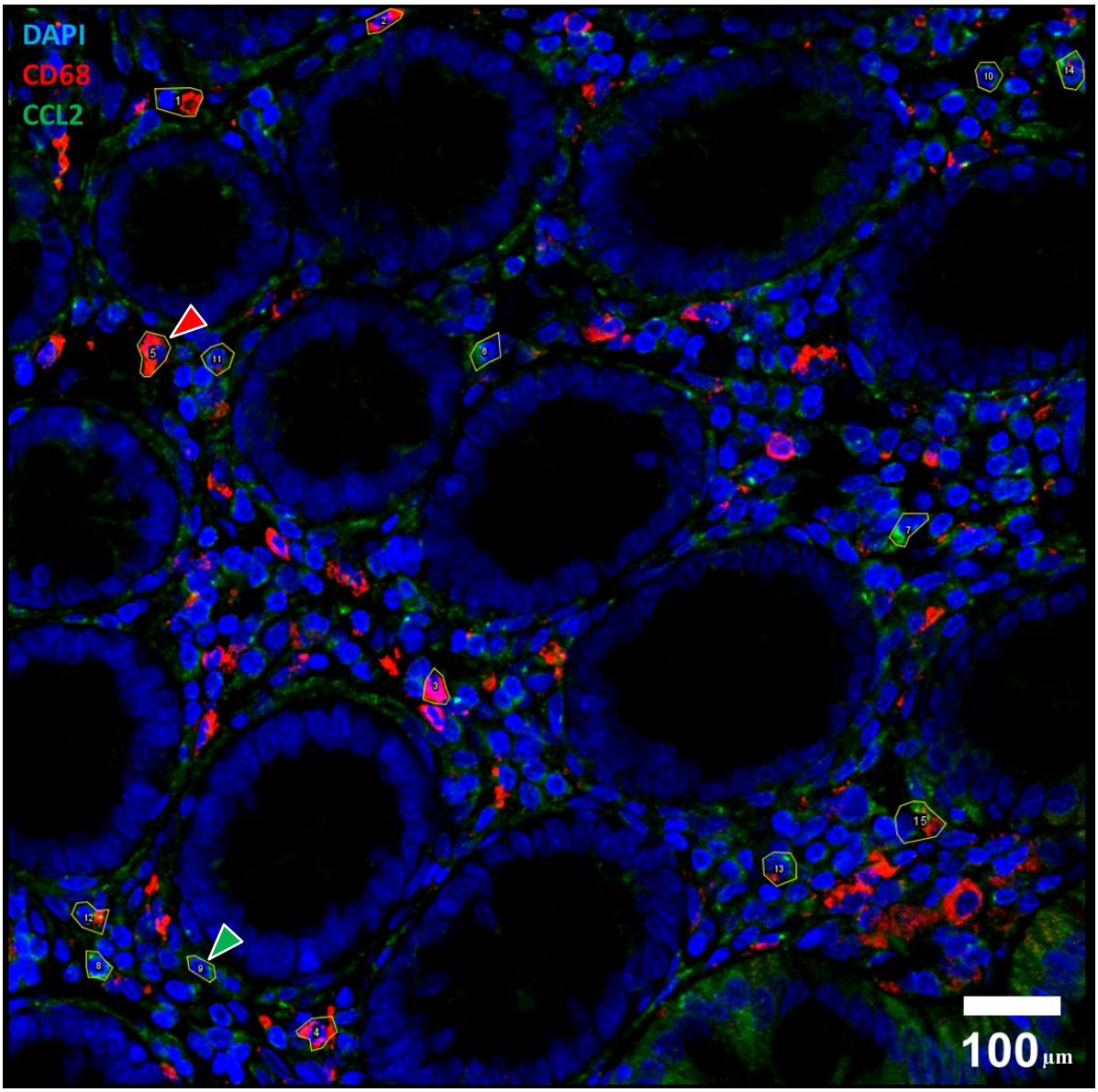

Figure 17: Defining ROIs in a CLSM image of healthy colon sample with ImageJ-Fiji.
Merged image of representative healthy colon FFPE section. Cell nuclei stained with DAPI, macrophages with primary antibody for CD68 combined with secondary conjugated Alexa Fluor 647 (1:500) antibody and CCL2 expression with primary antibody for CCL2 combined with secondary conjugated Alexa Fluor 546 (1:500) antibody. Each ROI represents one cell. 15 ROIs were analyzed per image. Red arrow (Cell 5) points at a typical macrophage, green arrow (Cell 9) at a typical fibroblast.

A color histogram was calculated for every ROI (**Figure 18**) and means and standard deviations were exported to MS Excel 2016 afterwards. Next, cells were classified and related to one of three categories: CAFs, macrophages expressing no CCL2 or macrophages expressing CCL2. This was done for all cells among all samples (healthy and tumor). Finally, means were calculated from each category and compared to each other.

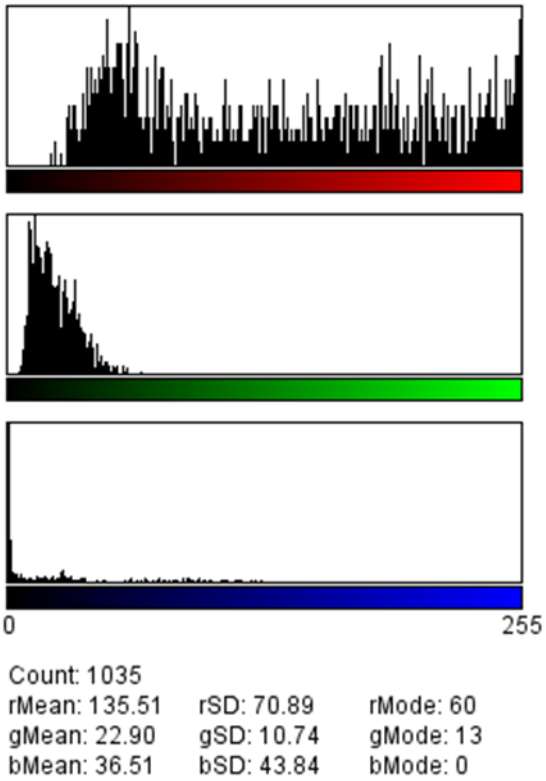

Figure 18: Color histogram calculation of selected ROI with ImageJ-Fiji.
Illustration of a representative macrophage color histogram (
Figure 17**:** Cell 5). Mean fluorescence intensities (MFIs) of macrophage marker CD68 (red), CCL2 expression marker (green) and cell nuclei marker DAPI (blue) with belonging standard deviations are calculated below histograms. Images were processed in 8-bit format with linear scaling from min-max to 0-255 for all three channels.

2.5.5.1. IgG subtraction

IgG controls were prepared for every sample. 10 ROIs were defined (**Figure 19**) as described in previous topic, belonging color histograms with MFIs were calculated and exported. Calculated MFI values were later subtracted from actual samples.

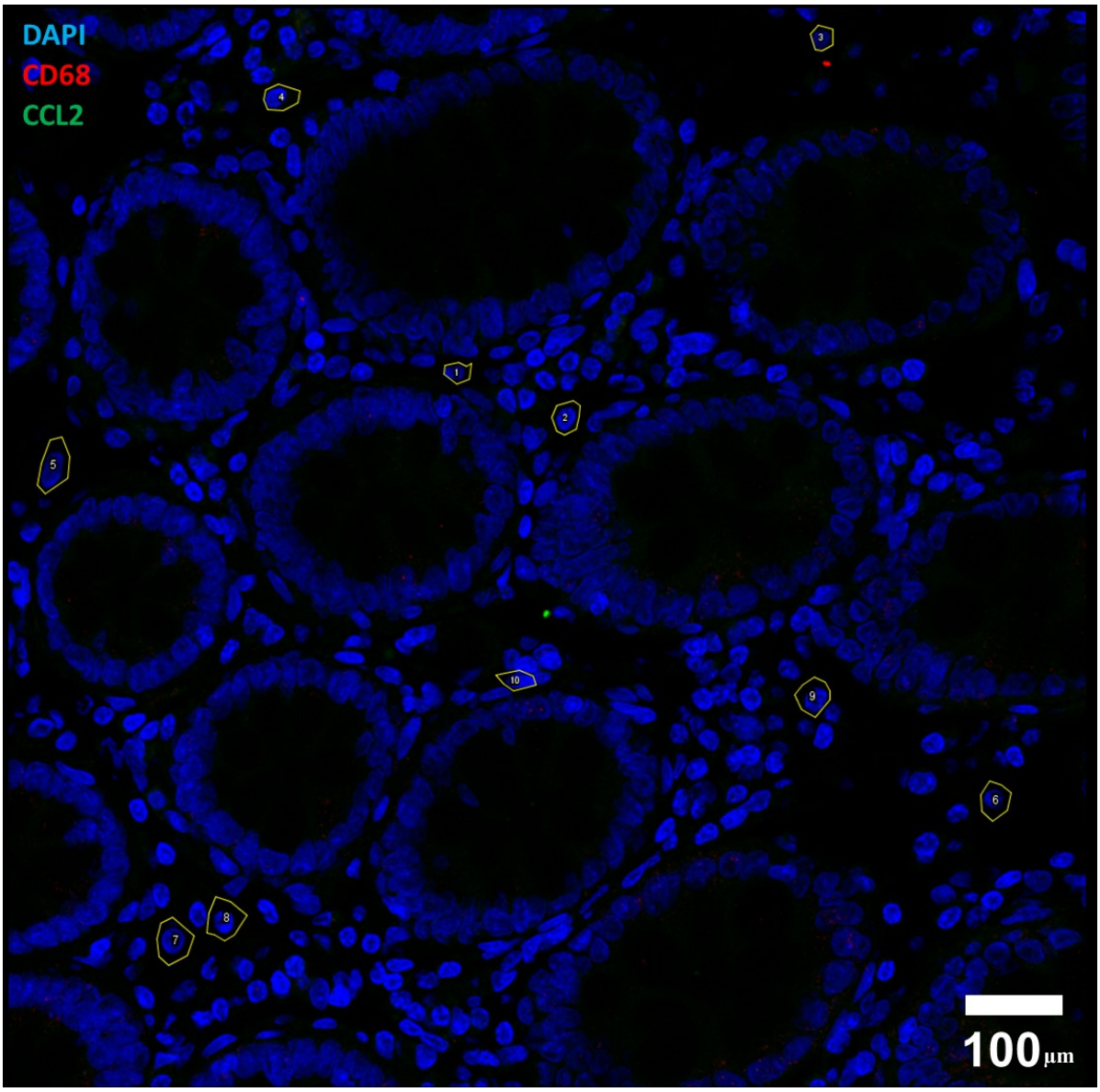

Figure 19: Defining ROIs in IgG control of healthy colon sample with ImageJ-Fiji.
Merged image of healthy colon IgG control. Cell nuclei stained with DAPI, macrophages controlled by mIgG combined with secondary conjugated Alexa Fluor 647 (1:500) antibody and CCL2 expression controlled by rIgG combined with secondary conjugated Alexa Fluor 546 (1:500) antibody. Each ROI represents one cell. 10 ROIs were analyzed per image.

3. Results

3.1. Titration and evaluation of Zombie NIR™ Fixable Viability Kit for dead cell staining – all cell populations shift

A precise flow cytometry analysis requires proper discrimination between alive and dead cells. Zombie NIR™ Fixable Viability Kit was used according to protocol to assess live vs. dead status of cells. It is an amine reactive fluorescent dye, which is water soluble and suitable for multi-color detection with red fluorescence at the far end of the light spectrum. Zombie NIR™ is supposed to be permeable to cells with compromised membranes only.

First, we titrated for optimum concentration per $1x10^6$ cells in 100 µl final volume in monocultured HCT116 cells and CAF3 cells. Three dilutions were chosen: 1:250, 1:500 and 1:1000. We observed a positive correlation between signal and concentration (**Figure 20**). The higher the concentration (or the lower the dilution), the stronger the signal was. Both cell types showed highest mean fluorescence intensity (MFI) for the 1:250 dilution and lowest MFI for the 1:1000 dilution. Surprisingly, the staining procedure shows effects on alive cells, meaning signals also shifting towards stronger intensity compared to unstained control. This becomes clear in **Figure 21 A and B**, where only cores (**Figure 21 C**) of several populations were gated and overlay-plotted with adjunct histograms. However, the negative population remains clearly distinguishable from alive cells among all samples. Secondly, we tested the 1:1000 dilution in cells treated with either plain DMEM or Staurosporine for 24h and compared it to normally cultured cells. By this we harvested a higher proportion of dead cells which made it easier to separate the populations (data not shown). As the more economical 1:1000 dilution allowed clear discrimination, we decided to use it for all subsequent experiments.

3.2. CCL2 and M-CSF signaling in 2D *in vitro* monoculture. Expression analysis of corresponding receptors CCR2 and M-CSFR in specific cell types by flow cytometry

Our current hypothesis is that CAFs instruct recruited monocytes to differentiate and polarize into M2-like macrophages. CCL2 and M-CSF have been identified as promising key players in this interaction. Moreover, CCL2 si-RNA-knockdown-CAFs displayed a reduction in cell number indicating a proliferative and/or cell survival phenotype.

Cells need to express the ligand-specific receptors for signal-transduction. Hence, to determine receptor expression in each cell type individually, we monocultured CAF3 and HCT116 cells

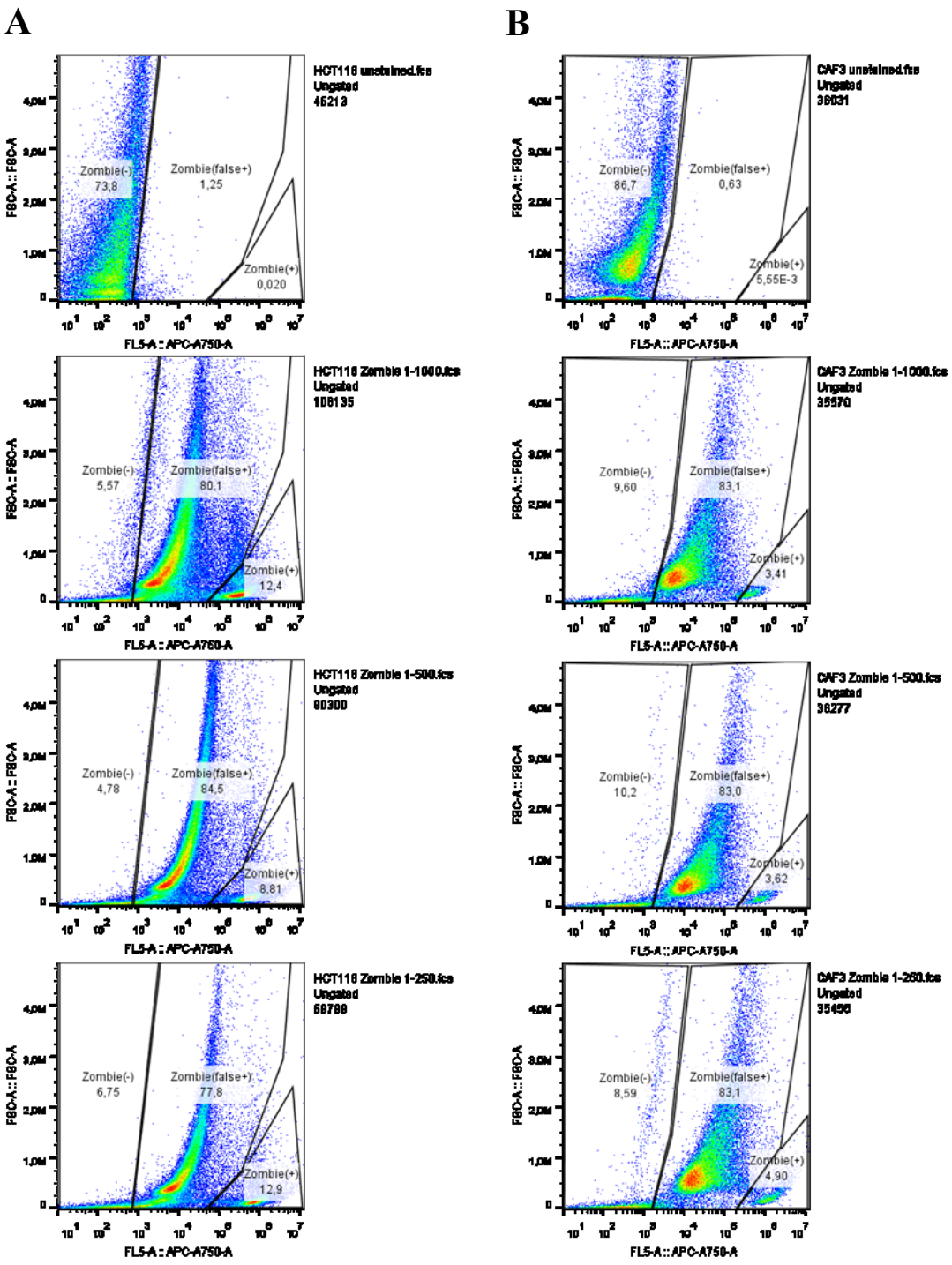

Figure 20: Flow cytometry data for titration of Zombie NIR™ Fixable Viability Kit in HCT116 (A) and CAF3 (B) cells.

HCT116 and CAF3 cells were mono-cultured in corresponding media until confluency. 1x10^6 cells per 100 µl each were stained with Zombie NIR™ Fixable Viability Kit at either 1:1000, 1:500 or 1:250 dilution. Cells were plotted by APC-A750-A vs. FSC-A. The distribution of cell populations is depicted among three gates: Zombie (-), Zombie (false+) and Zombie (+). First row shows unstained cells, followed by three titration conditions with increasing concentration. Zombie (+) gate marks dead cells.

and additionally isolated PBMCs. The latter were either directly used for flow cytometry or cultured, differentiated and polarized towards M1- or M2-like macrophages. For flow cytometry analysis we subdivided the PBMCs into monocytes and lymphocytes by gating for CD14 and CD86 positive cells, which are, in contrast to lymphocytes, both highly expressed in monocytes (data not shown). Next all cells were stained for CCR2 and M-CSFR for flow cytometry.

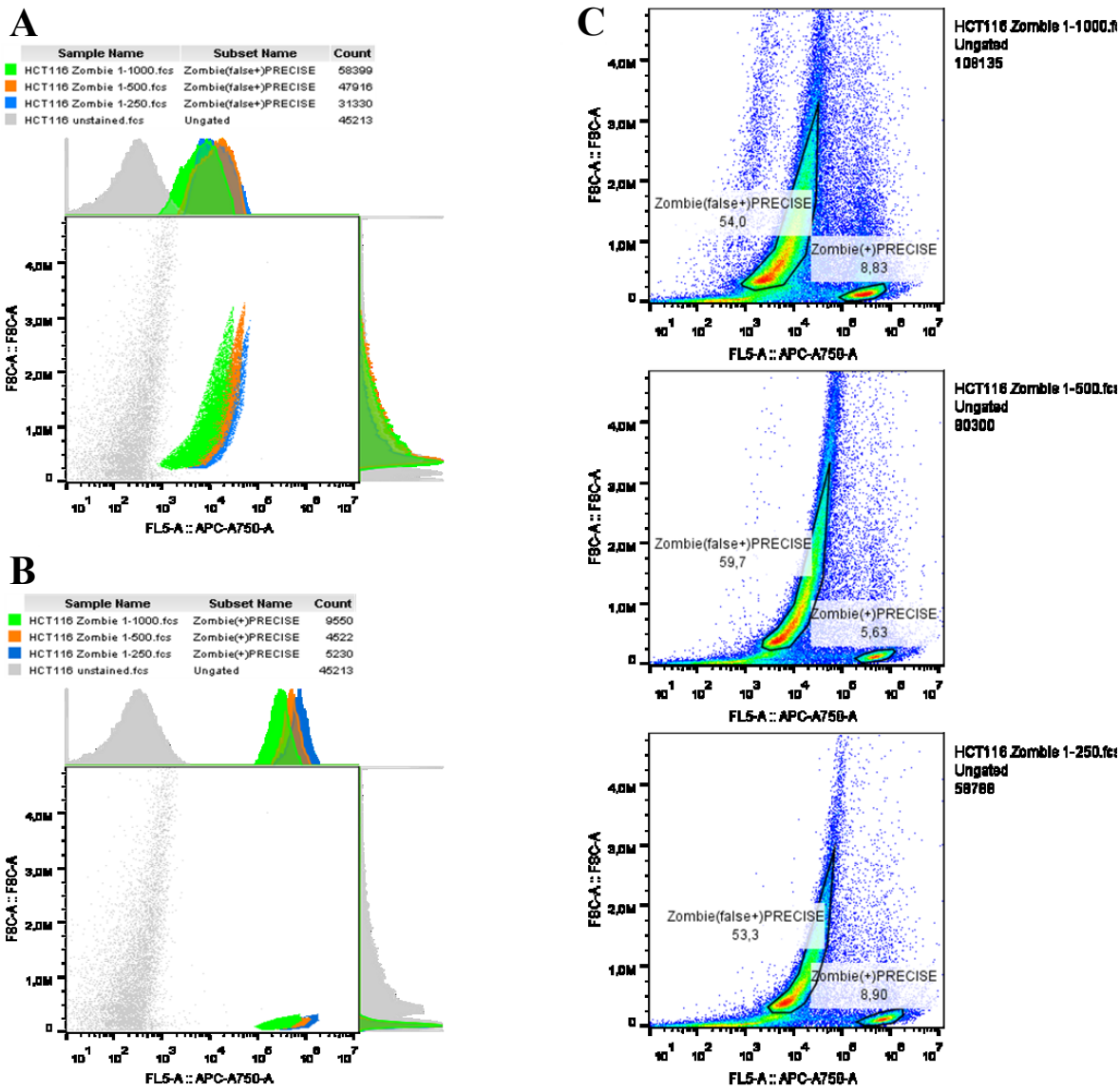

Figure 21: Flow cytometry overlay plots of Zombie NIR™ Fixable Viability Kit dilutions in HCT116 cells. HCT116 cells were chosen as representative example to illustrate dilution-dependent signal shift. Data from Figure 20 A was reevaluated by gating only the population cores. **A** Plotted overlay of gated Zombie(false+) core for 1:1000 (green), 1:500 (orange) and 1:250 (blue) dilutions. **B** Plotted overlay of gated Zombie(+) core for 1:1000 (green), 1:500 (orange) and 1:250 (blue) dilutions. **C** Precise gating of population cores.

3.2.1. M-CSFR is expressed among all cell types. CCR2 is expressed in CAFs, monocytes and lymphocytes – not in HCTs.

Quantification of flow cytometry data revealed highly significant (P = < 0,0001) CCR2 expression in CAFs, monocytes and lymphocytes (**Figure 22: A,C,D**), while no expression was observed in HCT116 cells (**Figure 22: B**). For M-CSFR highly significant (P = < 0,0001) expression was detected among all cell types (**Figure 22: A,B,C,D**). We double-controlled results with unstained and IgG control each. Unstained controls served as evaluation of IgG controls. IgG controls were used for final evaluation of results as they are more accurate.

Figure 23 A compares all previous CCR2 samples with subtracted IgG values embedded in one scale. Lymphocytes (MFI = 144) and CAFs (MFI = 119) show similar and low CCR2 expression levels. No CCR2 expression was observed in HCT116 (**Figure 22: B**). Monocytes (MFI = 5.407) express CCR2 at ~40 times more than lymphocytes and CAFs.

M-CSFR is expressed at low comparable levels in CAFs and lymphocytes (MFI ~ 380), while HCTs (MFI ~ 2.790) display an ~7-fold increased CCR2 expression. Monocytes reveal highest expression levels (MFI = 10.260) being ~3.5 fold higher as in HCT116 cells (**Figure 23: B**).

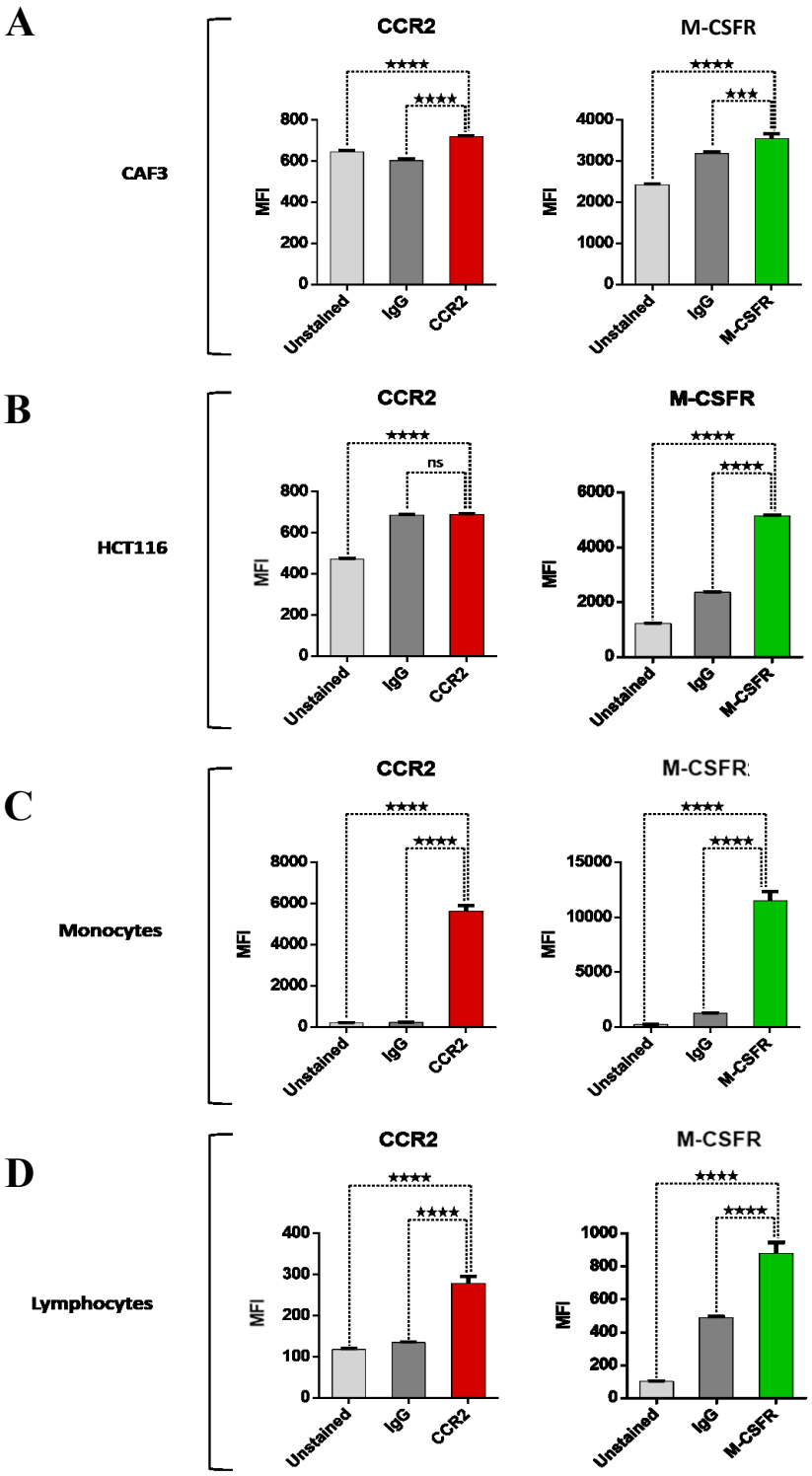

Figure 22: Cell type specific expression levels of CCR2 and MCSFR in 2D quantified by flow cytometry analysis.

A,B,C,D show quantified MFI of CCR2/APC and M-CSFR/PE for CAF3s, HCT116s, monocytes and lymphocytes (three biological replicates each, for *N see* **Figure 23**). CAFs and HCTs were monocultured in 2D, while PBMCs were isolated from healthy male donor and directly prepared for flow cytometry analysis. Monocytes were distinguished from lymphocytes by CD14 and CD86. Unstained controls were directly stained after trypsinization. mIgG1/APC served as IgG control for CCR2, mIgG1/PE for M-CSFR and were stained according to protocol of actual samples. Error bars depict the standard error of mean (SEM). Significance is indicated by stars. Non-significant comparisons are labeled with ns. For P-values see **Supplementary Table 1,2,3,4**.

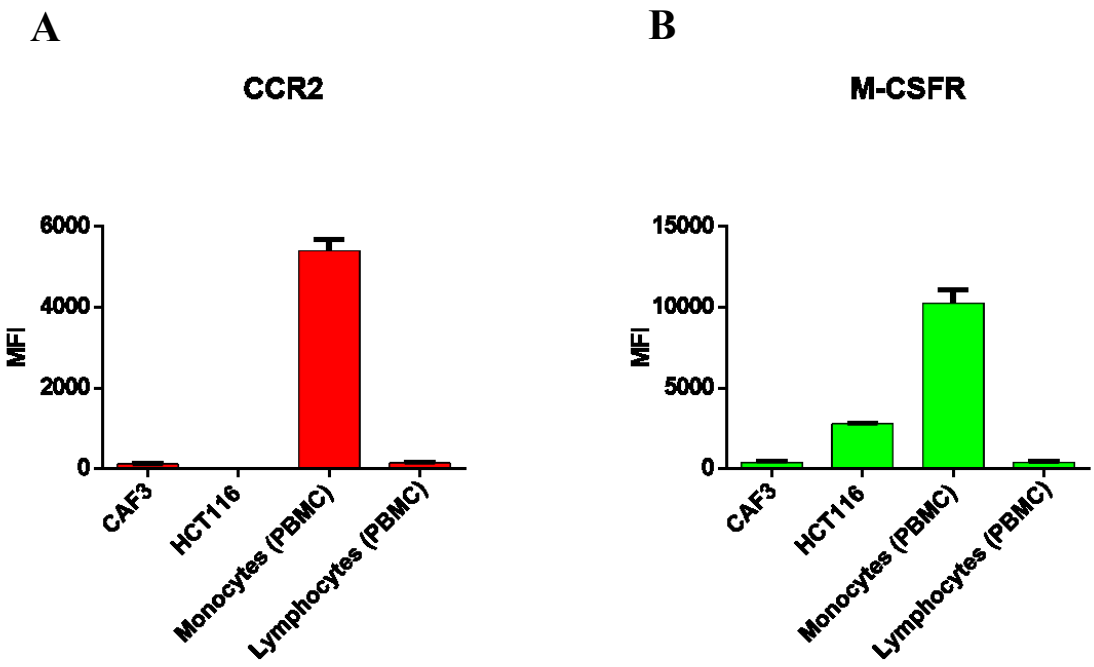

Figure 23: Comparison of cell type specific expression of CCR2 and M-CSFR by flow cytometry.
Comparison of CCR2 and M-CSFR expression levels determined in (**Figure 22**). Each bar represents mean fluorescence intensity (MFI) with subtracted IgG values. **A** CCR2 expression (red). **B** M-CSFR expression (green). Error bars depict the standard error of mean (SEM). *N*(CAF3): 67.291; *N*(/HCT116): 145.987; *N*(/Monocytes): 3118; *N*(/Lymphocytes): 17.112. *N* = gated singlets.

3.2.2. Differential expression of specific markers in M1- and M2-like macrophages

Monocytes isolated from PBMCs were differentiated and polarized into M1-like macrophages by GM-CSF, LPS and IFN-γ and into M2-like macrophages by M-CSF. Given that M2-like macrophages have in contrast to M1-like macrophages rather been associated with immunosuppressive functions in the tumor microenvironment, we further investigated their expression profile for specific monocyte lineage markers in addition to CCR2 and M-CSFR. Namely: CD45 as marker for hematopoietic cells, CD68 which is highly expressed by human monocytes and tissue macrophages, CD86 as marker for antigen-presenting cells, CD163 as specific marker for M2-like macrophages and CD14 as monocyte/macrophage specific marker.

3.2.2.1. M1- and M2-like macrophages are CCR2-negative. M-CSFR only expressed in M2-like macrophages

M1-like or M2-like macrophages were monocultured and derived from monocytes isolated from PBMCs. Both polarized cell types do not express CCR2 in our experiments as unstained and IgG controls show far more MFI (**Figure 24 A**). Interestingly, M1-like macrophages are negative for M-CSFR, while M2-like macrophages show strong (P = < 0,0001) expression (**Figure 24 B**).

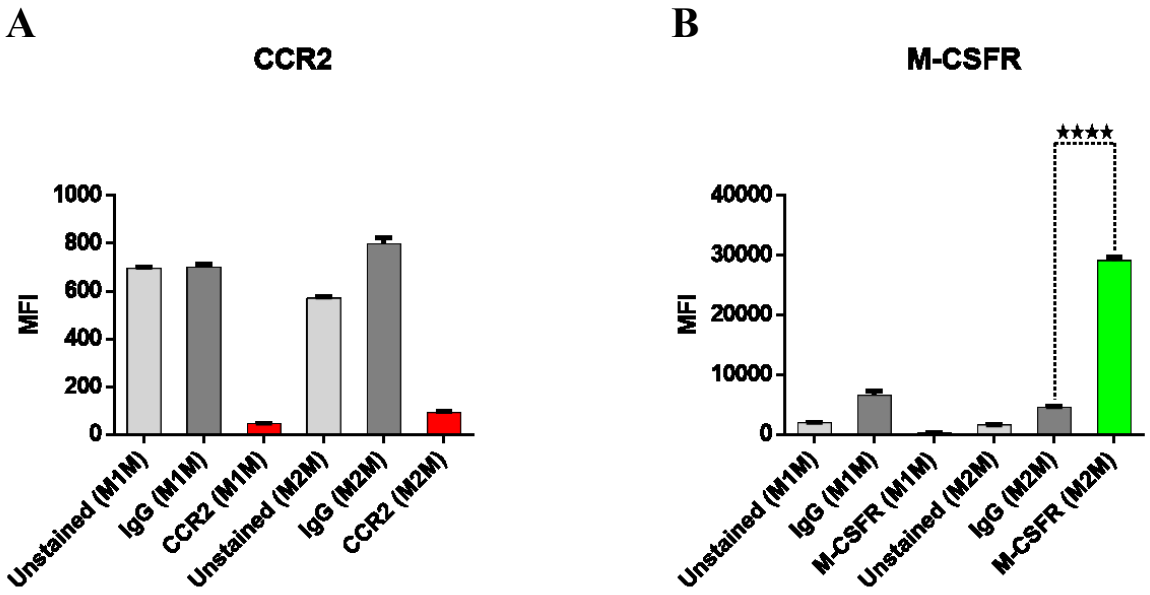

Figure 24: Flow cytometry data of CCR2 and M-CSFR expression levels in M1-like (M1M) and M2-like (M2M) macrophages.
PBMC-derived monocytes were differentiated and polarized towards M1- or M2-like status in 2D monoculture. They were either stained with conjugated CCR2/APC or M-CSFR/PE antibody. Bars represent MFI signals of unstained, IgG and CCR2 samples of M1M and M2M depicted for CCR2 (red) in **A**, for M-CSFR (green) in **B**. Error bars indicate the Standard Error of Mean (SEM). Significance is illustrated by stars. For P-values see **Supplementary Table 5**. *N*(Unstained(M1M)): 10.252; *N*(IgG(M1M)): 16.755; *N*(CCR2/M-CSFR(M1M)): 17.492. *N*(Unstained(M2M)): 9.373; *N*(IgG(M2M)): 10.335; *N*(CCR2/M-CSFR(M2M)): 16.624. *N* = gated singlets.

3.2.2.2. Differential monocyte/macrophage marker signature of M1- and M2-like macrophages

Several polarization types have been reported in the past. M1- and M2- like are considered as the two far extremes. However, intermediate forms make it difficult to distinguish and classify. We asked, if we can assign a specific marker signature for artificially polarized M1- and M2-

like macrophage extremes. Both types show highly significant (P = < 0,0001) expression of CD45, CD68 and CD86 (**Figure 25 A,B,C**). Still, when comparing them among each other, M1-like macrophages seem to express considerably more of all three markers. M2-specific marker CD163 was expressed highly (P = < 0,0001) in M2-like macrophages and its expression is low in M1-like cells (**Figure 25 D**). CD14 is a monocyte specific marker but was only observed in M2-like macrophages (**Figure 25 E**).

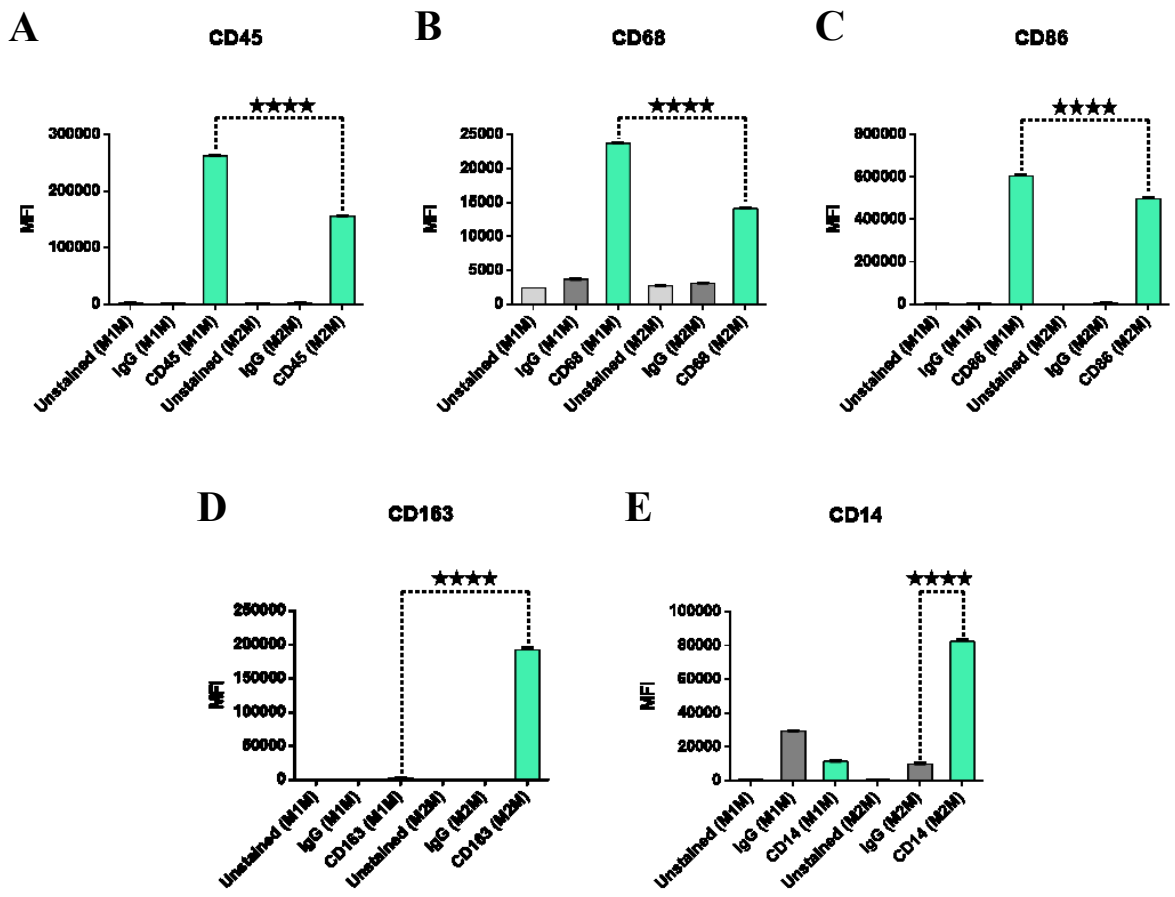

Figure 25: Flow cytometry data of monocyte/macrophage specific markers in M1-like (M1M) and M2-like (M2M) macrophages.
PBMC-derived monocytes were differentiated and polarized towards M1- or M2-like status in 2D monoculture. Bars represent MFI of unstained control, IgG control and specific markers for both M1- and M2-like macrophages. This panel contains several monocyte/macrophage specific markers: **A** CD45/Brilliant Violet 421 as marker for hematopoietic lineage; **B** CD68/Alexa Fluor 488 as monocyte/macrophage marker; **C** CD86/Alexa Fluor 488 as monocyte/macrophage marker; **D** CD163/Alexa Fluor 647 as specific marker for M2-like macrophages; **E** CD14/APC as monocyte/macrophage marker. Error bars indicate the standard error of mean (SEM). Relevant significances illustrated by stars. For P-values see **Supplementary Table 5**. *N*(Unstained(M1M)): 10.252; *N*(IgG(M1M)): 11.900; *N*(CCR2/M-CSFR(M1M)): 12.656. *N*(Unstained(M2M)): 9.373; *N*(IgG(M2M)): 11.811; *N*(CCR2/M-CSFR(M2M)): 11.976. *N* = gated singlets.

3.3. Targeting CCR2 and M-CSFR axis in 3D collagen gel *in vitro* setting. Effects of small molecule inhibitors RS 504393 and BLZ 945 on specific markers

3D culture settings are known for more closely mimicking the physiological situation. Hence, we decided to interfere the signaling axis of CCR2 and M-CSFR in 3D collagen gel settings with focus on the crosstalk between cancer associated fibroblasts and macrophages only, as previous experiments revealed CAFs as important mediators of macrophage polarization but not the tumor cells. For the experimental readout, flow cytometry antibodies against following markers were used: CCR2 as receptor for CCL2; M-CSFR as receptor for M-CSF; CD86 as marker for antigen-presenting monocytes/macrophages; CD163 as specific marker for M2-like macrophages; CD45 as marker for the hematopoietic cells; Vimentin as mesenchymal cell marker; and CCL2 (only in cocultured CAFs and macrophages). For blocking receptor mediated signaling of CCR2 we used the small molecule inhibitor RS 504393, while M-CSFR was blocked with the small molecule inhibitor BLZ 945. As control, gels were treated with DMSO. Every experimental setup contained one gel treated with DMSO for control, one gel treated with RS 504393 and one with BLZ 945 – the treatment was performed for 6 days with media and factor change every 48 hours. These experiments were performed in at least three biological replicates. Experiments were carried out in mono- and cocultures with CAFs or/and macrophages.

3.3.1. Effects of RS 504393 and BLZ 945 in 3D monocultured CAFs and macrophages

Previously, we demonstrated that 2D monocultured CAFs show significant expression of CCR2 and M-CSFR. In this 3D setting, they did not show significant expression for both CCR2 and M-CSFR in any of the three conditions compared to IgG control. Also, as expected, no expression for monocyte/macrophage lineage markers CD86, CD163 and CD45 were observed. Expression of Vimentin was detected among all conditions (P(DMSO) = 0,0063; P(RS 504393) = 0,0031; P(BLZ 945) = 0,0056), but without differences in between (**Figure 26**).

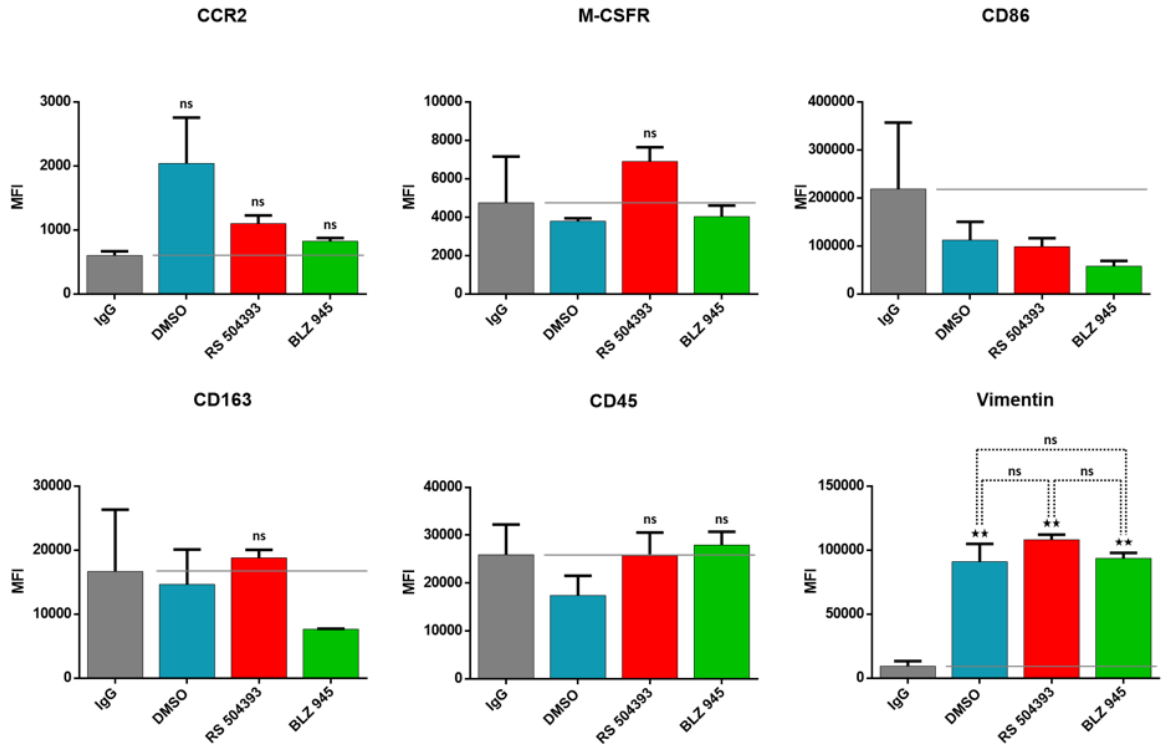

Figure 26: Effects of RS 504393 and BLZ 945 on specific markers in 3D monocultured CAFs analyzed by flow cytometry.
CAFs (300.000 cells per gel) were imbedded in 3D collagen type 1 gels and treated with either DMSO control (blue), CCR2 small molecule inhibitor RS 504393 (2 µM, red) or M-CSFR small molecule inhibitor BLZ 945 (1 µM, green) for 6 days (media and factor refresh all 48 hours). Each bar represents the MFI of combined replicates (at least 2, for individual data see **Supplementary Figure 1 and 3**). Mean MFI of unstained- and IgG-controls was taken as reference for expression evaluation and is illustrated as gray horizontal line among samples. Error bars indicate the SEM and relevant significances are illustrated by stars while non-significant comparisons are labeled with ns. Significance results directly clipped to the error bar account for MFI differences between treatments and IgG control, presupposed being significantly higher. For P-values see **Supplementary Table 6**. CCR2 as receptor for CCL2; M-CSFR as receptor for M-CSF; CD86 as monocyte/macrophage marker; CD163 as specific marker for M2-like macrophages; CD45 as marker for the hematopoietic lineage and Vimentin as mesenchymal cell marker were detected by following conjugated antibodies: CCR2/APC; M-CSFR/PE; CD163/PerCP7Cy5.5; CD45/Alexa Fluor 488 and Vimentin/Alexa Fluor 594. *N*(IgG): 19.732; *N*(DMSO): 12.971; *N*(RS 504393): 31.889; *N*(BLZ 945): 23.140. *N* = gated singlets.

In contrast, the monocultured macrophages showed CCR2 (P = 0,0179) and M-CSFR (P = 0,0002) expression in DMSO controls and CCR2 inhibition by RS 504393 did not show any significant effect. However, treatment with the M-CSFR inhibitor BLZ 945 resulted in significant downregulation of CCR2 (P = 0,0457) and M-CSFR (P = 0,0008) in the myeloid cells. On the other hand, myeloid cells treated with BLZ 945 displayed significant CD86 expression (P = 0,0196). The M2-like macrophage marker CD163 was decreased by both treatments in comparison to the DMSO controls, specifically evident under M-CSFR inhibition. CD45 and Vimentin did not show significant differences.

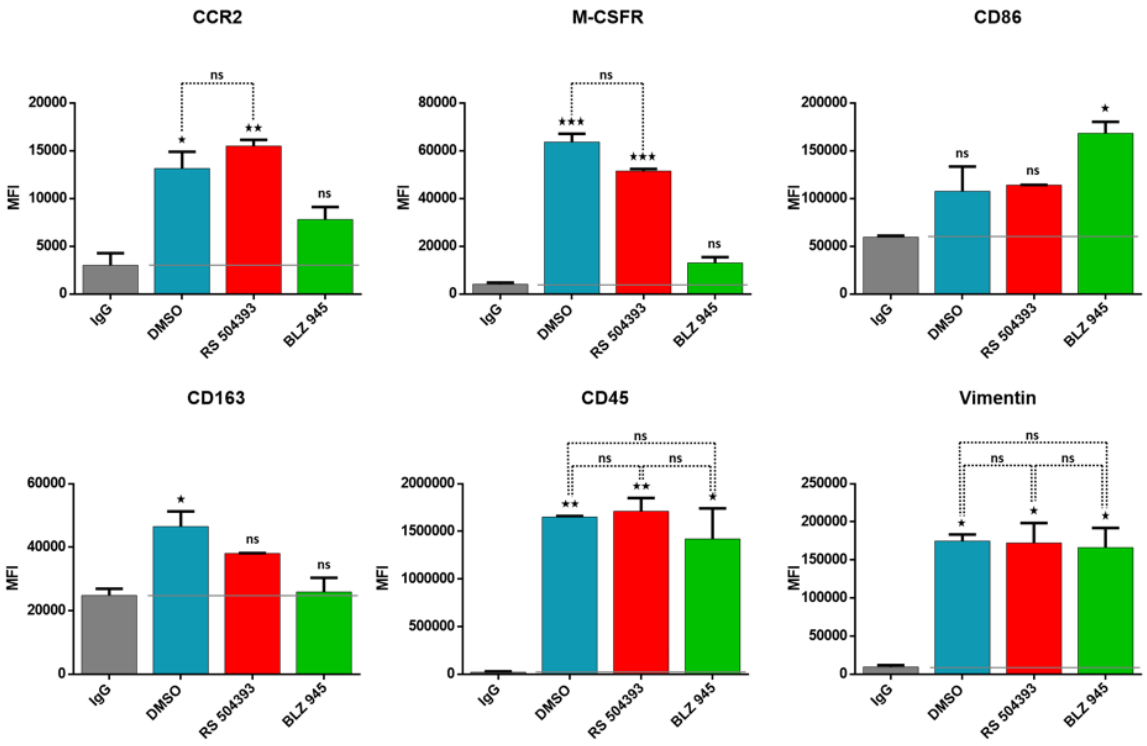

Figure 27: Effects of RS 504393 and BLZ 945 on specific markers in 3D monocultured macrophages analyzed by flow cytometry.
From PBMC isolated into macrophage differentiated monocytes (300.000 cells per gel) were imbedded in 3D collagen type 1 gels and treated with either DMSO control (blue), CCR2 small molecule inhibitor RS 504393 (2 µM, red) or M-CSFR small molecule inhibitor BLZ 945 (1 µM, green) for 6 days (media and factor refresh all 48 hours). Each bar represents MFI of combined gel replicates (at least 2, for individual data see **Supplementary Figure 1 and 4**). Means MFI of Unstained- and IgG-controls was taken as reference for expression evaluation and is illustrated as gray horizontal line among samples. Error bars indicate the SEM and relevant significances are illustrated by stars while non-significant comparisons are labeled with ns. Significance results directly clipped to the error bar account for MFI differences between treatments and IgG control, presupposed being significantly higher. For P-values see **Supplementary Table 7**. CCR2 as receptor for CCL2; M-CSFR as receptor for M-CSF; CD86 as monocyte/macrophage marker; CD163 as specific marker for M2-like macrophages; CD45 as marker for the hematopoietic lineage and Vimentin as mesenchymal cell marker were detected by following conjugated antibodies: CCR2/APC; M-CSFR/PE; CD163/PerCP7Cy5.5; CD45/Alexa Fluor 488 and Vimentin/Alexa Fluor 594. *N*(IgG): 25.256; *N*(DMSO): 37.948; *N*(RS 504393): 38.817; *N*(BLZ 945): 32.848. *N* = gated singlets.

3.3.2. Effects of RS 504393 and BLZ 945 in 3D cocultured CAFs and macrophages

The next step was the 3D cocultivation of CAFs and macrophages. In addition to above analyzed markers, we investigated the effects of the small molecule inhibitors on the expression level of CCL2 – the major ligand of CCR2. Earlier experiments in the Dolznig Lab showed strong CCL2 induction in both CAFs and macrophages when coculturing them in 3D (Pudelko, 2016). Thus, we were interested, whether interference with CCL2 and/or M-CSFR signaling

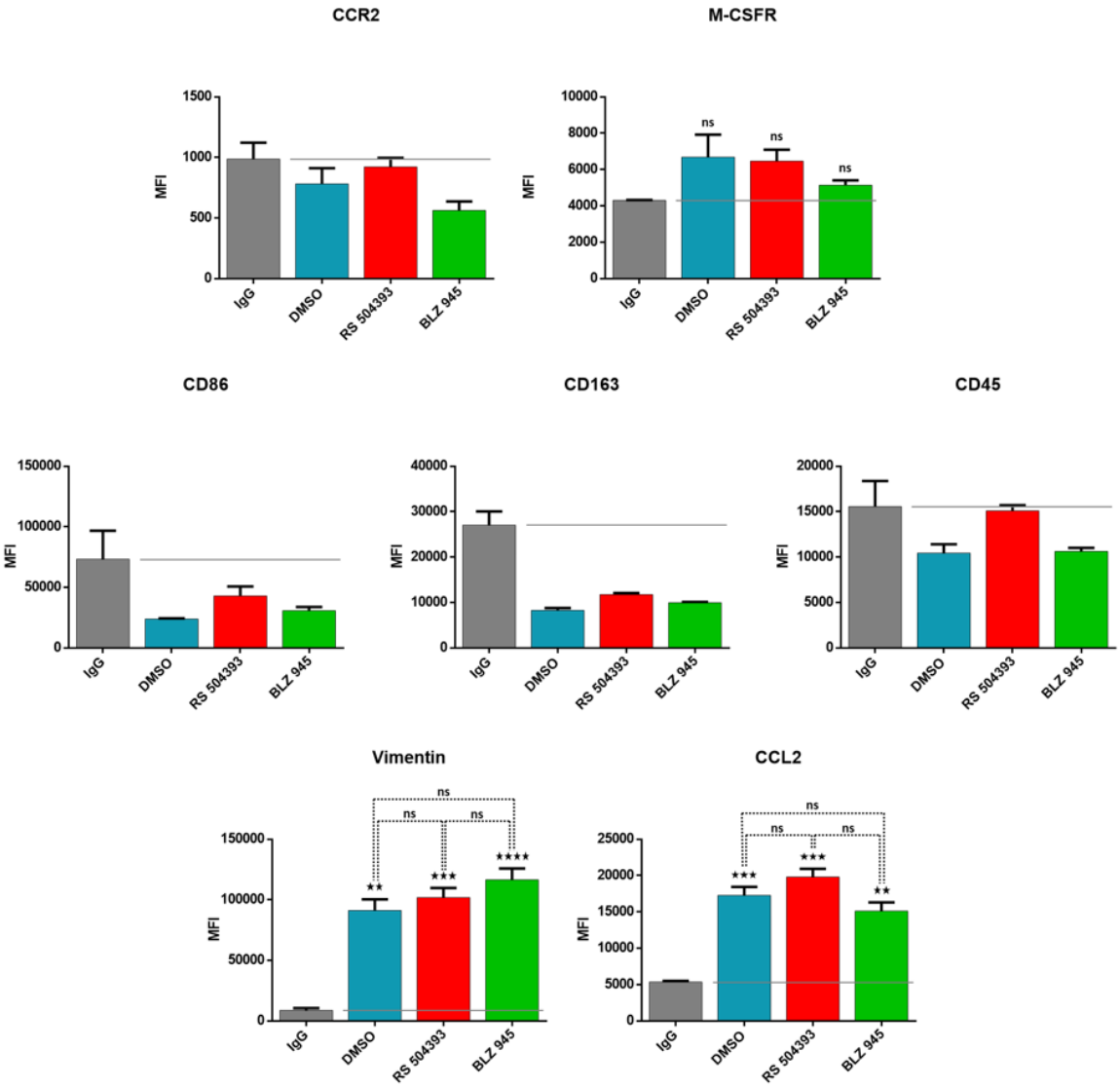

Figure 28: Effects of RS 504393 and BLZ 945 on specific markers in 3D cocultured CAFs analyzed by flow cytometry.

CAFs and macrophages (300.000 cells each per gel) were cocultured in 3D collagen type 1 gels and treated with either DMSO (control, blue), the CCR2 small molecule inhibitor RS 504393 (2 µM, red) or the M-CSFR small molecule inhibitor BLZ 945 (1 µM, green) for 6 days (media and factor refresh all 48 hours). Each bar represents MFI of gated CAFs from combined gel replicates (at least 3, for individual data see **Supplementary Figure 2 and 5**). Mean MFI of unstained- and IgG-controls was taken as reference for expression evaluation and is illustrated as gray horizontal line among samples. Error bars indicate the standard error of mean (SEM) and relevant significances are illustrated by stars while non-significant comparisons are labeled with ns. Significance results directly clipped to the error bar account for MFI differences between treatments and IgG control, presupposed being significantly higher. For P-values see **Supplementary Table 8**. The ligand CCL2; CCR2 as receptor for CCL2; M-CSFR as receptor for M-CSF; CD86 as monocyte/macrophage marker; CD163 as specific marker for M2-like macrophages; CD45 as marker for the hematopoietic lineage and Vimentin as mesenchymal cell marker were detected by following conjugated antibodies: CCL2/PE; CCR2/APC; M-CSFR/PE; CD163/PerCP7Cy5.5; CD45/Alexa Fluor 488 and Vimentin/Alexa Fluor. *N*(IgG):27.630; *N*(DMSO): 23.154; *N*(RS 504393): 29.712; *N*(BLZ 945): 66.805. *N* = gated singlets.

might change CCL2 expression in the cocultures. For better detectability of CCL2 the cells int the gels were pretreated with Brefeldin A for four hours prior to flow cytometry analysis. By

this, the Golgi apparatus-mediated export of proteins is inhibited and leads to accumulation of cytokines and chemokines inside of the cell (Alvarez and Sztul, 1999), which then are better detectable in flow cytometry.

Cells were gated according to our established protocol, first discriminating against dead cells by Zombie NIR Fixable Viability Kit, then gating out debris and separating singlets. CAFs were separated from macrophages by CD45/Alexa Fluor 488 – only the latter express CD45.

We detected highly significant expression of Vimentin (P(DMSO) = 0,0012; P(RS 504393) = 0,0003; P(BLZ 945) = < 0,0001) among all three treatments in CAFs, with no significant differences in between the groups. Also, we found essential levels of CCL2 expression (P(DMSO) = 0,0009; P(RS 504393) = 0,0003; P(BLZ 945) = 0,003) in all groups – again with no significant differences. CCR2, M-CSFR, CD86, CD163 and CD45 are not unexpressed under any conditions, as expected (**Figure 28**).

In macrophages, CCR2 expression (P = 0,0039) was increased to significant levels under CCR2 inhibitor treatment. Interestingly, CCR2 levels dropped to undetectable levels (equaling the IgG controls) in M-CSFR inhibitor treated cells. Similarly, also M-CSFR expression was substantially reduced in the myeloid cells as compared to controls (P = < 0,0001), when it's signaling was inhibited in the co-cultures. In contrast, CCR2 inhibition displayed no inhibitory effect on M-CRF levels in the macrophages. CD86 expression was low to undetectable compared to IgG control. In line with previous results, the M2-like macrophage marker CD163 was expressed in the myeloid cells in DMSO controls (P = 0,0025). CCR2 inhibition had no effect on CD163 expression in macrophages, whereas it was significantly reduced to IgG control levels under BLZ 945 treatment (P = < 0,0001), implicating total loss of CD163 expression. Vimentin (P(DMSO) = 0,0003; P(RS 504393) = 0,0024; P(BLZ 945) = 0,004) and CD45 (P(DMSO) = < 0,0001; P(RS 504393) = < 0,0001; P(BLZ 945) = 0,0008) were highly expressed in all groups, however, interestingly CD45 levels also dropped under M-CSFR inhibitor conditions. Most importantly, high CCL2 expression in macrophages (P = 0,0294) could be detected in DMSO treated CAF-myeloid cell co-cultures, validating our previous findings. This high CCL2 expression was substantially increased (P = < 0,0001) when the gels were treated with the CCR2 inhibitor, and was significantly decreased (P = 0,0251) to low levels equaling IgG controls when M-CSFR signaling was inhibited (**Figure 29**).

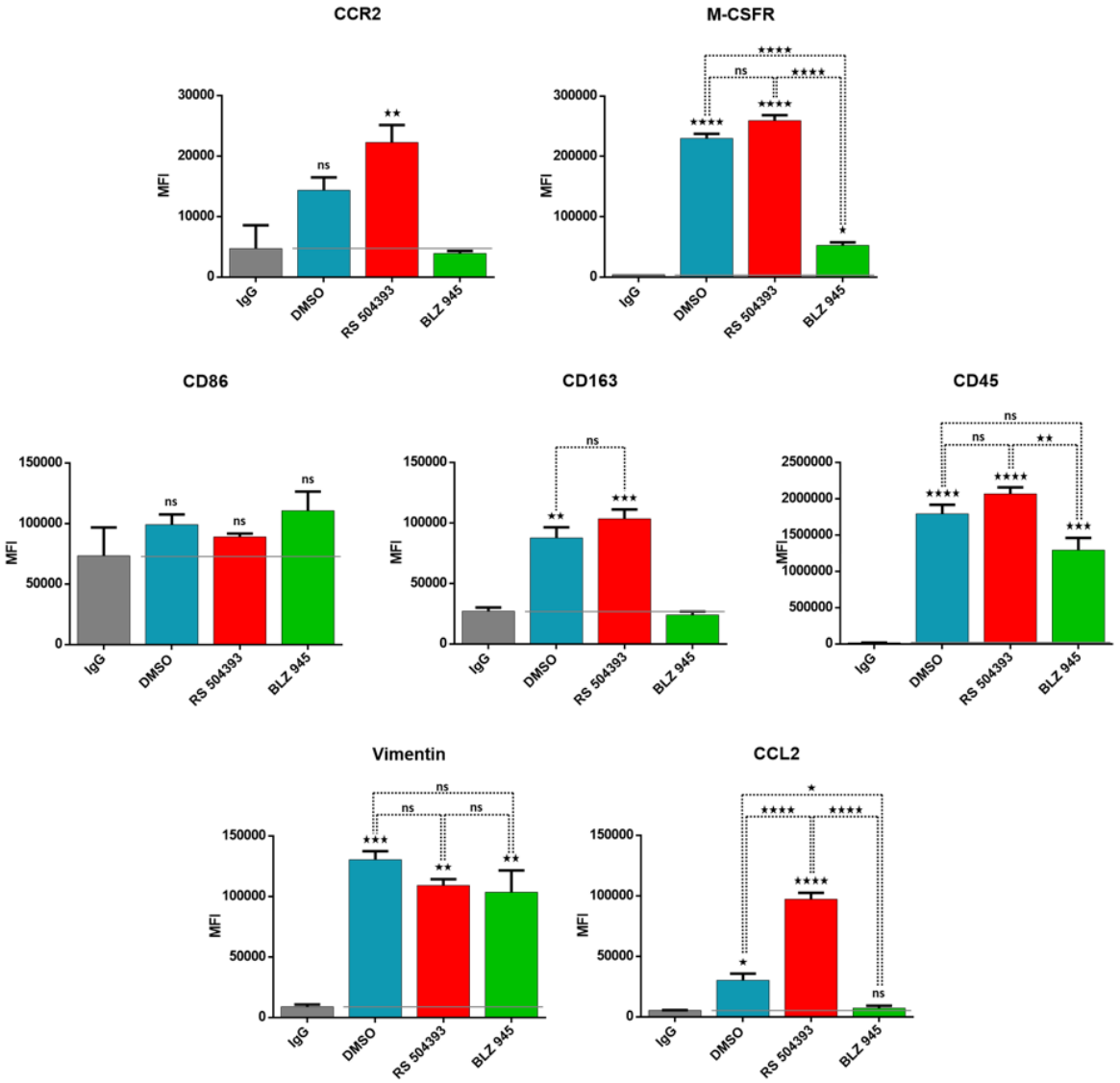

Figure 29: Effects of RS 504393 and BLZ 945 on specific markers in 3D cocultured macrophages analyzed by flow cytometry.

CAFs and macrophages (300.000 cells each per gel) were cocultured in 3D collagen type 1 gels and treated with either DMSO (control, blue), CCR2 small molecule inhibitor RS 504393 (2 µM, red) or M-CSFR small molecule inhibitor BLZ 945 (1 µM, green) for 6 days (media and factor refresh all 48 hours). Each bar represents MFI of gated macrophages from combined gel replicates (at least 3, for individual data see **Supplementary Figure 2 and 6**). Mean MFI of unstained- and IgG-controls was taken as reference for expression evaluation and is illustrated as gray horizontal line among samples. Error bars indicate the Standard Error of Mean (SEM) and relevant significances are illustrated by stars while non-significant comparisons are labeled with ns. Significance results directly clipped to the error bar account for MFI differences between treatments and IgG control, presupposed being significantly higher. For P-values see **Supplementary Table 9**. The ligand CCL2; CCR2 as receptor for CCL2; M-CSFR as receptor for M-CSF; CD86 as monocyte/macrophage marker; CD163 as specific marker for M2-like macrophages; CD45 as marker for the hematopoietic lineage and Vimentin as mesenchymal cell marker were detected by following conjugated antibodies: CCL2/PE; CCR2/APC; M-CSFR/PE; CD163/PerCP7Cy5.5; CD45/Alexa Fluor 488 and Vimentin/Alexa Fluor. *N*(IgG):27.630; *N*(DMSO): 23.154; *N*(RS 504393): 29.712; *N*(BLZ 945): 66.805. *N* = gated singlets.

3.3.3. Effects of small molecule inhibitors RS 504393 and BLZ 945 on phenotype

During cultivation we checked the cell phenotypes and appearance of gels with phase contrast microscopy. It is of importance to note that making focused and clear shots of 3D collagen gels

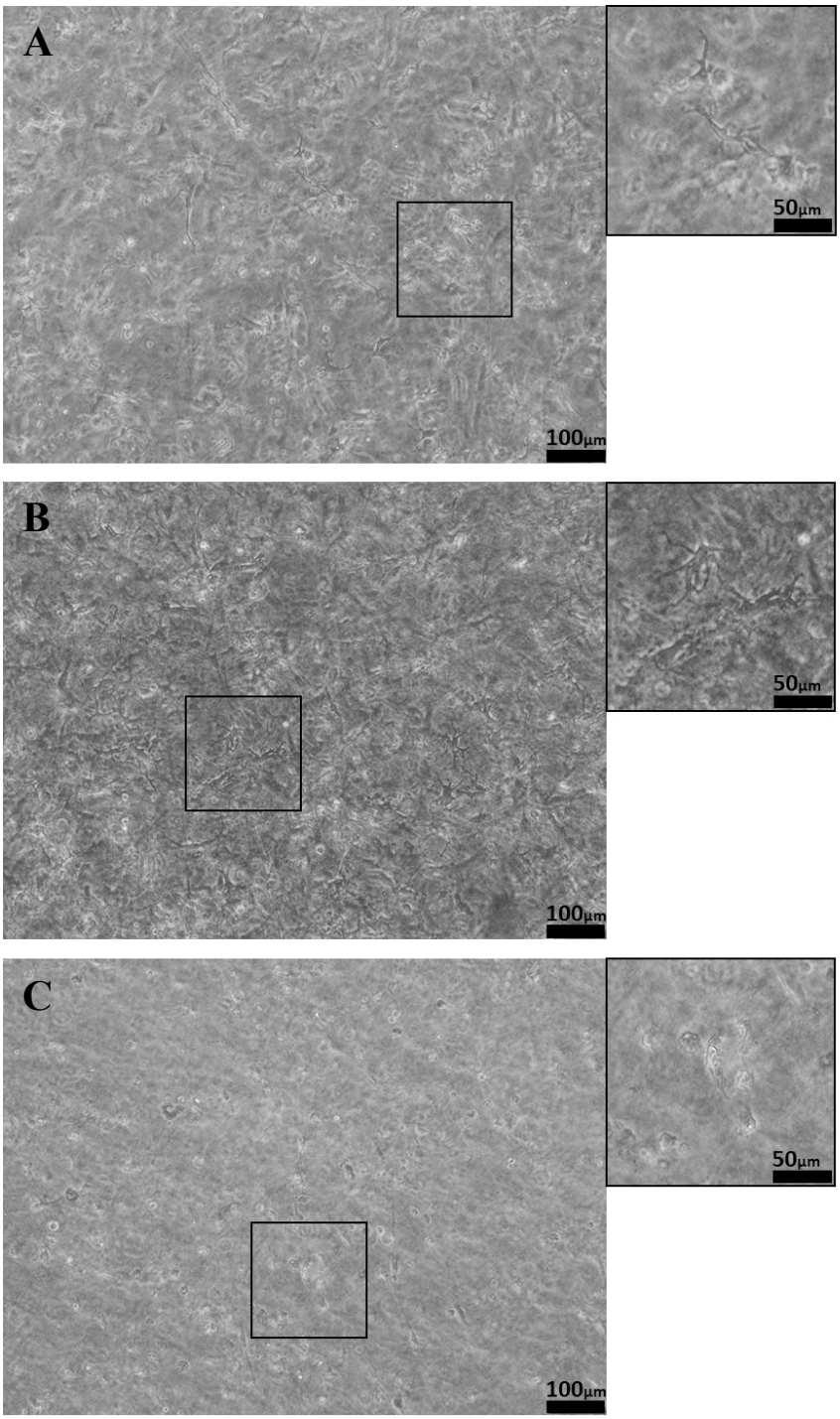

Figure 30: Effects of small molecule inhibitors RS 504393 and BLZ 945 on phenotype of 3D coculture gels. **A,B,C** visualize representative cell and gel appearance under Olympus IX51 light microscope at 10x magnification. Images of gels were captured every 48 hours for 6 days. In this case, the last time point at 144 hours is shown for all conditions: **A** DMSO control; **B** CCR2 small molecule inhibitor RS 504393; **C** M-CSFR small molecule inhibitor BLZ 945. Black-framed images show zoomed in regions with interwoven CAFs and macrophages.

with a light microscope – light needs to pass through certain thickness and density of material – is not trivial.

Figure 30 illustrates the visual appearance of gels after 144 hours. RS 504393 treatment results in darkest collagen gel appearance and higher cell density with a more sellate like appearance of the cells (**Figure 30 B**). In contrast, BLZ 945 treatment results in brighter appearing gels with less and more roundup phenotype. This indicated that also at the cell phenotype level clear different response were detectable.

3.4. *In vivo* Confocal Laser Scanning Microscopy (CLSM) analysis of CCL2 expression in healthy and tumor FFPE samples

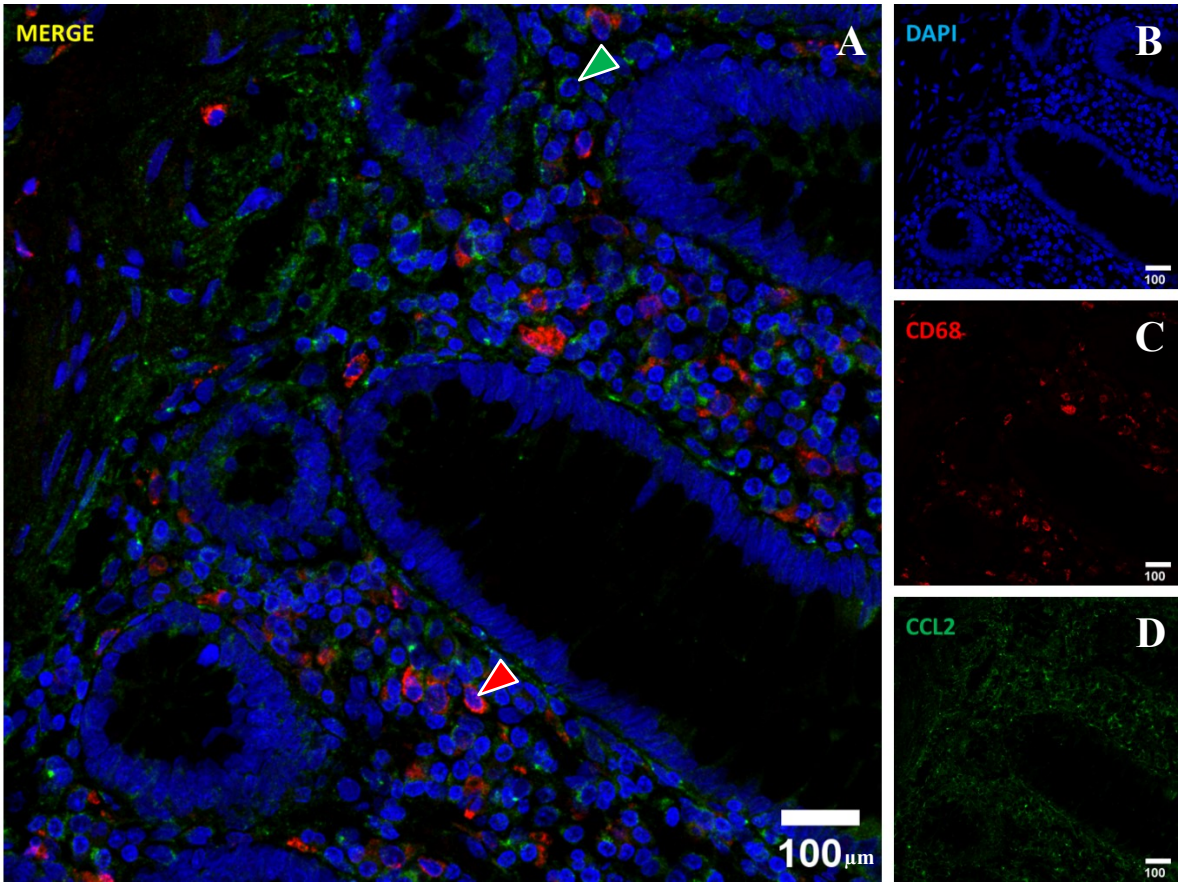

Figure 31: CLSM maximum projection image of healthy colon sample.
A Merged image of representative healthy colon FFPE section (4 µm). The right part of the image shows two crypts cut longitudinally. The red arrowhead points to a representative CD68 positive macrophage, the green arrowhead at a CCL2 expressing fibroblast. **B** Cell nuclei were stained with DAPI. **C** Moderate macrophage infiltration stained with conjugated CD68-Alexa Fluor 546 (1:500) and **D** CCL2 expression with CCL2-Alexa Fluor 647 (1:500). Ten optical sections in 3 µm stack size were maximum projected and analyzed.

To complement the previous *in vitro* findings that both CAFs and myeloid cells express significant amounts of CCL2 in the tumor stroma by further *in vivo* analysis, we performed a

CLSM analysis of patient material to detect CCL2 in certain cell types. For this, we received FFPE material of five CRC patients from the Pathology Institute of the Medical University of Vienna in cooperation with the Department of Surgery (Prof. Rudolf Oehler). Patient matched healthy as well as tumor samples were available. Microtome sections were stained for macrophage marker CD68-Alexa Fluor 546 and CCL2-Alexa Fluor 647.

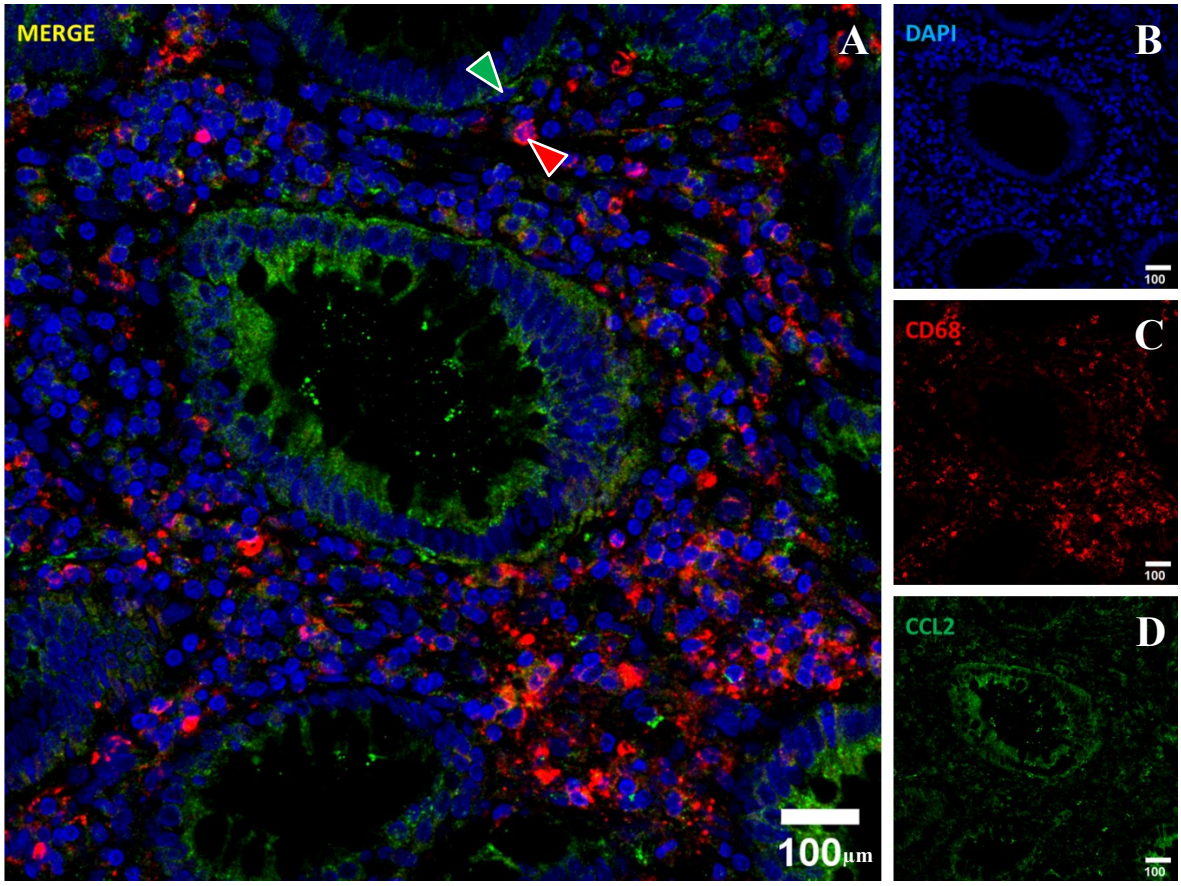

Figure 32: CLSM maximum projection image of tumor colon sample.
A Merged image of representative tumor colon FFPE section (4 µm). The red arrowhead points at a representative CD68 positive macrophage, the green arrowhead at a CCL2 expressing fibroblast. **B** Cell nuclei were stained with DAPI. **C** Substantial macrophage infiltration marked with conjugated CD68-Alexa Fluor 546 (1:500) and **D** CCL2 expression with CCL2-Alexa Fluor 647 (1:500). Ten optical sections in 3 µm stack size were maximum projected and analyzed.

Healthy colonic crypts sectioned perpendicularly and longitudinally are depicted in **Figure 31**. Cell nuclei were stained with DAPI, macrophages were stained for CD68 and are especially visible in close vicinity to crypts. CCL2 ubiquitously occurs in and around the cells. The corresponding tumor sample (**Figure 32**) shows less organized tissue structure. Macrophage infiltration appears at larger extent and CCL2 levels seem elevated. The staining in the tumor epithelial cells is background as it appeared similarly in the IgG controls, whereas stromal parts were clearly negative in the IgG controls.

3.4.1. Expression level dependent categorization of fibroblasts and macrophages

Previous *in vitro* experiments showed CCL2 expression of CAFs and macrophages in 3D cell culture models. With the following experiments we wanted to investigate, if this also applies for human patient samples *in vivo*.

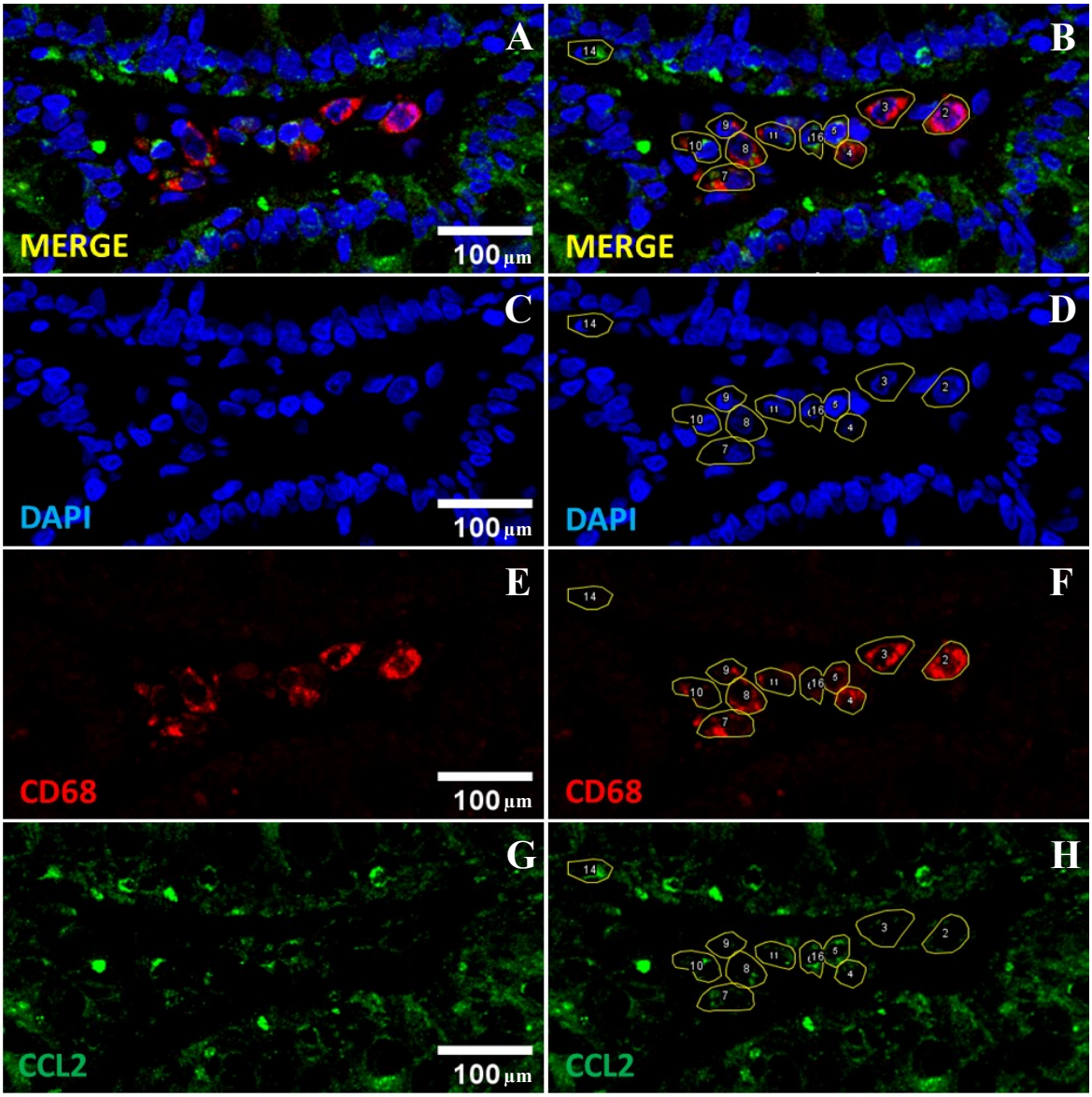

Figure 33: CLSM maximum projection image of selected macrophages and fibroblasts in healthy colon sample.

A,B show merged tissue sample. **C,D** Cell nuclei were stained with DAPI, **E,F** macrophages with primary antibody to CD68 and **G,H** CCL2 with primary antibody to CCL2. **B,D,F,H** are replicates of **A,C,E,F** depicting several cells of interest. Cell 14 shows CCL2 expression and is a representative example for fibroblasts. Cells 2, 3, 6 and 10 are infiltrating macrophages with high CD68 expression. For corresponding color histograms see (**Figure 34**).

After visual selection (**Figure 33**), of CAFs ($CCL2^{+}/CD68^{-}$) and macrophages ($CD68^{+}$) among all patient sample maximum projections further color histogram analysis revealed cell specific expression levels of CCL2 and CD68 (**Figure 34**). By closer analysis three different patterns could be identified. Cells with high red (CD68) intensity and low to absent green (CCL2), cells with high green and low to absent red staining and cells which were simultaneously positive

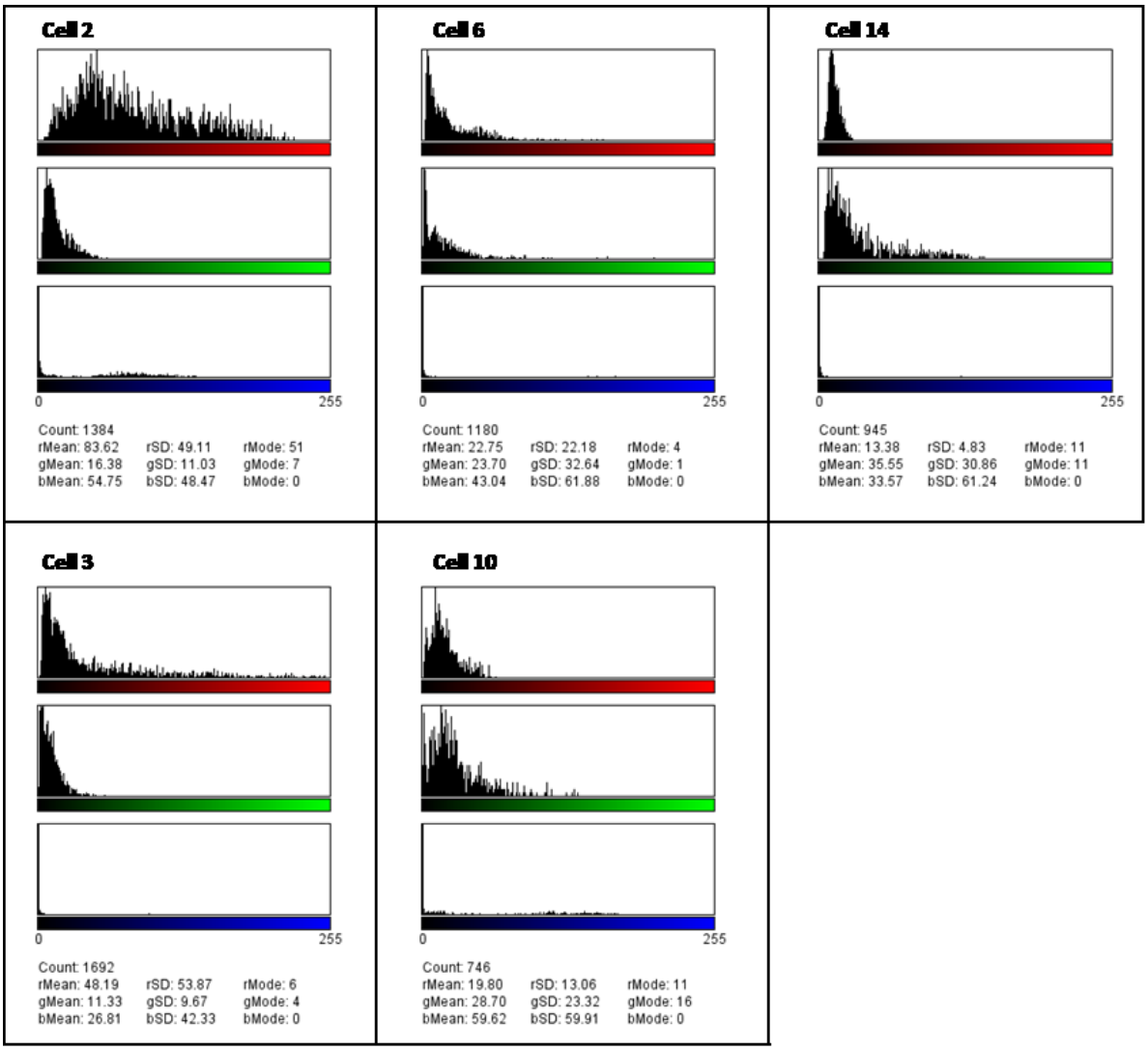

Figure 34: Color histograms of selected macrophages and fibroblast.
Color histograms and therefrom derived means with standard deviations were calculated for DAPI, CD68 and CCL2 of all selected cells of interest. Images were processed with ImageJ software in 8-bit format with linear scaling from min-max to 0-255 for all three channels. Five representative cells are depicted (see **Figure 33**). **Cells 2 and 3** represent macrophages with CD68 expression and no CCL2 expression. **Cells 6 and 10** represent macrophages with CCL2 expression. **Cell 14** shows a representative fibroblast with high levels of CCL2.

for red and green. We considered these cells as CCL2 expressing macrophages, whereas green cells alone were assigned as CCL2 expressing CAFs. Red cells with low to absent green fluorescence signals are macrophages without obvious CCL2 expression. We consequently categorized the cells depending on their CD68/CCL2 ratio as follows:

Fibroblasts expressing CCL2:	**[(CD68/CCL2) ≤ 0.5]**
Macrophages expressing CCL2:	**[0.5 ≤ (CD68/CCL2) ≤ 2.0]**
Macrophages devoid of CCL2:	**[(CD68/CCL2) ≥ 2.0]**

3.4.2. CCL2-expressing fibroblasts and macrophages in healthy and in tumor tissue

The analysis of 346 cells among healthy and tumor FFPE samples of 5 CRC patients (**Supplementary Figure 7,4,5,6,7,8**) revealed, according to our previous classification, the existence of CCL2 expressing fibroblasts and macrophages in both healthy and tumor tissue samples. Moreover, macrophages devoid of CCL2 were also identified in normal and tumor samples.

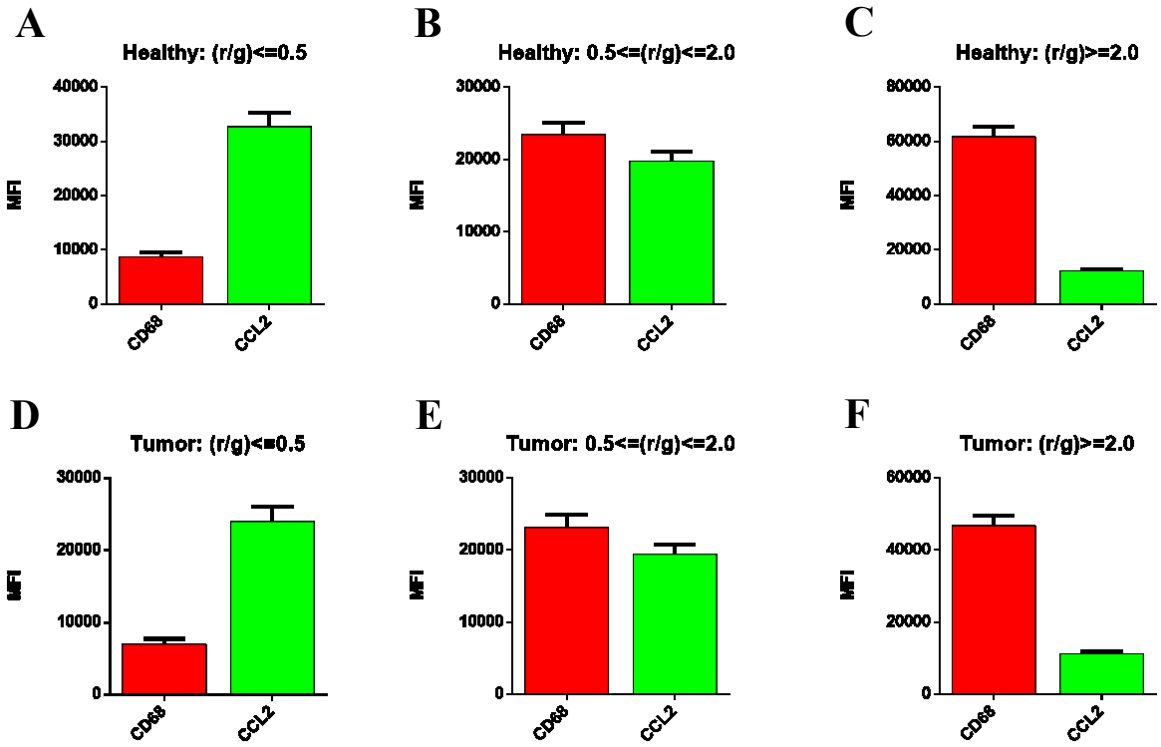

Figure 35: Mean expression levels of categorized fibroblasts and macrophages.
A total of 346 cells **(Supplementary Figure 7,8,9,10,11,12**) were analyzed and categorized as follows: Fibroblasts expressing CCL2: [(CD68/CCL2) ≤ 0.5]; Macrophages expressing CCL2: [0.5 ≤ (CD68/CCL2) ≤ 2.0]; Macrophages expressing no CCL2: [(CD68/CCL2) ≥ 2.0]. **A,B,C** show MFI means of macrophage marker CD68 (red) and CCL2 expression (green) in healthy FFPE samples of 5 patients, **D,E,F** in tumor samples. Analysis of healthy samples yielded **A** 31 CCL2 expressing fibroblasts (MFI-CD68 = 8.720; MFI-CCL2 = 32.652), **B** 49 CCL2 expressing macrophages (MFI-CD68 = 23.427; MFI-CCL2 = 19.768) and **C** 72 macrophages expressing no CCL2 (MFI-CD68 = 61.672; MFI-CCL2 = 12.283). Analysis of tumor samples showed **D** 39 CCL2 expressing fibroblasts (MFI-CD68 = 6.914; MFI-CCL2 = 23.908), **E** 59 CCL2 expressing macrophages (MFI-CD68 = 23.099; MFI-CCL2 = 19.431) and **F** 96 macrophages expressing no CCL2 (MFI-CD68 = 46.733; MFI-CCL2 = 11.252).

Based on this analysis, fibroblasts show higher CCL2 expression MFI than macrophages – healthy fibroblasts accounting for more than tumor fibroblasts (**Figure 35 A,D**). CCL2 expressing macrophages have similar CD68 expression and CCL2 production when comparing healthy with tumor (**Figure 35 B,E**). In healthy tissue, macrophages without CCL2 expression seem to have higher CD68 expression compared to tumor macrophages (**Figure 35 C,F**). However, these semiquantitative results need further validation by more accurate quantitative methods such as flow cytometric analysis of digested fresh patient tissue samples. Taken together, these results clearly demonstrate that CCL2 expressing myeloid cells co-exist with CCL2 expressing fibroblasts in the normal stroma as well as in the tumor microenvironment of human CRC.

4. Discussion

Worldwide, colorectal cancer ranks among the top three cancer types in terms of incidence and mortality, making it prone for research (Bray *et al.*, 2018). In the past, environmental lifestyle factors – such as alcohol consumption, physical inactivity or obesity – but also major mutated genes (APC, KRAS, TP53) have been identified as crucial influences on CRC development and progression (Kuipers *et al*., 2015).

Tumor progression is highly dependent on the interaction with the surrounding tumor stroma – also referred to as tumor microenvironment. The two major cell types present in the stroma are cancer-associated fibroblasts (CAFs) and tumor-associated macrophages (TAMs). The latter are permanently recruited and regulated by soluble chemo-attractants (Peddareddigari, Wang and Dubois, 2010) which interact in highly dynamic and complex networks.

Earlier experiments in our lab suggested CCL2 and M-CSF as major factors in our hypothesis that CAFs instruct recruited monocytes to differentiate and polarize towards M2-like phenotype, which is characterized by creating a rather immunosuppressive environment. The colon is unique in terms of TAM-recruitment dynamics, as its high self-renewal rate and ongoing confrontation with microbes and pathogens requires continuous recruitment (Round and Mazmanian, 2009; Smith *et al.*, 2011; Peterson and Artis, 2014). CCL2 is one of the most studied chemokines and has been associated with progression of many cancer types. Still, its role in colorectal cancer remains elusive. With this work we are trying to contribute to a better understanding of its regulation.

Here, we first investigated the roles of CCL2/CCR2 and M-CSF/M-CSFR signaling in the communication of CAFs with myeloid cells in 2D and 3D *in vitro* cell culture settings. The source of CCL2 in CRC still remains debated, often it is introduced as tumor derived factor, which implicates that the tumor stroma is also a possible contributor. In recent work we have shown that secretion of the soluble factor CCL2 was induced in colonic CAFs and macrophages in 3D coculture systems (Pudelko, 2016). To be able to react to CCL2 signaling, cells must express the corresponding receptor CCR2. With our first set of 2D monoculture experiments we provide evidence that CAFs and PBMC-derived monocyte and lymphocyte fractions significantly express CCR2. However, expression levels of CAFs and lymphocytes appear marginal compared to monocytes. High expression of both splicing variants of CCR2 (CCR2A and B) in monocytes were also reported by others (Lim *et al.*, 2016). Indeed, the conjugated antibody used in this study is supposed to target both variants. In the future, it would be

interesting to more specifically analyze the expression of CCR2A or CCR2B and individually target these receptors.

Of note, we differentiated and polarized PBMC-derived monocytes into either of the two distinct M1- or M2-like macrophage phenotypes. Surprisingly, none of them did express CCR2 in our 2D experiments, despite the fact, that the myeloid fraction of the PBMC input cells express high levels of the receptors. Thus, we conclude that under these culture conditions CCR2 expression is lost independent of the polarization status of the cells.

Our analysis further revealed that HCT116 colon cancer cells were CCR2-negative. In opposition to this finding, other colon cancer cell lines such as KM12C and KM12SM have been shown to express CCR2 (Torres *et al.*, 2013), suggesting differences due to heterogeneity in epithelial tumor cells. Hence, further analysis is needed to clarify whether the majority of epithelial CRC cells or only a minority express CCR2. This might have an impact on the response of CRC to CCR2 inhibition in clinical trials.

M-CSFR was, as expected, expressed in CAFs, HCT116 cells, monocytes and at very low levels also in lymphocytes. We thus concluded, that CAFs and monocytes should be able to respond to both CCL2 and M-CSF signaling.

Before we moved on to 3D culture methods, we wanted to check the expression of selected markers in established *in vitro* models for M1-like and M2-like macrophages by multicolor flow cytometry. Therefore, we employed a widely accepted differentiation and polarization protocol for PBMC derived monocytes. Indeed, CD163, which is commonly accepted as M2-like macrophage marker (Tommelein *et al.*, 2015), and CD14 was highly expressed in our M2-like macrophages only. We also compared expression of the hematopoietic cell marker CD45, the human monocyte and macrophage markers CD68 and CD86 which is expressed by antigen-presenting cells. They were all highly expressed in both types of polarization, however M1-like macrophages clearly displayed increased expression of these markers compared to M2-like macrophages. This might support the believed immune-stimulating roles of M1-like macrophages, as CD45 and CD86 have been shown to play roles in T cell activation (Janeway, 1992; Gool *et al.*, 1996).

Since we showed that CAFs monocultured in 2D and monocytes express CCR2 as well as M-CSFR, we further investigated their interactions in a more complex 3D collagen type 1 gel setups. Moreover, we interfered signaling with two small molecule inhibitors: RS 504393 (targeting CCR2) or BLZ 945 (inactivating M-CSFR). 3D culture methods have been shown to closer mimic physiological *in vivo* situations as they provide more spatial and architectural

complex environment than 2D methods (Kramer *et al.*, 2013; Unger *et al.*, 2014; Stadler *et al.*, 2015). Also, they enable modular ways of investigating cell-cell interactions by either mono- or coculturing multiple cell types of interest. Hence, we mono- or cocultured CAFs or/and M-CSF-derived macrophages, which have been described as rather immunosuppressive alternatively activated M2-like cells (Martinez *et al.*, 2006; Svensson *et al.*, 2011), and compared the effects of the above mentioned inhibitors to DMSO controls.

Surprisingly, monocultured CAFs in the collagen gels did not express CCR2 or M-CSFR – as we previously showed in our 2D experiments – in neither of the three conditions. At this point it is important to mention, that defining positivity during flow cytometry is not trivial. Proper controls are essential for evaluating expression of specific markers. We controlled our results with unstimulated controls, unstained controls, application of compensation matrices and IgG controls. The latter are limited in a way that isotype controls may not match the test antibody for background staining (Maecker and Trotter, 2006). We are aware that some researchers even renounce IgG controls for this reason. Nevertheless, we tried to find the best way in our context and decided to control with the mean of taken together unstained and IgG controls. Indeed, MFIs are clearly lower for CCR2 and M-CSFR in 3D monocultured CAFs compared to 2D ones. However, 3D cocultured CAFs recapitulated findings from 3D monocultured CAFs, suggesting that CAFs in 3D seem to lose the very low receptor expression. Thus, they are highly likely not responsive to CCL2 or M-CSF signaling through intrinsic receptor expression. At least for CCL2 we can exclude an autocrine effect. Further experiments should additionally address the expression of M-CSF. On the other hand, we could reveal similarly high CCL2 expression levels among all three conditions. First, this is supporting our current hypothesis of CAFs acting on monocytes by CCL2 mediated signaling in a paracrine manner. Second, the fact that neither CCL2 expression nor vimentin expression is altered in CAFs upon CCR2 or M-CSFR inhibition also is a hint that the receptors are not present on CAFs.

As expected, macrophages displayed high CD45 expression among all groups in both 3D mono- and coculture. Interestingly, BLZ 945 treated cocultured macrophages showed significantly lower levels compared to DMSO control and RS 504393 condition, suggesting loss of macrophage-specific features. This was strengthened by the complete loss of M2-like macrophage marker CD163 under BLZ 945 treatment compared to the high expression levels in DMSO and RS 504393 treated cells. Interestingly, these macrophages devoid of M-CSFR signaling also showed deficiency in CCL2 and CCR2 expression and considerably lower M-CSFR expression. This means that, M-CSF produced by CAFs (previous findings strongly support the notion that M-CSF is efficiently produced by CAFs) is a major regulator of the

macrophage phenotype. Loss of M-CSF/M-CSFR signaling in the macrophages obviously shuts down endogenous M-CSFR, CCR2 and CCL2 expression. It cannot be ruled out that the continuous treatment with the inhibitor induces another polarization state in the macrophages, which is characterized by low M-CSFR/CCL2/CCR2 expression. Obviously, macrophages and CAFs do generally not react with M-CSFR upregulation in case of BLZ 945 inhibition to compensate for the inactivation of the receptor. In contrast, when inhibiting 3D mono- or cocultured macrophages with the CCR2 small molecule inhibitor RS 504393 they clearly induce its expression to obviously compensate for less signaling strength. In line with this, CCL2 expression levels are also substantially induced in the myeloid cells under CCR2 inhibitor treatment. This suggests a tight regulation of CCL2/CCR2 signaling and a potential feedback mechanism to respond to decreased CCL2 levels or CCR2 signaling strength. In case of low CCL2 and or low CCR2 signaling, both the ligand and the receptor in the cells are upregulated. Of note, this might - at least in part – explain the failure of CCL2/CCR2 blockers to induce clinical response in human cancer patients (Galdiero, Marone and Mantovani, 2018). Indeed, both elevated CCL2 as well as upregulation of CCR2 have been reported. Thus, we might have identified the cellular source of CCL2 in CRC to be mainly the macrophages and a possible explanation of the mechanism of therapy resistance. At this point it would be also interesting to additionally block alternative CCL2 signaling by also inhibiting CCR4, which has also been reported to bind CCL2 (Zhang *et al.*, 2006; Françoise Bachelerie *et al.*, 2014).

In addition to quantitative flow cytometry analysis we made a qualitative analysis of light microscopy images of treated gels. Interestingly, gels treated with CCR2 small molecule inhibitor RS 504393 looked denser. Also, cells stretched out more and seemed to like the environment more than in BLZ 945 treated gels. We speculate, that maybe ECM production by CAFs is altered, as RS 504393 gels showed more M2-like macrophages, which are known for production of CAF promoting IL-4. Future experiments should investigate the M-CSF expression levels in this context. In tumors, M-CSF has been reported to contribute to M2-like polarization of macrophages (Erreni, Mantovani and Allavena, 2011). Generally, it seems to us that blocking CCR2 seems to cause an adverse effect of promoting an immunosuppressive environment with growing outstretching cells. Of note, even though RS 504393 treated gels appear substantially denser than BLZ945 treated gels, flow cytometry data revealed more than twice as many analyzed singlets for the former. A reason for that might be stronger clumping of large outstretching cells during flow cytometry preparation, which could then further lead to more cells remaining in the cell strainer. These larger cells might be CD163 positive M2-like

macrophages resulting from elevated CCL2 levels produced by macrophages and CAFs in autocrine or paracrine manner.

With our second aim, the *in vivo* analysis of colon cancer patient material, we could provide further evidence supporting our hypothesis of macrophage recruitment by CAF-derived mechanisms. We found several CCL2 expressing fibroblasts and CCL2 expressing macrophages in both healthy and tumor samples. We did not quantify data in terms of cells occurring per area of analyzed material. However, we found more cells among all three categories – CCL2 expressing fibroblasts, CCL2 expressing macrophages, macrophages without CCL2 expression – in tumor samples. This would be in line with earlier findings showing an accumulation of a CCL2-expressing variety of cells such as infiltrating macrophages at tumor sites (Deshmane *et al.*, 2009; Peddareddigari, Wang and Dubois, 2010; Komohara *et al.*, 2016).

From a technical point of view, we established a working multicolor flow cytometry protocol enabling readouts of cells digested out of previous 3D culture systems. Our side experiment with Zombie^{NIR} Fixable Viability Kit, which was supposed to re-evaluate the accuracy of dead cell discrimination, showed, that proper controls and preparation are absolutely crucial for later analysis. We show, that even established and widely used dyes show unwanted effects such as staining also alive cells. This must be taken into account, as shifting signals otherwise might be interpreted as false positive results.

In conclusion, we established a multicolor flow cytometry protocol suitable for accurate readouts of multiple 3D cocultured cell types. We provide further evidence supporting roles of CCL2/CCR2 signaling in the crosstalk between CAFs and macrophages – and an essential involvement of M-CSF/M-CSFR signaling. CAFs alone generally did not respond to neither the RS 504393 nor the BLZ 945 inhibitor. Why artificially polarized M1- and M2-like macrophages did not show CCR2 expression in 2D remains as open question. Maybe dose or the combination of factors are not perfectly matched yet.

Importantly, we could show substantial levels of CCL2 expression in fibroblasts and in CAFs *in vitro* and *in vivo*. Thus, we first of all validated previous findings in our lab, secondly, we extended our knowledge on the involvement of CCR2 and/or M-CSFR signaling in CRC, and third we could highlight in vivo relevance in humans by demonstrating CCL2 expression in macrophages and CAFs in CRC samples. We contribute to the understanding of CCL2 and M-CSF signaling by excluding a possible autocrine effect in CAFs, and rather encouraging paracrine mechanisms. Moreover, we suggest CCL2/CCR2 signaling interference via the M-

CSF/M-CSFR pathway by BLZ 945 as its treatment resulted in loss of CCL2 and CCR2 expression, downregulation of M-CSFR and loss of immunosuppressive CD163-positive M2-like macrophages. Similar effects of BLZ 945 were recently shown in animal studies (Pyonteck *et al.*, 2013; Pathria, Louis and Varner, 2019). In line with other groups (Bonapace *et al.*, 2014; Galdiero, Marone and Mantovani, 2018), direct interference of CCL2/CCR2 axis by RS 504393 showed adverse effects in terms of overcompensated CCR2, CCL2 and M-CSFR expression and increases in immunosuppressive M2-like macrophage polarization. Future research needs to be performed to functionally test the impact of these CAF-educated macrophages on T cell phenotypes and possible immunomodulatory effects. Furthermore, the T cell response will also be monitored in the educated macrophages treated with MCSFR or CCR2 inhibitors.

5. Supplementary

5.1. Supplementary figures

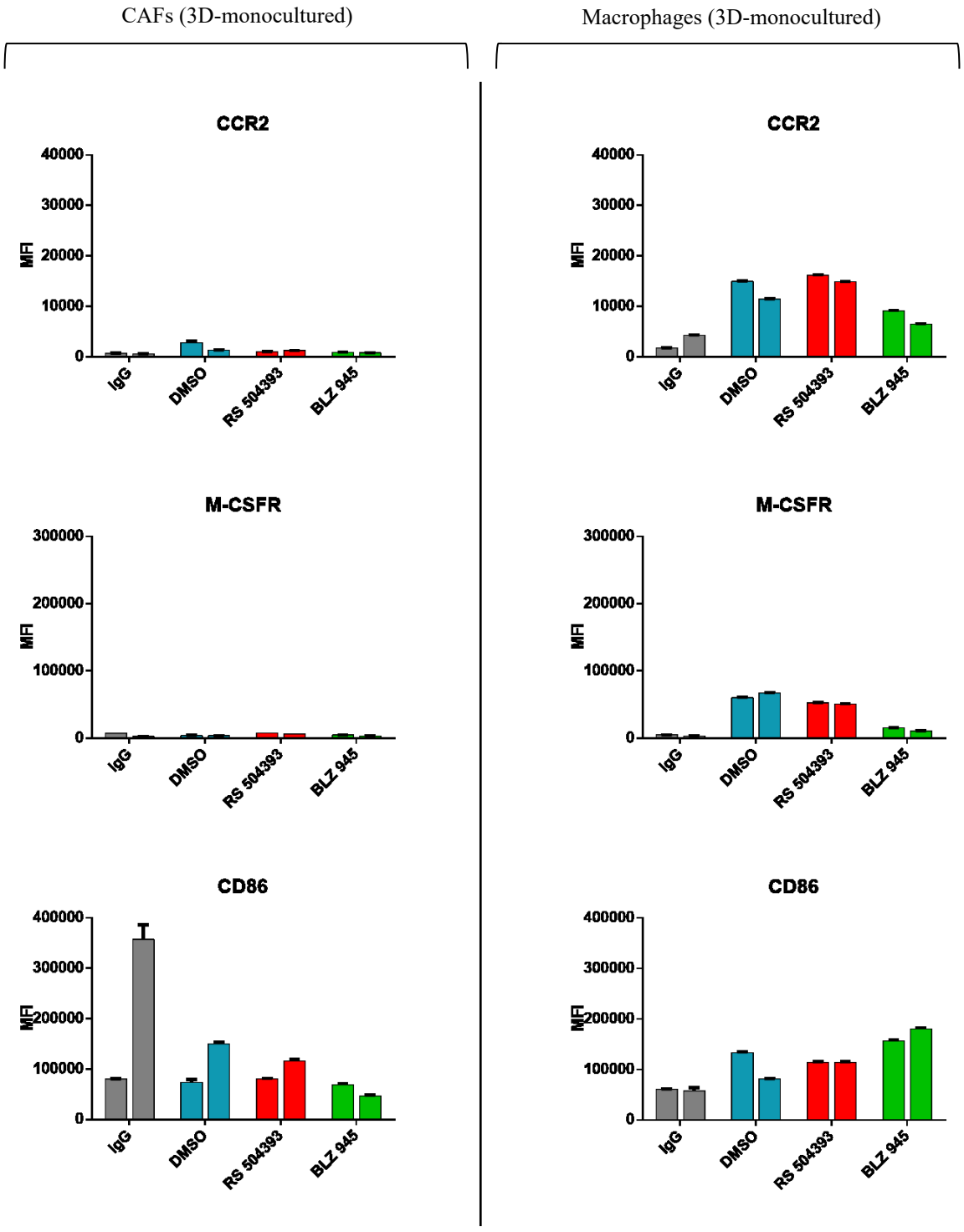

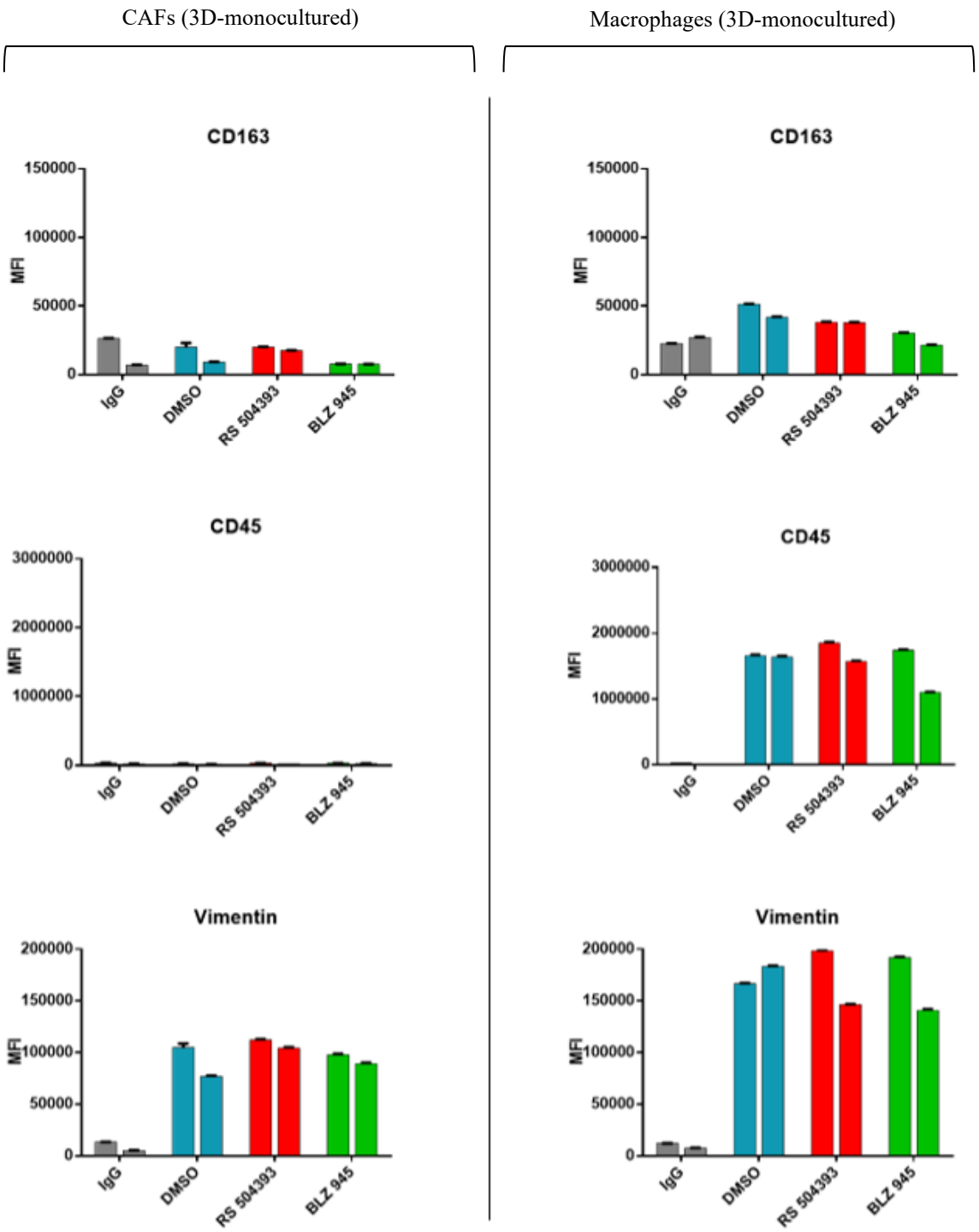

Supplementary Figure 1: Quantified flow cytometry data of individual CAF or macrophage gels treated with RS 504393 and BLZ 945 which were summarized in Figure 26 and 27.

CAFs or macrophages (300.000 cells per gel) were monocultured in 3D collagen type 1 gels and treated with either DMSO(control, blue), CCR2 small molecule inhibitor RS 504393 (2 µM, red) or M-CSFR small molecule inhibitor BLZ 945 (1 µM, green) for 6 days (media and factor refresh all 48 hours). Each bar represents MFI of cells digested out of one gel. Two replicates per setting. IgG control was conducted with cells digested out of DMSO treated gels. Error bars indicate the standard error of mean (SEM). CCR2 as receptor for CCL2; M-CSFR as receptor for M-CSF; CD86 as monocyte/macrophage marker; CD163 as specific marker for M2-like macrophages; CD45 as marker for the hematopoietic lineage and Vimentin as mesenchymal cell marker were detected by following conjugated antibodies: CCR2/APC; M-CSFR/PE; CD163/PerCP7Cy5.5; CD45/Alexa Fluor 488 and Vimentin/Alexa Fluor 594.

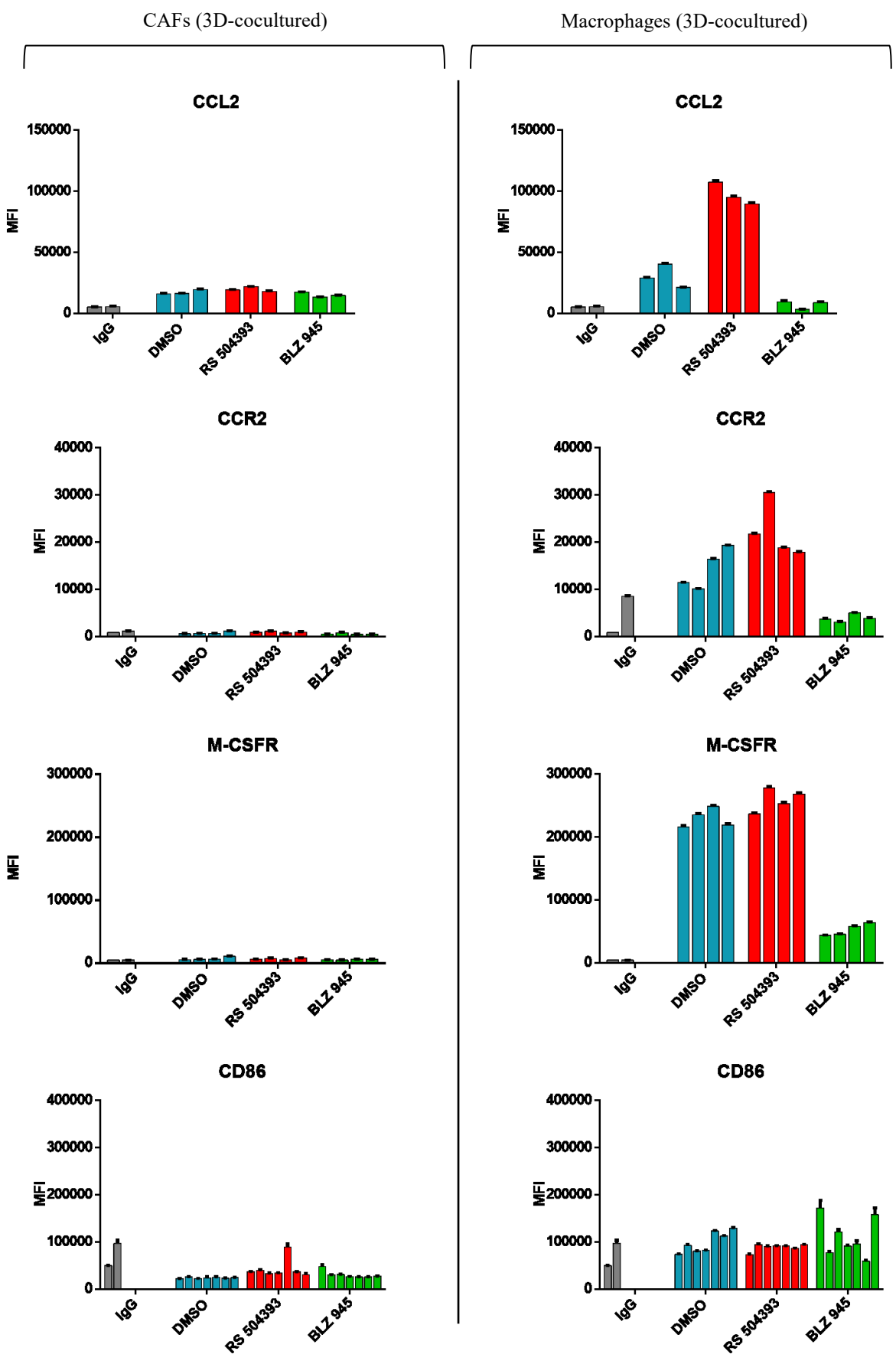
CAFs (3D-cocultured)
Macrophages (3D-cocultured)
CCL2
CCR2
M-CSFR
CD86
MFI
IgG
DMSO
RS 504393
BLZ 945

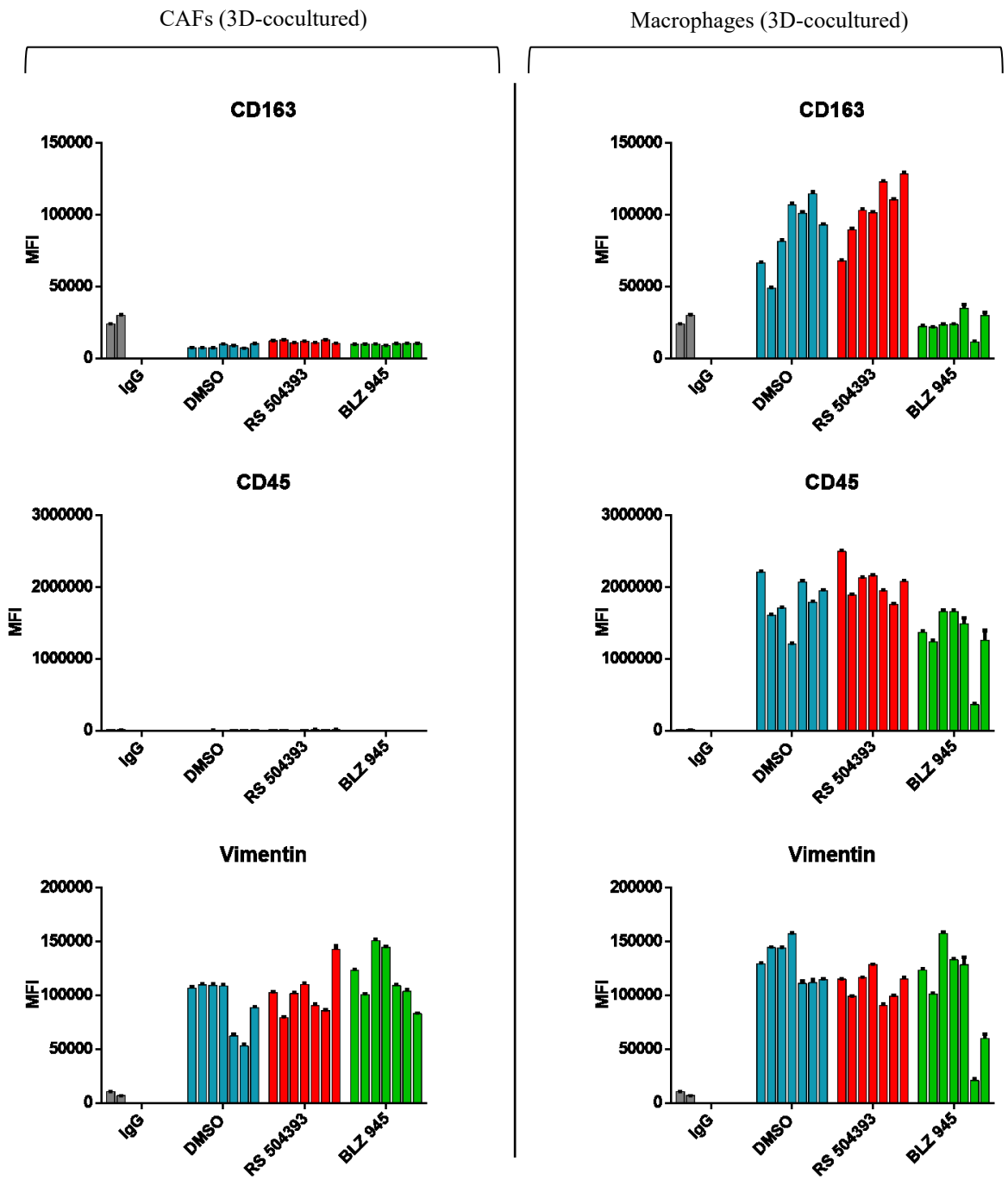

Supplementary Figure 2: Quantified flow cytometry data of individual coculture gels treated with RS 504393 and BLZ 945 which were summarized in Figure 28 and 29.

CAFs and macrophages (300.000 cells each per gel) were cocultured in 3D collagen type 1 gels and treated with either DMSO (control, blue), CCR2 small molecule inhibitor RS 504393 (2 µM, red) or M-CSFR small molecule inhibitor BLZ 945 (1 µM, green) for 6 days (media and factor refresh all 48 hours). Each bar represents MFI of cells digested out of one gel. At least three - up to seven - replicates per setting. IgG control was conducted with cells digested out of DMSO treated gels. Error bars indicate the standard error of mean (SEM). The ligand CCL2; CCR2 as receptor for CCL2; M-CSFR as receptor for M-CSF; CD86 as monocyte/macrophage marker; CD163 as specific marker for M2-like macrophages; CD45 as marker for the hematopoietic lineage and Vimentin as mesenchymal cell marker were detected by following conjugated antibodies: CCL2/PE; CCR2/APC; M-CSFR/PE; CD163/PerCP7Cy5.5; CD45/Alexa Fluor 488 and Vimentin/Alexa Fluor.

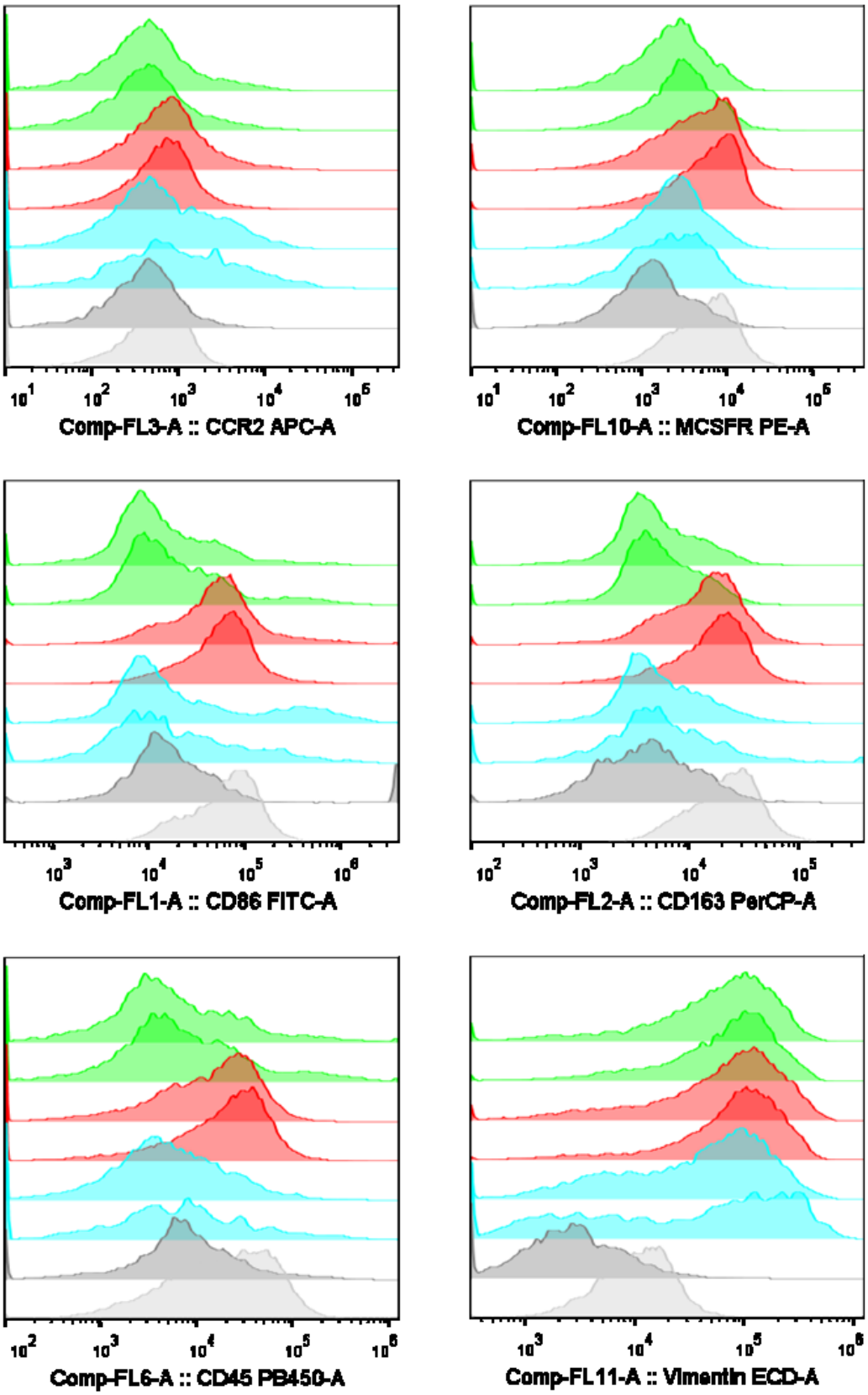

Supplementary Figure 3: Quantified flow cytometry data of individual 3D monocultured CAF gels treated with RS 504393 and BLZ 945 which were summarized in Figure 26.

FlowJo histograms of individual gels are depicted. They were either treated with DMSO control (blue), CCR2 small molecule inhibitor RS 504393 (red) or M-CSFR small molecule inhibitor BLZ 945 (green).

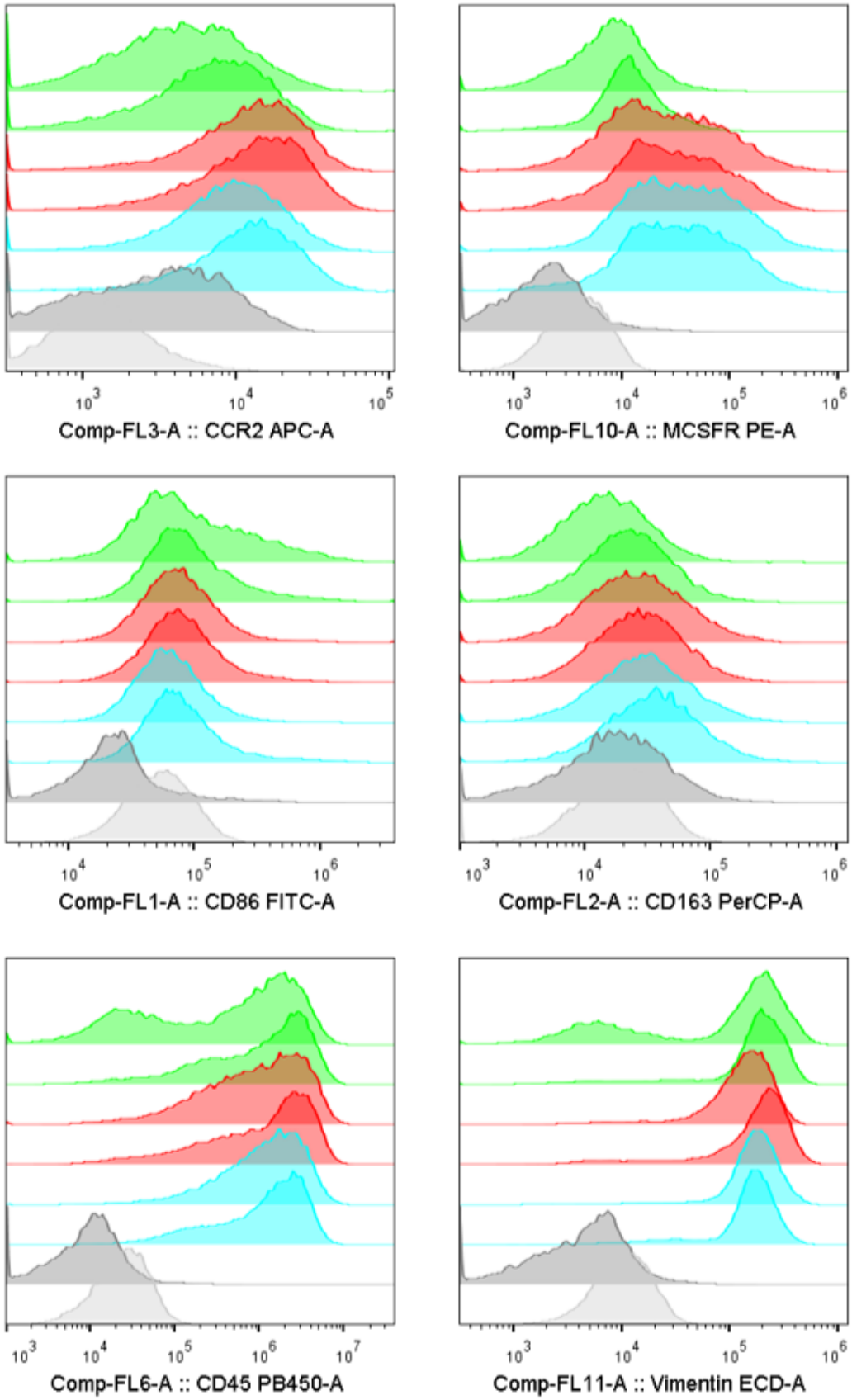

Supplementary Figure 4: Quantified flow cytometry data of individual 3D monocultured macrophage gels treated with RS 504393 and BLZ 945 which were summarized in Figure 27.
FlowJo histograms of individual gels are depicted. They were either treated with DMSO control (blue), CCR2 small molecule inhibitor RS 504393 (red) or M-CSFR small molecule inhibitor BLZ 945 (green).

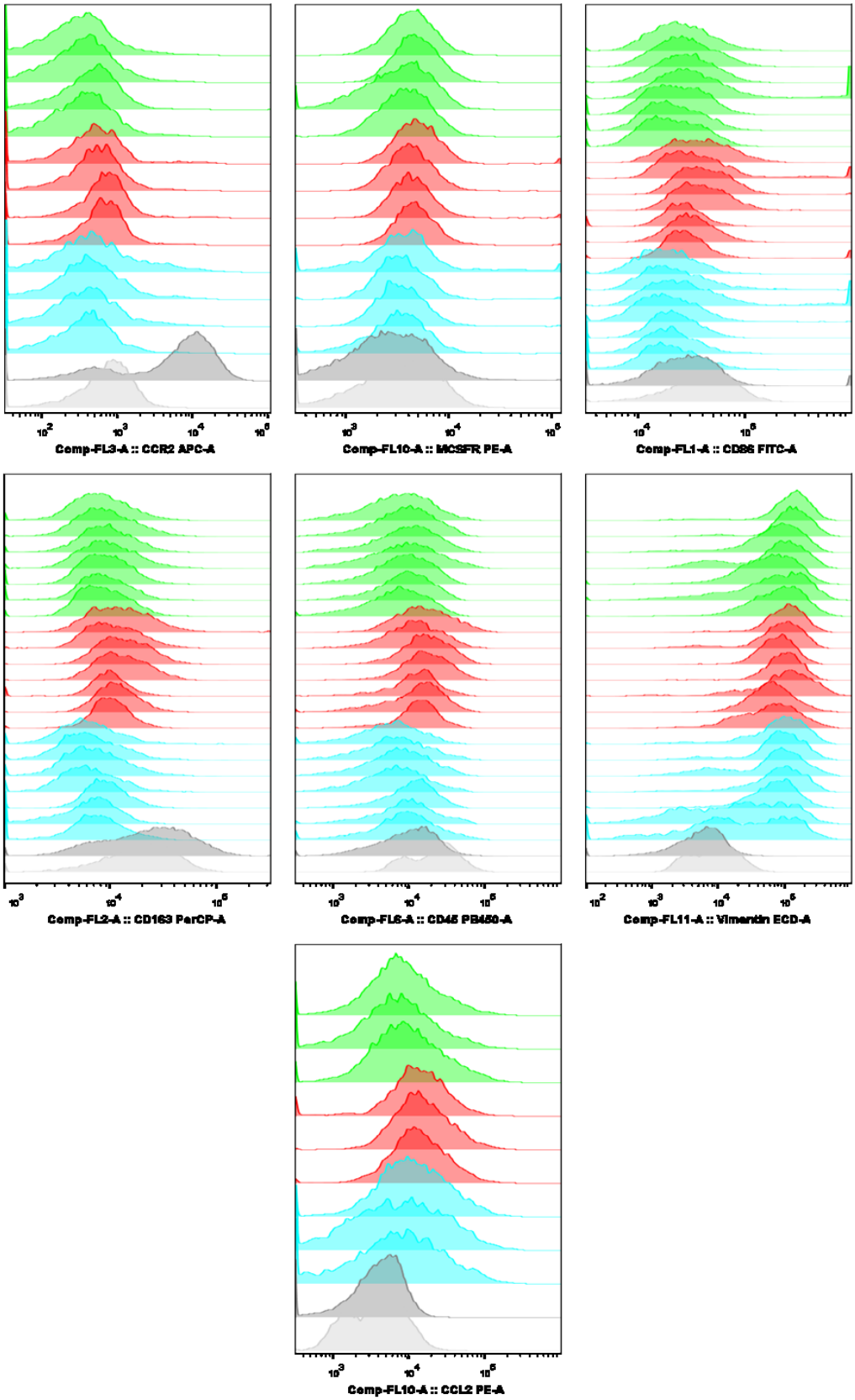

Supplementary Figure 5: Quantified flow cytometry data of individual cocultured CAFs treated with RS 504393 and BLZ 945 which were summarized in Figure 28.
FlowJo histograms of individual gels are depicted. They were either treated with DMSO control (blue), CCR2 small molecule inhibitor RS 504393 (red) or M-CSFR small molecule inhibitor BLZ 945 (green).

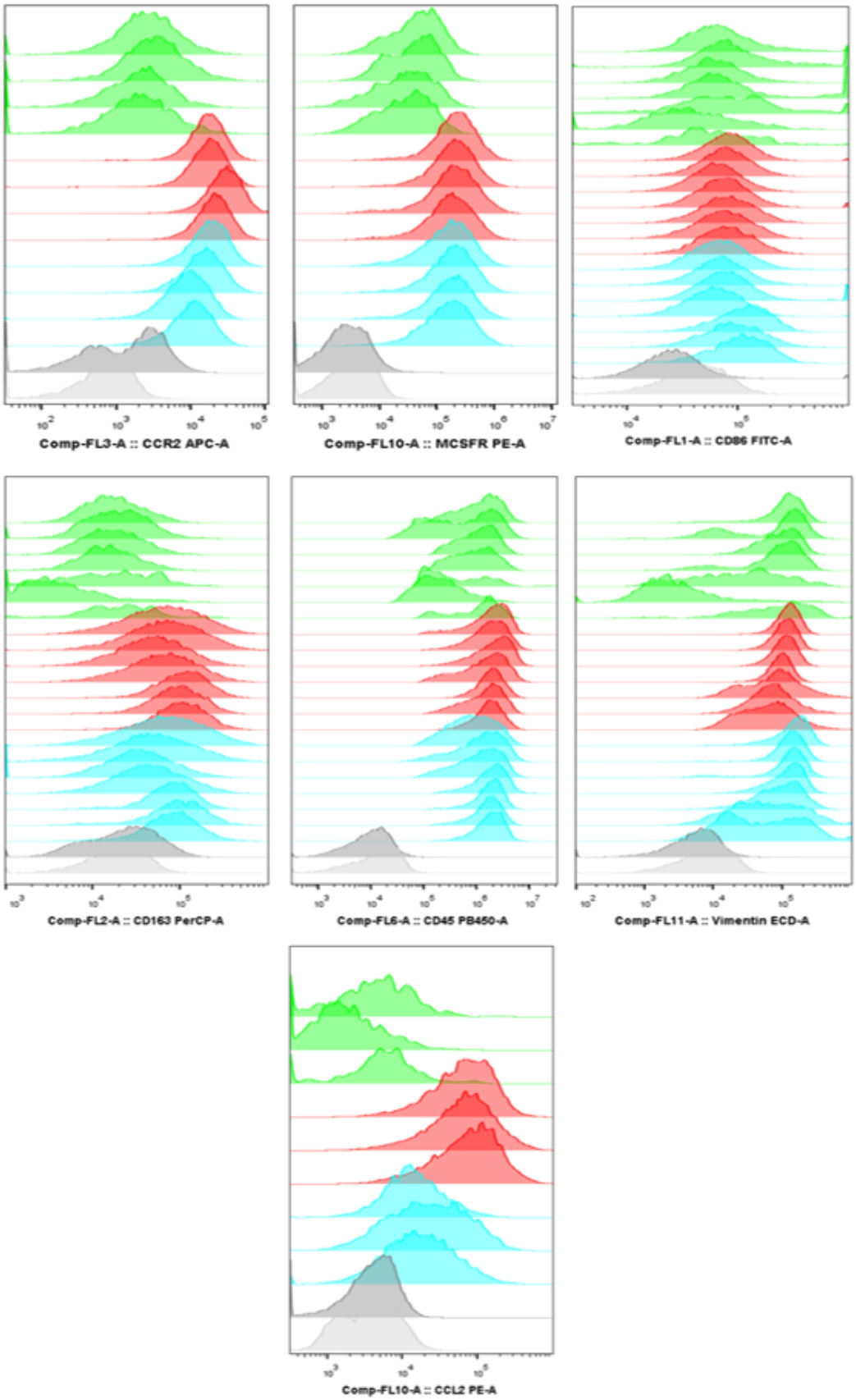

Supplementary Figure 6: Quantified flow cytometry data of individual cocultured macrophages treated with RS 504393 and BLZ 945 which were summarized in Figure 29.

FlowJo histograms of individual gels are depicted. They were either treated with DMSO control (blue), CCR2 small molecule inhibitor RS 504393 (red) or M-CSFR small molecule inhibitor BLZ 945 (green).

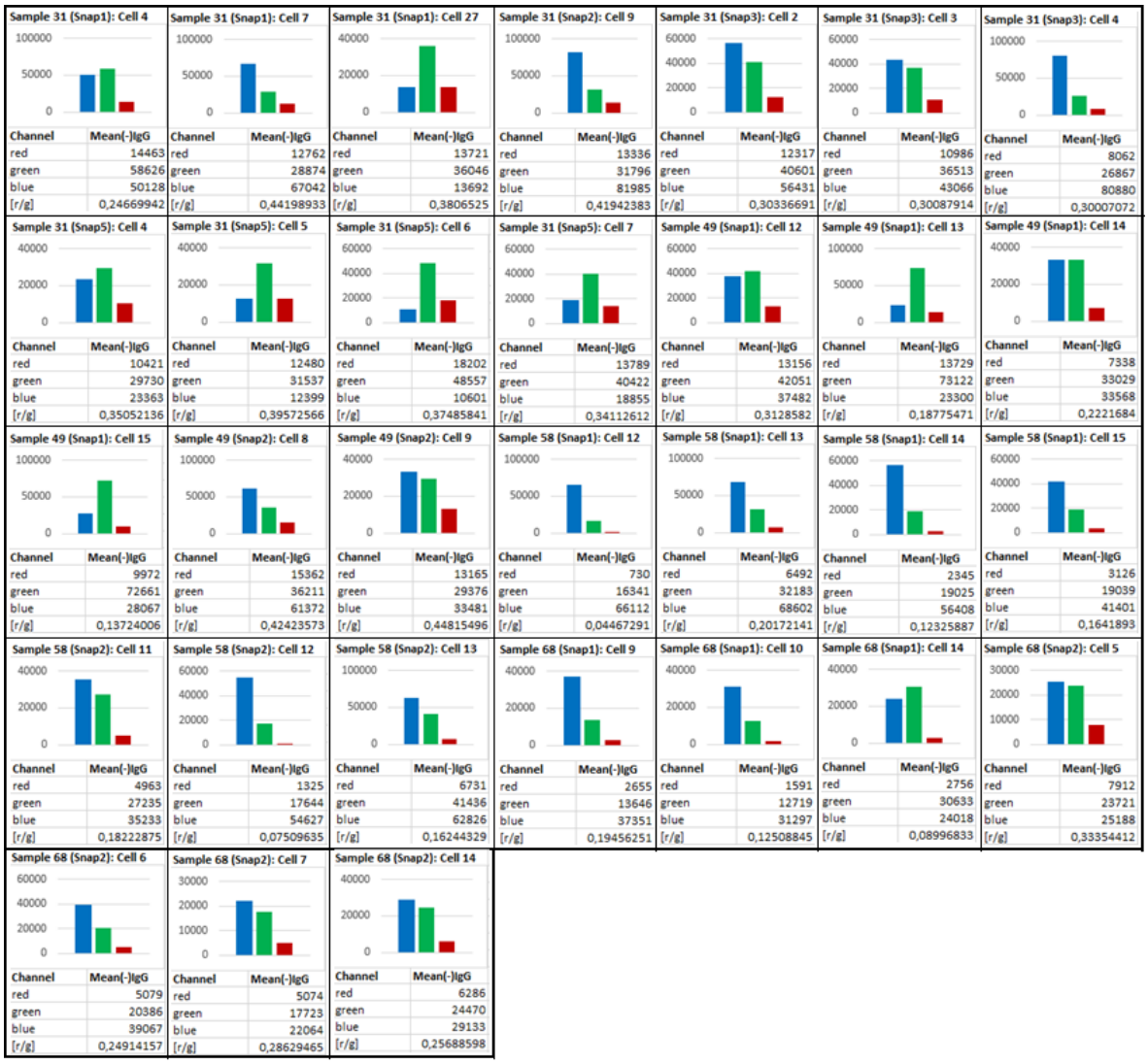

Supplementary Figure 7: Quantitative color histogram data of healthy individual cells categorized as fibroblasts expressing CCL2.

31 cells out of 346 cells in total were categorized as CCL2 expressing fibroblasts according to formula: [(CD68/CCL2) ≤ 0.5]. Color histogram derived means (IgG-subtracted) are shown for three analyzed channels of each cell: CD68 (red), CCL2 (green), DAPI (blue). Exact quotients of CD68/CCL2 (marked as [r/g]) are given below channel means.

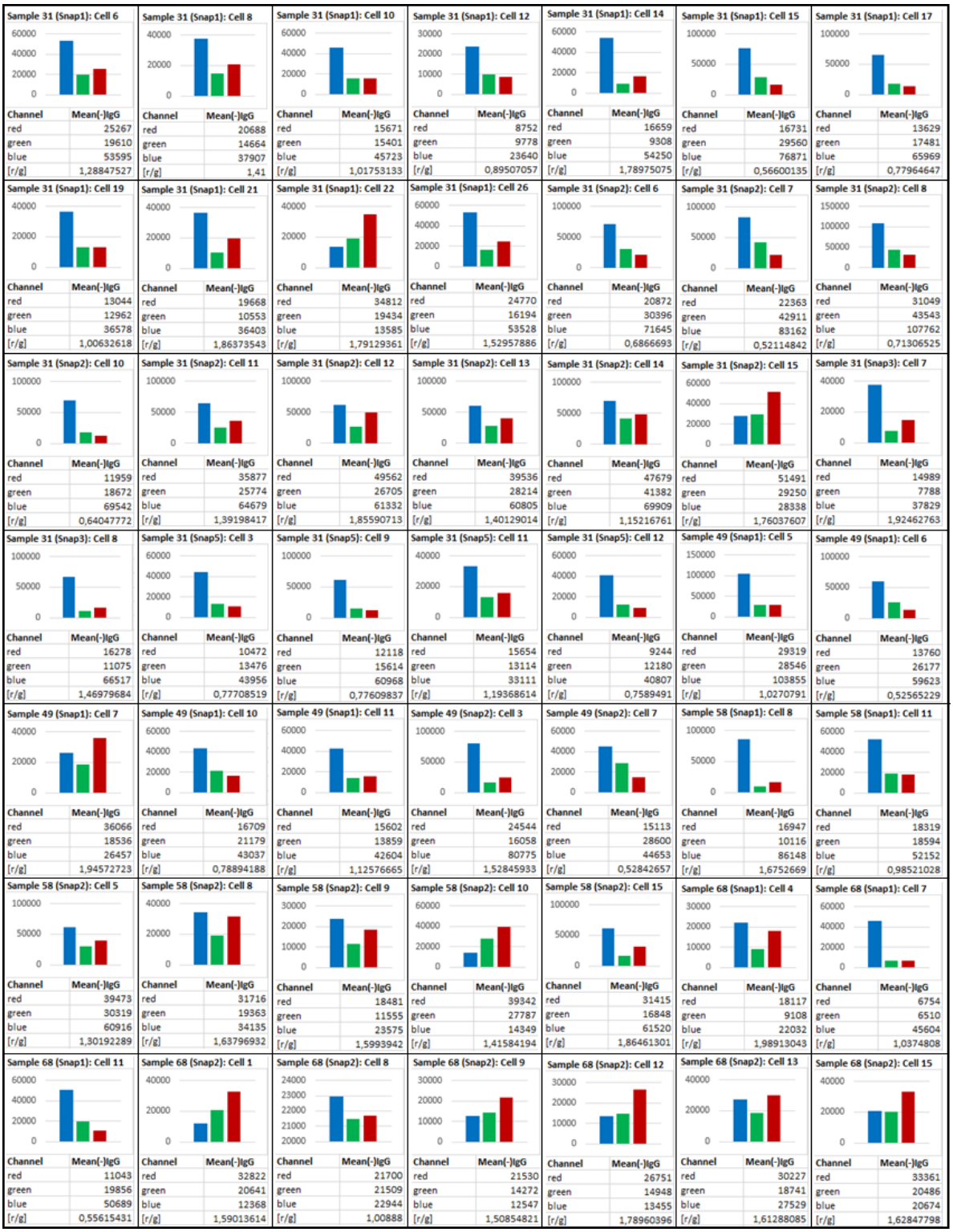

Supplementary Figure 8: Quantitative color histogram data of healthy individual cells categorized as macrophages expressing CCL2.

49 cells out of 346 cells in total were categorized as CCL2 expressing macrophages according to formula: [0.5 ≤ (CD68/CCL2) ≤ 2.0]. Color histogram derived means (IgG-subtracted) are shown for three analyzed channels of each cell: CD68 (red), CCL2 (green), DAPI (blue). Exact quotients of CD68/CCL2 (marked as [r/g]) are given below channel means.

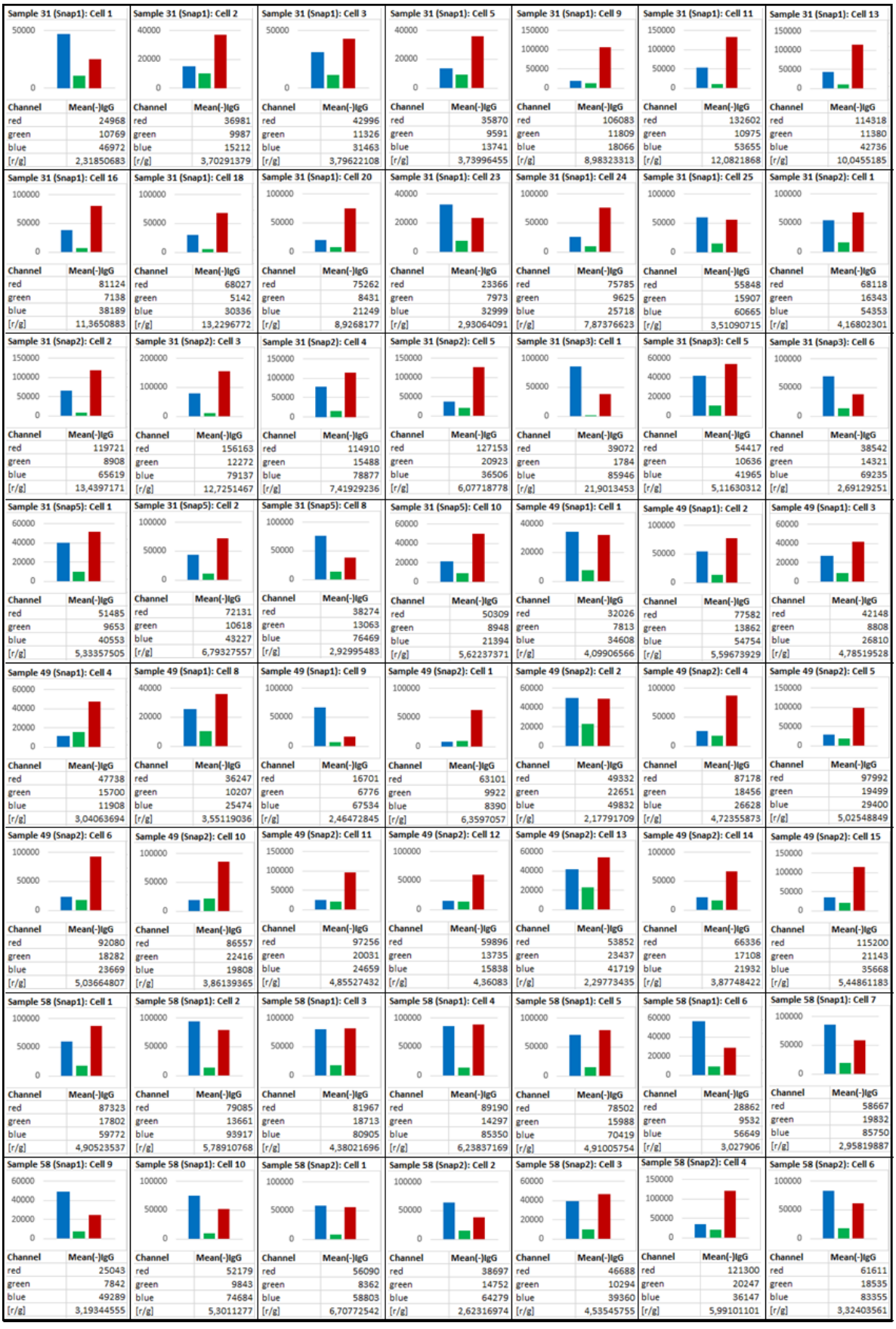
Sample 31 (Snap1): Cell 1
Channel Mean(-)IgG
red 24968
green 10769
blue 46972
[r/g] 2,31850683
Sample 31 (Snap1): Cell 2
Channel Mean(-)IgG
red 36981
green 9987
blue 15212
[r/g] 3,70291379
Sample 31 (Snap1): Cell 3
Channel Mean(-)IgG
red 42996
green 11326
blue 31463
[r/g] 3,79622108
Sample 31 (Snap1): Cell 5
Channel Mean(-)IgG
red 35870
green 9591
blue 13741
[r/g] 3,73996455
Sample 31 (Snap1): Cell 9
Channel Mean(-)IgG
red 106083
green 11809
blue 18066
[r/g] 8,98323313
Sample 31 (Snap1): Cell 11
Channel Mean(-)IgG
red 132602
green 10975
blue 53655
[r/g] 12,0821868
Sample 31 (Snap1): Cell 13
Channel Mean(-)IgG
red 114318
green 11380
blue 42736
[r/g] 10,0455185
Sample 31 (Snap1): Cell 16
Channel Mean(-)IgG
red 81124
green 7138
blue 38189
[r/g] 11,3650883
Sample 31 (Snap1): Cell 18
Channel Mean(-)IgG
red 68027
green 5142
blue 30336
[r/g] 13,2296772
Sample 31 (Snap1): Cell 20
Channel Mean(-)IgG
red 75262
green 8431
blue 21249
[r/g] 8,9268177
Sample 31 (Snap1): Cell 23
Channel Mean(-)IgG
red 23366
green 7973
blue 32999
[r/g] 2,93064091
Sample 31 (Snap1): Cell 24
Channel Mean(-)IgG
red 75785
green 9625
blue 25718
[r/g] 7,87376623
Sample 31 (Snap1): Cell 25
Channel Mean(-)IgG
red 55848
green 15907
blue 60665
[r/g] 3,51090715
Sample 31 (Snap2): Cell 1
Channel Mean(-)IgG
red 68118
green 16343
blue 54353
[r/g] 4,16802301
Sample 31 (Snap2): Cell 2
Channel Mean(-)IgG
red 119721
green 8908
blue 65619
[r/g] 13,4397171
Sample 31 (Snap2): Cell 3
Channel Mean(-)IgG
red 156163
green 12272
blue 79137
[r/g] 12,7251467
Sample 31 (Snap2): Cell 4
Channel Mean(-)IgG
red 114910
green 15488
blue 78877
[r/g] 7,41929236
Sample 31 (Snap2): Cell 5
Channel Mean(-)IgG
red 127153
green 20923
blue 36506
[r/g] 6,07718778
Sample 31 (Snap3): Cell 1
Channel Mean(-)IgG
red 39072
green 1784
blue 85946
[r/g] 21,9013453
Sample 31 (Snap3): Cell 5
Channel Mean(-)IgG
red 54417
green 10636
blue 41965
[r/g] 5,11630312
Sample 31 (Snap3): Cell 6
Channel Mean(-)IgG
red 38542
green 14321
blue 69235
[r/g] 2,69129251
Sample 31 (Snap5): Cell 1
Channel Mean(-)IgG
red 51485
green 9653
blue 40553
[r/g] 5,33357505
Sample 31 (Snap5): Cell 2
Channel Mean(-)IgG
red 72131
green 10618
blue 43227
[r/g] 6,79327557
Sample 31 (Snap5): Cell 8
Channel Mean(-)IgG
red 38274
green 13063
blue 76469
[r/g] 2,92995483
Sample 31 (Snap5): Cell 10
Channel Mean(-)IgG
red 50309
green 8948
blue 21394
[r/g] 5,62237371
Sample 49 (Snap1): Cell 1
Channel Mean(-)IgG
red 32026
green 7813
blue 34608
[r/g] 4,09906566
Sample 49 (Snap1): Cell 2
Channel Mean(-)IgG
red 77582
green 13862
blue 54754
[r/g] 5,59673929
Sample 49 (Snap1): Cell 3
Channel Mean(-)IgG
red 42148
green 8808
blue 26810
[r/g] 4,78519528
Sample 49 (Snap1): Cell 4
Channel Mean(-)IgG
red 47738
green 15700
blue 11908
[r/g] 3,04063694
Sample 49 (Snap1): Cell 8
Channel Mean(-)IgG
red 36247
green 10207
blue 25474
[r/g] 3,55119036
Sample 49 (Snap1): Cell 9
Channel Mean(-)IgG
red 16701
green 6776
blue 67534
[r/g] 2,46472845
Sample 49 (Snap2): Cell 1
Channel Mean(-)IgG
red 63101
green 9922
blue 8390
[r/g] 6,3597057
Sample 49 (Snap2): Cell 2
Channel Mean(-)IgG
red 49332
green 22651
blue 49832
[r/g] 2,17791709
Sample 49 (Snap2): Cell 4
Channel Mean(-)IgG
red 87178
green 18456
blue 26628
[r/g] 4,72355873
Sample 49 (Snap2): Cell 5
Channel Mean(-)IgG
red 97992
green 19499
blue 29400
[r/g] 5,02548849
Sample 49 (Snap2): Cell 6
Channel Mean(-)IgG
red 92080
green 18282
blue 23669
[r/g] 5,03664807
Sample 49 (Snap2): Cell 10
Channel Mean(-)IgG
red 86557
green 22416
blue 19808
[r/g] 3,86139365
Sample 49 (Snap2): Cell 11
Channel Mean(-)IgG
red 97256
green 20031
blue 24659
[r/g] 4,85527432
Sample 49 (Snap2): Cell 12
Channel Mean(-)IgG
red 59896
green 13735
blue 15838
[r/g] 4,36083
Sample 49 (Snap2): Cell 13
Channel Mean(-)IgG
red 53852
green 23437
blue 41719
[r/g] 2,29773435
Sample 49 (Snap2): Cell 14
Channel Mean(-)IgG
red 66336
green 17108
blue 21932
[r/g] 3,87748422
Sample 49 (Snap2): Cell 15
Channel Mean(-)IgG
red 115200
green 21143
blue 35668
[r/g] 5,44861183
Sample 58 (Snap1): Cell 1
Channel Mean(-)IgG
red 87323
green 17802
blue 59772
[r/g] 4,90523537
Sample 58 (Snap1): Cell 2
Channel Mean(-)IgG
red 79085
green 13661
blue 93917
[r/g] 5,78910768
Sample 58 (Snap1): Cell 3
Channel Mean(-)IgG
red 81967
green 18713
blue 80905
[r/g] 4,38021696
Sample 58 (Snap1): Cell 4
Channel Mean(-)IgG
red 89190
green 14297
blue 85350
[r/g] 6,23837169
Sample 58 (Snap1): Cell 5
Channel Mean(-)IgG
red 78502
green 15988
blue 70419
[r/g] 4,91005754
Sample 58 (Snap1): Cell 6
Channel Mean(-)IgG
red 28862
green 9532
blue 56649
[r/g] 3,027906
Sample 58 (Snap1): Cell 7
Channel Mean(-)IgG
red 58667
green 19832
blue 85750
[r/g] 2,95819887
Sample 58 (Snap1): Cell 9
Channel Mean(-)IgG
red 25043
green 7842
blue 49289
[r/g] 3,19344555
Sample 58 (Snap1): Cell 10
Channel Mean(-)IgG
red 52179
green 9843
blue 74684
[r/g] 5,3011277
Sample 58 (Snap2): Cell 1
Channel Mean(-)IgG
red 56090
green 8362
blue 58803
[r/g] 6,70772542
Sample 58 (Snap2): Cell 2
Channel Mean(-)IgG
red 38697
green 14752
blue 64279
[r/g] 2,62316974
Sample 58 (Snap2): Cell 3
Channel Mean(-)IgG
red 46688
green 10294
blue 39360
[r/g] 4,53545755
Sample 58 (Snap2): Cell 4
Channel Mean(-)IgG
red 121300
green 20247
blue 36147
[r/g] 5,99101101
Sample 58 (Snap2): Cell 6
Channel Mean(-)IgG
red 61611
green 18535
blue 83355
[r/g] 3,32403561

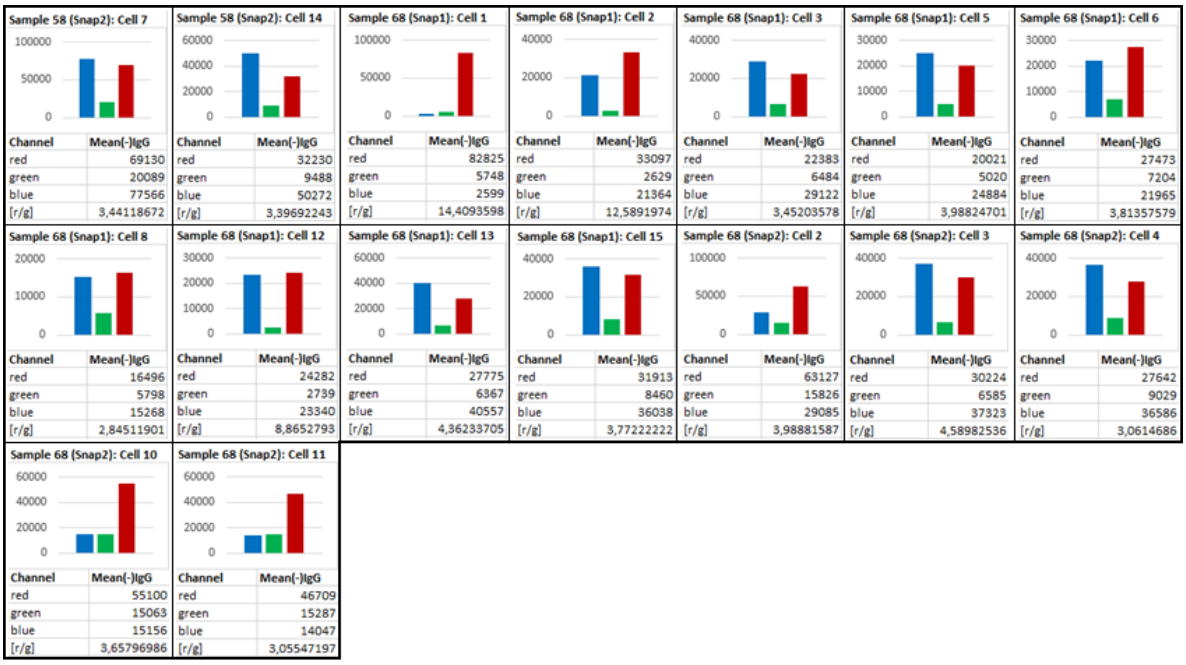

Supplementary Figure 9: Quantitative color histogram data of healthy individual cells categorized as macrophages expressing no CCL2.

72 cells out of 346 cells in total were categorized as macrophages without CCL2 expression according to formula: [(CD68/CCL2) ≥ 2.0]. Color histogram derived means (IgG-subtracted) are shown for three analyzed channels of each cell: CD68 (red), CCL2 (green), DAPI (blue). Exact quotients of CD68/CCL2 (marked as [r/g]) are given below channel means.

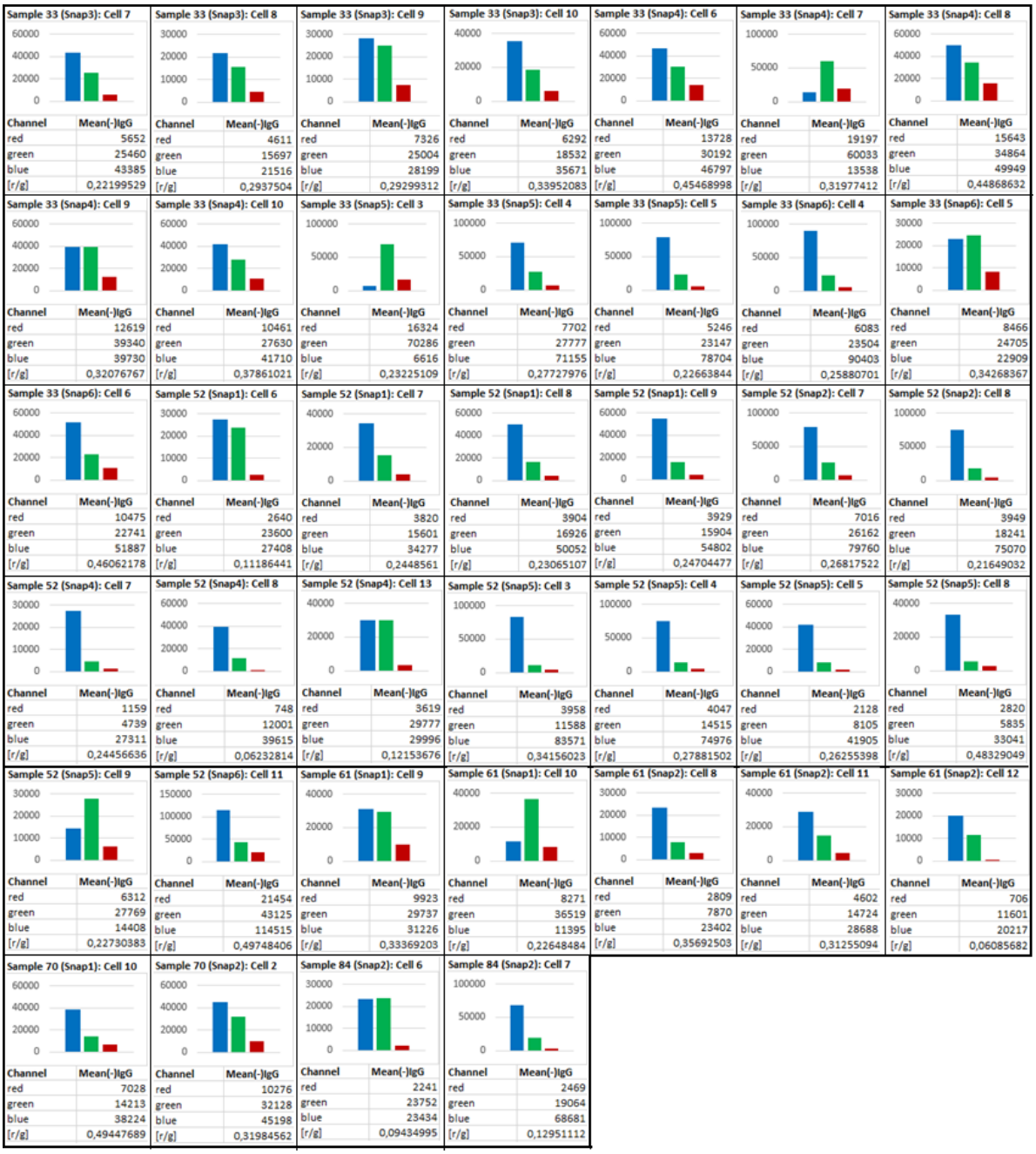

Supplementary Figure 10: Quantitative color histogram data of tumor individual cells categorized as fibroblasts expressing CCL2.

39 cells out of 346 cells in total were categorized as CCL2 expressing fibroblasts according to formula: [(CD68/CCL2) ≤ 0.5]. Color histogram derived means (IgG-subtracted) are shown for three analyzed channels of each cell: CD68 (red), CCL2 (green), DAPI (blue). Exact quotients of CD68/CCL2 (marked as [r/g]) are given below channel means.

Sample 33 (Snap3): Cell 6	
Channel	Mean(-)IgG
red	24064
green	41553
blue	30803
[r/g]	0,57911583

Sample 33 (Snap3): Cell 11	
Channel	Mean(-)IgG
red	46831
green	28504
blue	57610
[r/g]	1,64296239

Sample 33 (Snap3): Cell 12	
Channel	Mean(-)IgG
red	45141
green	29286
blue	45306
[r/g]	1,54138496

Sample 33 (Snap3): Cell 13	
Channel	Mean(-)IgG
red	47720
green	28696
blue	34652
[r/g]	1,66294954

Sample 33 (Snap3): Cell 14	
Channel	Mean(-)IgG
red	36542
green	30091
blue	24392
[r/g]	1,21438304

Sample 33 (Snap4): Cell 12	
Channel	Mean(-)IgG
red	42505
green	23533
blue	78760
[r/g]	1,80618706

Sample 33 (Snap4): Cell 13	
Channel	Mean(-)IgG
red	50483
green	44352
blue	39932
[r/g]	1,13823503

Sample 33 (Snap4): Cell 14	
Channel	Mean(-)IgG
red	28729
green	14929
blue	30398
[r/g]	1,92437538

Sample 33 (Snap4): Cell 15	
Channel	Mean(-)IgG
red	32522
green	24150
blue	46912
[r/g]	1,34666667

Sample 33 (Snap5): Cell 7	
Channel	Mean(-)IgG
red	18836
green	18384
blue	50750
[r/g]	1,0245866

Sample 33 (Snap5): Cell 8	
Channel	Mean(-)IgG
red	12663
green	15546
blue	67462
[r/g]	0,81455037

Sample 33 (Snap5): Cell 9	
Channel	Mean(-)IgG
red	18702
green	17317
blue	89075
[r/g]	1,07997921

Sample 33 (Snap6): Cell 7	
Channel	Mean(-)IgG
red	45752
green	55049
blue	25169
[r/g]	0,8311141

Sample 33 (Snap6): Cell 8	
Channel	Mean(-)IgG
red	14268
green	21131
blue	40720
[r/g]	0,67521651

Sample 33 (Snap6): Cell 9	
Channel	Mean(-)IgG
red	25519
green	12944
blue	59140
[r/g]	1,97149258

Sample 33 (Snap6): Cell 10	
Channel	Mean(-)IgG
red	35071
green	23576
blue	110623
[r/g]	1,48757211

Sample 33 (Snap6): Cell 11	
Channel	Mean(-)IgG
red	26161
green	31539
blue	33153
[r/g]	0,82948096

Sample 52 (Snap1): Cell 5	
Channel	Mean(-)IgG
red	14333
green	9292
blue	71057
[r/g]	1,54250969

Sample 52 (Snap2): Cell 6	
Channel	Mean(-)IgG
red	5271
green	9258
blue	71199
[r/g]	0,56934543

Sample 52 (Snap2): Cell 15	
Channel	Mean(-)IgG
red	25908
green	18907
blue	25801
[r/g]	1,37028614

Sample 52 (Snap): Cell 6	
Channel	Mean(-)IgG
red	9961
green	19609
blue	38522
[r/g]	0,50798103

Sample 52 (Snap): Cell 7	
Channel	Mean(-)IgG
red	14507
green	16115
blue	44112
[r/g]	0,90021719

Sample 52 (Snap): Cell 8	
Channel	Mean(-)IgG
red	25274
green	14156
blue	49346
[r/g]	1,78539135

Sample 52 (Snap): Cell 13	
Channel	Mean(-)IgG
red	35503
green	19503
blue	52503
[r/g]	1,82038661

Sample 52 (Snap): Cell 15	
Channel	Mean(-)IgG
red	31228
green	17972
blue	81798
[r/g]	1,73759181

Sample 52 (Snap4): Cell 4	
Channel	Mean(-)IgG
red	11946
green	8988
blue	48903
[r/g]	1,32910547

Sample 52 (Snap4): Cell 6	
Channel	Mean(-)IgG
red	5303
green	9974
blue	14450
[r/g]	0,53168237

Sample 52 (Snap4): Cell 9	
Channel	Mean(-)IgG
red	17853
green	20606
blue	17082
[r/g]	0,86639814

Sample 52 (Snap4): Cell 11	
Channel	Mean(-)IgG
red	8110
green	5152
blue	33525
[r/g]	1,57414596

Sample 52 (Snap4): Cell 12	
Channel	Mean(-)IgG
red	8252
green	5047
blue	63900
[r/g]	1,63503071

Sample 52 (Snap5): Cell 1	
Channel	Mean(-)IgG
red	21913
green	18010
blue	28150
[r/g]	1,21671294

Sample 52 (Snap5): Cell 2	
Channel	Mean(-)IgG
red	10925
green	14791
blue	85828
[r/g]	0,73862484

Sample 52 (Snap5): Cell 7	
Channel	Mean(-)IgG
red	8104
green	8476
blue	92491
[r/g]	0,95611137

Sample 52 (Snap5): Cell 10	
Channel	Mean(-)IgG
red	3484
green	3158
blue	28837
[r/g]	1,10322989

Sample 52 (Snap6): Cell 2	
Channel	Mean(-)IgG
red	74036
green	40781
blue	82311
[r/g]	1,81545327

Sample 52 (Snap6): Cell 6	
Channel	Mean(-)IgG
red	35185
green	22080
blue	97333
[r/g]	1,59352355

Sample 52 (Snap6): Cell 8	
Channel	Mean(-)IgG
red	31380
green	33876
blue	115186
[r/g]	0,92631952

Sample 52 (Snap6): Cell 13	
Channel	Mean(-)IgG
red	22691
green	15452
blue	118752
[r/g]	1,46848304

Sample 52 (Snap6): Cell 14	
Channel	Mean(-)IgG
red	24537
green	24837
blue	112693
[r/g]	0,98792125

Sample 61 (Snap1): Cell 3	
Channel	Mean(-)IgG
red	24610
green	13513
blue	53434
[r/g]	1,82120921

Sample 61 (Snap1): Cell 5	
Channel	Mean(-)IgG
red	24017
green	26914
blue	17924
[r/g]	0,89236085

Sample 61 (Snap1): Cell 6	
Channel	Mean(-)IgG
red	31871
green	22352
blue	30053
[r/g]	1,42586793

Sample 61 (Snap1): Cell 7	
Channel	Mean(-)IgG
red	15331
green	19703
blue	30803
[r/g]	0,77810486

Sample 61 (Snap1): Cell 8	
Channel	Mean(-)IgG
red	21432
green	11494
blue	29959
[r/g]	1,86462502

Sample 61 (Snap1): Cell 11	
Channel	Mean(-)IgG
red	24402
green	14403
blue	24039
[r/g]	1,69423037

Sample 61 (Snap1): Cell 12	
Channel	Mean(-)IgG
red	10773
green	13596
blue	30057
[r/g]	0,7923654

Sample 61 (Snap1): Cell 13	
Channel	Mean(-)IgG
red	28327
green	21283
blue	81980
[r/g]	1,33096838

Sample 61 (Snap1): Cell 14	
Channel	Mean(-)IgG
red	20519
green	22246
blue	36367
[r/g]	0,92236807

Sample 61 (Snap1): Cell 15	
Channel	Mean(-)IgG
red	12791
green	19604
blue	26263
[r/g]	0,65246888

Sample 61 (Snap2): Cell 2	
Channel	Mean(-)IgG
red	17430
green	13864
blue	12987
[r/g]	1,25721293

Sample 61 (Snap2): Cell 6	
Channel	Mean(-)IgG
red	8899
green	9842
blue	25700
[r/g]	0,90418614

Sample 61 (Snap2): Cell 7	
Channel	Mean(-)IgG
red	22019
green	7070
blue	29134
[r/g]	3,11442716

Sample 61 (Snap2): Cell 9	
Channel	Mean(-)IgG
red	13991
green	16440
blue	16446
[r/g]	0,85103406

Sample 61 (Snap2): Cell 10	
Channel	Mean(-)IgG
red	22582
green	13157
blue	66747
[r/g]	1,71634871

Sample 61 (Snap2): Cell 15	
Channel	Mean(-)IgG
red	7308
green	10895
blue	15678
[r/g]	0,67076641

Sample 70 (Snap2): Cell 6	
Channel	Mean(-)IgG
red	17294
green	26009
blue	61175
[r/g]	0,66492368

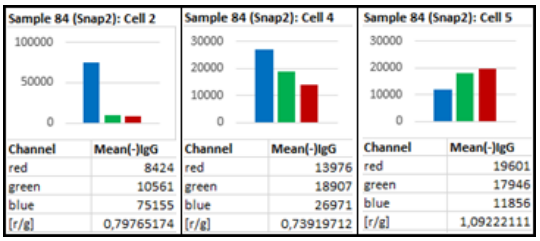

Supplementary Figure 11: Quantitative color histogram data of tumor individual cells categorized as macrophages expressing CCL2.

59 cells out of 346 cells in total were categorized as CCL2 expressing macrophages according to formula: [0.5 ≤ (CD68/CCL2) ≤ 2.0]. Color histogram derived means (IgG-subtracted) are shown for three analyzed channels of each cell: CD68 (red), CCL2 (green), DAPI (blue). Exact quotients of CD68/CCL2 (marked as [r/g]) are given below channel means.

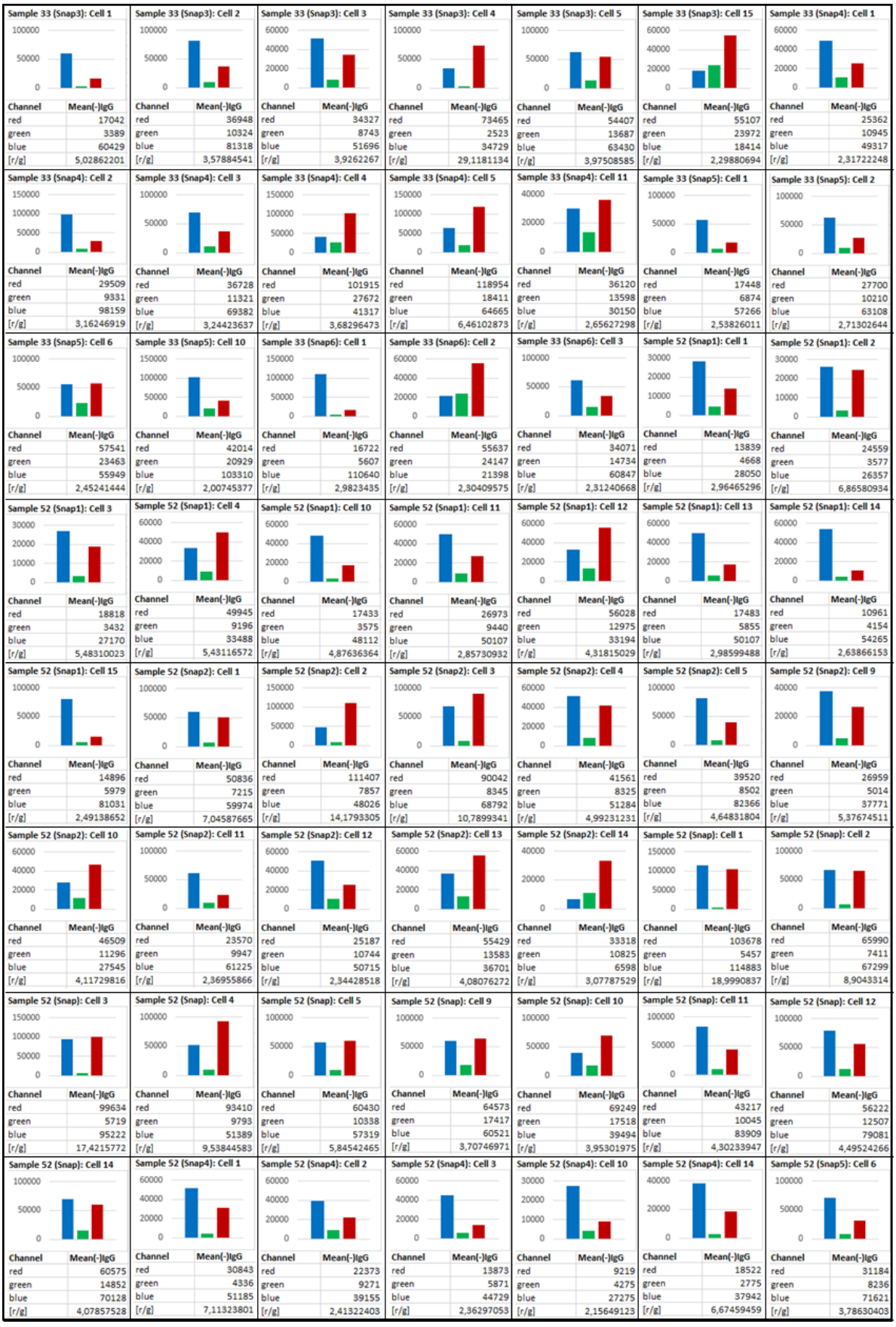
Sample 33 (Snap3): Cell 1
Channel Mean(-)IgG
red 17042
green 3389
blue 60429
[r/g] 5,02862201
Sample 33 (Snap3): Cell 2
Channel Mean(-)IgG
red 36948
green 10324
blue 81318
[r/g] 3,57884541
Sample 33 (Snap3): Cell 3
Channel Mean(-)IgG
red 34327
green 8743
blue 51696
[r/g] 3,9262267
Sample 33 (Snap3): Cell 4
Channel Mean(-)IgG
red 73465
green 2523
blue 34729
[r/g] 29,1181134
Sample 33 (Snap3): Cell 5
Channel Mean(-)IgG
red 54407
green 13687
blue 63430
[r/g] 3,97508585
Sample 33 (Snap3): Cell 15
Channel Mean(-)IgG
red 55107
green 23972
blue 18414
[r/g] 2,29880694
Sample 33 (Snap4): Cell 1
Channel Mean(-)IgG
red 25362
green 10945
blue 49317
[r/g] 2,31722248
Sample 33 (Snap4): Cell 2
Channel Mean(-)IgG
red 29509
green 9331
blue 98159
[r/g] 3,16246919
Sample 33 (Snap4): Cell 3
Channel Mean(-)IgG
red 36728
green 11321
blue 69382
[r/g] 3,24423637
Sample 33 (Snap4): Cell 4
Channel Mean(-)IgG
red 101915
green 27672
blue 41317
[r/g] 3,68296473
Sample 33 (Snap4): Cell 5
Channel Mean(-)IgG
red 118954
green 18411
blue 64665
[r/g] 6,46102873
Sample 33 (Snap4): Cell 11
Channel Mean(-)IgG
red 36120
green 13598
blue 30150
[r/g] 2,65627298
Sample 33 (Snap5): Cell 1
Channel Mean(-)IgG
red 17448
green 6874
blue 57266
[r/g] 2,53826011
Sample 33 (Snap5): Cell 2
Channel Mean(-)IgG
red 27700
green 10210
blue 63108
[r/g] 2,71302644
Sample 33 (Snap5): Cell 6
Channel Mean(-)IgG
red 57541
green 23463
blue 55949
[r/g] 2,45241444
Sample 33 (Snap5): Cell 10
Channel Mean(-)IgG
red 42014
green 20929
blue 103310
[r/g] 2,00745377
Sample 33 (Snap6): Cell 1
Channel Mean(-)IgG
red 16722
green 5607
blue 110640
[r/g] 2,9823435
Sample 33 (Snap6): Cell 2
Channel Mean(-)IgG
red 55637
green 24147
blue 21398
[r/g] 2,30409575
Sample 33 (Snap6): Cell 3
Channel Mean(-)IgG
red 34071
green 14734
blue 60847
[r/g] 2,31240668
Sample 52 (Snap1): Cell 1
Channel Mean(-)IgG
red 13839
green 4668
blue 28050
[r/g] 2,96465296
Sample 52 (Snap1): Cell 2
Channel Mean(-)IgG
red 24559
green 3577
blue 26357
[r/g] 6,86580934
Sample 52 (Snap1): Cell 3
Channel Mean(-)IgG
red 18818
green 3432
blue 27170
[r/g] 5,48310023
Sample 52 (Snap1): Cell 4
Channel Mean(-)IgG
red 49945
green 9196
blue 33488
[r/g] 5,43116572
Sample 52 (Snap1): Cell 10
Channel Mean(-)IgG
red 17433
green 3575
blue 48112
[r/g] 4,87636364
Sample 52 (Snap1): Cell 11
Channel Mean(-)IgG
red 26973
green 9440
blue 50107
[r/g] 2,85730932
Sample 52 (Snap1): Cell 12
Channel Mean(-)IgG
red 56028
green 12975
blue 33194
[r/g] 4,31815029
Sample 52 (Snap1): Cell 13
Channel Mean(-)IgG
red 17483
green 5855
blue 50107
[r/g] 2,98599488
Sample 52 (Snap1): Cell 14
Channel Mean(-)IgG
red 10961
green 4154
blue 54265
[r/g] 2,63866153
Sample 52 (Snap1): Cell 15
Channel Mean(-)IgG
red 14896
green 5979
blue 81031
[r/g] 2,49138652
Sample 52 (Snap2): Cell 1
Channel Mean(-)IgG
red 50836
green 7215
blue 59974
[r/g] 7,04587665
Sample 52 (Snap2): Cell 2
Channel Mean(-)IgG
red 111407
green 7857
blue 48026
[r/g] 14,1793305
Sample 52 (Snap2): Cell 3
Channel Mean(-)IgG
red 90042
green 8345
blue 68792
[r/g] 10,7899341
Sample 52 (Snap2): Cell 4
Channel Mean(-)IgG
red 41561
green 8325
blue 51284
[r/g] 4,99231231
Sample 52 (Snap2): Cell 5
Channel Mean(-)IgG
red 39520
green 8502
blue 82366
[r/g] 4,64831804
Sample 52 (Snap2): Cell 9
Channel Mean(-)IgG
red 26959
green 5014
blue 37771
[r/g] 5,37674511
Sample 52 (Snap2): Cell 10
Channel Mean(-)IgG
red 46509
green 11296
blue 27545
[r/g] 4,11729816
Sample 52 (Snap2): Cell 11
Channel Mean(-)IgG
red 23570
green 9947
blue 61225
[r/g] 2,36955866
Sample 52 (Snap2): Cell 12
Channel Mean(-)IgG
red 25187
green 10744
blue 50715
[r/g] 2,34428518
Sample 52 (Snap2): Cell 13
Channel Mean(-)IgG
red 55429
green 13583
blue 36701
[r/g] 4,08076272
Sample 52 (Snap2): Cell 14
Channel Mean(-)IgG
red 33318
green 10825
blue 6598
[r/g] 3,07787529
Sample 52 (Snap): Cell 1
Channel Mean(-)IgG
red 103678
green 5457
blue 114883
[r/g] 18,9990837
Sample 52 (Snap): Cell 2
Channel Mean(-)IgG
red 65990
green 7411
blue 67299
[r/g] 8,9043314
Sample 52 (Snap): Cell 3
Channel Mean(-)IgG
red 99634
green 5719
blue 95222
[r/g] 17,4215772
Sample 52 (Snap): Cell 4
Channel Mean(-)IgG
red 93410
green 9793
blue 51389
[r/g] 9,53844583
Sample 52 (Snap): Cell 5
Channel Mean(-)IgG
red 60430
green 10338
blue 57319
[r/g] 5,84542465
Sample 52 (Snap): Cell 9
Channel Mean(-)IgG
red 64573
green 17417
blue 60521
[r/g] 3,70746971
Sample 52 (Snap): Cell 10
Channel Mean(-)IgG
red 69249
green 17518
blue 39494
[r/g] 3,95301975
Sample 52 (Snap): Cell 11
Channel Mean(-)IgG
red 43217
green 10045
blue 83909
[r/g] 4,30233947
Sample 52 (Snap): Cell 12
Channel Mean(-)IgG
red 56222
green 12507
blue 79081
[r/g] 4,49524266
Sample 52 (Snap): Cell 14
Channel Mean(-)IgG
red 60575
green 14852
blue 70128
[r/g] 4,07857528
Sample 52 (Snap4): Cell 1
Channel Mean(-)IgG
red 30843
green 4336
blue 51185
[r/g] 7,11323801
Sample 52 (Snap4): Cell 2
Channel Mean(-)IgG
red 22373
green 9271
blue 39155
[r/g] 2,41322403
Sample 52 (Snap4): Cell 3
Channel Mean(-)IgG
red 13873
green 5871
blue 44729
[r/g] 2,36297053
Sample 52 (Snap4): Cell 10
Channel Mean(-)IgG
red 9219
green 4275
blue 27275
[r/g] 2,15649123
Sample 52 (Snap4): Cell 14
Channel Mean(-)IgG
red 18522
green 2775
blue 37942
[r/g] 6,67459459
Sample 52 (Snap5): Cell 6
Channel Mean(-)IgG
red 31184
green 8236
blue 71621
[r/g] 3,78630403

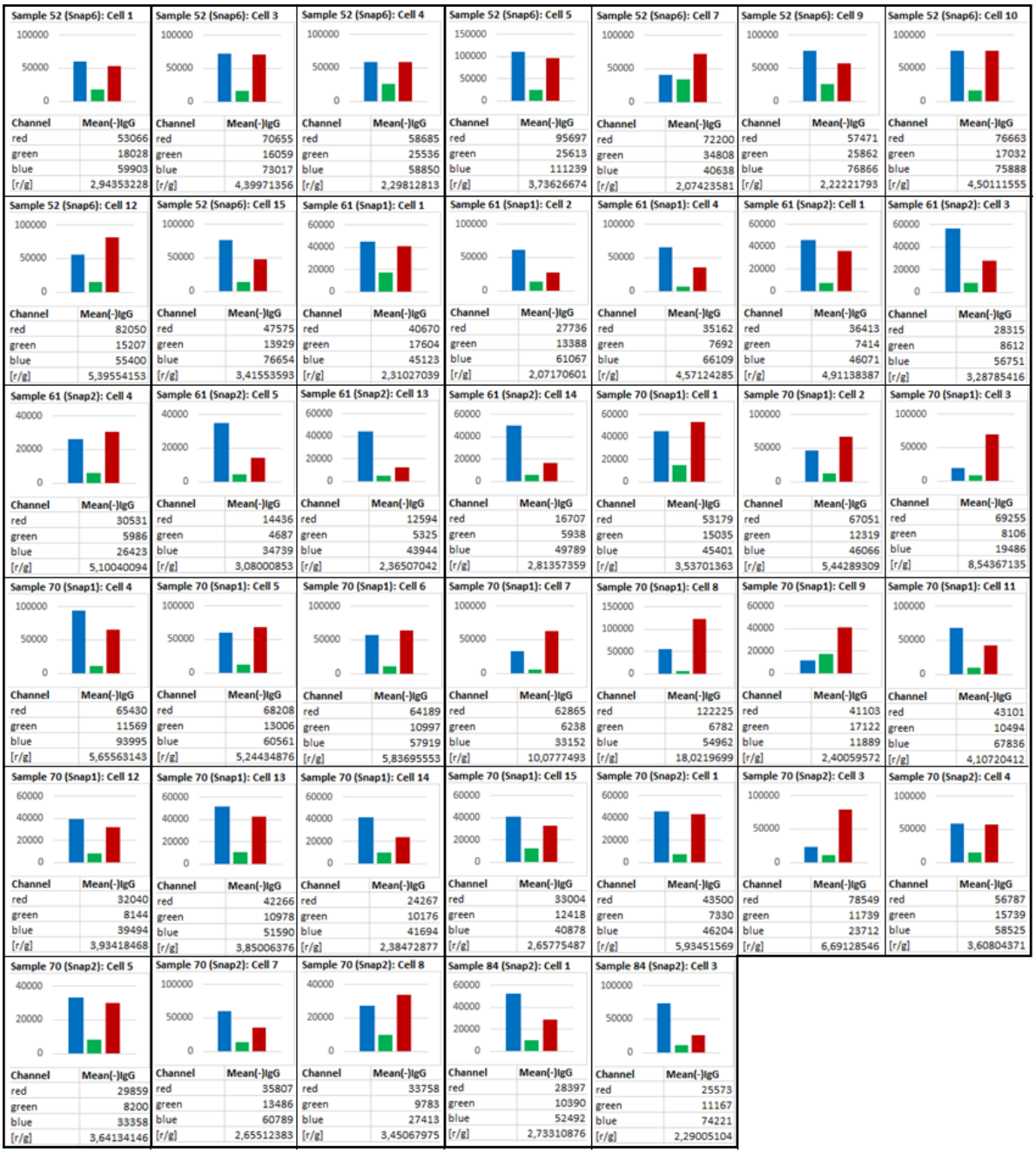

Supplementary Figure 12: Quantitative color histogram data of tumor individual cells categorized as macrophages expressing no CCL2.

96 cells out of 346 cells in total were categorized as macrophages without CCL2 expression according to formula: [(CD68/CCL2) ≥ 2.0]. Color histogram derived means (IgG-subtracted) are shown for three analyzed channels of each cell: CD68 (red), CCL2 (green), DAPI (blue). Exact quotients of CD68/CCL2 (marked as [r/g]) are given below channel means.

5.2. Supplementary tables

Supplementary Table 1: P-values of CCR2 and M-CSFR for CAFs in Figure 22

CCR2

Unpaired t test	*One- or two-tailed P value?*	*Significantly different? (P < 0.05)*	*P value summary*	*P value*
Unstained vs. CCR2	Two-tailed	Yes	****	< 0,0001
IgG vs. CCR2	Two-tailed	Yes	****	< 0,0001

M-CSFR

Unpaired t test	*One- or two-tailed P value?*	*Significantly different? (P < 0.05)*	*P value summary*	*P value*
Unstained vs. M-CSFR	Two-tailed	Yes	****	< 0,0001
IgG vs. M-CSFR	Two-tailed	Yes	***	0,0007

Supplementary Table 2: P-values of CCR2 and M-CSFR for HCT116 cells in Figure 22

CCR2

Unpaired t test	*One- or two-tailed P value?*	*Significantly different? (P < 0.05)*	*P value summary*	*P value*
Unstained vs. CCR2	Two-tailed	Yes	****	< 0,0001
IgG vs. CCR2	Two-tailed	No	ns	0,3908

M-CSFR

Unpaired t test	*One- or two-tailed P value?*	*Significantly different? (P < 0.05)*	*P value summary*	*P value*
Unstained vs. M-CSFR	Two-tailed	Yes	****	< 0,0001
IgG vs. M-CSFR	Two-tailed	Yes	***	0,0007

Supplementary Table 3: P-values of CCR2 and M-CSFR for monocytes in Figure 22

CCR2

Unpaired t test	*One- or two-tailed P value?*	*Significantly different? (P < 0.05)*	*P value summary*	*P value*
Unstained vs. CCR2	Two-tailed	Yes	****	< 0,0001
IgG vs. CCR2	Two-tailed	Yes	****	< 0,0001

M-CSFR

Unpaired t test	*One- or two-tailed P value?*	*Significantly different? (P < 0.05)*	*P value summary*	*P value*
Unstained vs. M-CSFR	Two-tailed	Yes	****	< 0,0001
IgG vs. M-CSFR	Two-tailed	Yes	****	< 0,0001

Supplementary Table 4: P-values of CCR2 and M-CSFR for lymphocytes in Figure 22

CCR2

Unpaired t test	*One- or two-tailed P value?*	*Significantly different? (P < 0.05)*	*P value summary*	*P value*
Unstained vs. CCR2	Two-tailed	Yes	****	< 0,0001
IgG vs. CCR2	Two-tailed	Yes	****	< 0,0001

M-CSFR

Unpaired t test	*One- or two-tailed P value?*	*Significantly different? (P < 0.05)*	*P value summary*	*P value*
Unstained vs. M-CSFR	Two-tailed	Yes	****	< 0,0001
IgG vs. M-CSFR	Two-tailed	Yes	****	< 0,0001

Supplementary Table 5: P-values for M1- and M2-like macrophages in Figure 24 & 25

Unpaired t test	*One- or two-tailed P value?*	*Significantly different? (P < 0.05)*	*P value summary*	*P value*
IgG (M2M) vs. M-CSFR (M2M)	Two-tailed	Yes	****	< 0,0001
CD45 (M1M) vs. CD45 (M2M)	Two-tailed	Yes	****	< 0,0001
CD68 (M1M) vs. CD68 (M2M)	Two-tailed	Yes	****	< 0,0001
CD86 (M1M) vs. CD86 (M2M)	Two-tailed	Yes	****	< 0,0001
CD163 (M1M) vs. CD163 (M2M)	Two-tailed	Yes	****	< 0,0001
IgG (M2M) vs. CD14 (M2M)	Two-tailed	Yes	****	< 0,0001

Supplementary Table 6: P-values of monocultured CAFs in Figure 26

	Adjusted P Value					
Tukey's multiple comparisons test	***CCR2***	***M-CSFR***	***CD86***	***CD163***	***CD45***	***Vimentin***
IgG vs. DMSO	0,1531	0,9492	0,7398	0,9933	0,6145	0,0063
IgG vs. RS 504393	0,7794	0,6705	0,6734	0,992	> 0,9999	0,0031
IgG vs. BLZ 945	0,9704	0,9767	0,4841	0,69	0,9885	0,0056
DMSO vs. RS 504393	0,383	0,4286	0,999	0,9483	0,6262	0,489
DMSO vs. BLZ 945	0,2302	0,9991	0,9479	0,8151	0,4717	0,9939
RS 504393 vs. BLZ 945	0,9476	0,4824	0,9763	0,5557	0,9858	0,6043

Supplementary Table 7: P-values of monocultured macrophages in Figure 27

	Adjusted P Value					
Tukey's multiple comparisons test	***CCR2***	***M-CSFR***	***CD86***	***CD163***	***CD45***	***Vimentin***
IgG vs. DMSO	0,0179	0,0002	0,2252	0,036	0,0095	0,0116
IgG vs. RS 504393	0,0084	0,0004	0,1658	0,1569	0,0083	0,0122
IgG vs. BLZ 945	0,1795	0,1372	0,0196	0,995	0,0164	0,014
DMSO vs. RS 504393	0,6198	0,0561	0,9869	0,4075	0,9942	0,9997
DMSO vs. BLZ 945	0,1352	0,0003	0,1235	0,0428	0,7923	0,9864
RS 504393 vs. BLZ 945	0,0457	0,0008	0,1664	0,1953	0,6715	0,9949

Supplementary Table 8: P-values of cocultured CAFs in Figure 28

	Adjusted P Value						
Tukey's multiple comparisons test	***CCL2***	***CCR2***	***M-CSFR***	***CD86***	***CD163***	***CD45***	***Vimentin***
IgG vs. DMSO	0,0009	0,6238	0,3334	0,0024	< 0,0001	0,0238	0,0012
IgG vs. RS 504393	0,0003	0,9797	0,4069	0,0773	< 0,0001	0,9918	0,0003
IgG vs. BLZ 945	0,003	0,1118	0,9221	0,0087	< 0,0001	0,0307	< 0,0001
DMSO vs. RS 504393	0,4134	0,7335	0,9972	0,1002	0,0007	0,0019	0,8157
DMSO vs. BLZ 945	0,5311	0,4138	0,5127	0,8108	0,1321	0,9978	0,1913
RS 504393 vs. BLZ 945	0,0692	0,0954	0,6231	0,42	0,0969	0,0028	0,6261

Supplementary Table 9: P-values of cocultured macrophages in Figure 29

	Adjusted P Value						
Tukey's multiple comparisons test	***CCL2***	***CCR2***	***M-CSFR***	***CD86***	***CD163***	***CD45***	***Vimentin***
IgG vs. DMSO	0,0294	0,1068	< 0,0001	0,6592	0,0025	< 0,0001	0,0003
IgG vs. RS 504393	< 0,0001	0,0039	< 0,0001	0,8961	0,0002	< 0,0001	0,0024
IgG vs. BLZ 945	0,9917	0,9963	0,0117	0,3635	0,9963	0,0008	0,004
DMSO vs. RS 504393	< 0,0001	0,1027	0,0595	0,9001	0,372	0,447	0,5521
DMSO vs. BLZ 945	0,0251	0,0283	< 0,0001	0,8649	< 0,0001	0,0544	0,3539
RS 504393 vs. BLZ 945	< 0,0001	0,0006	< 0,0001	0,4776	< 0,0001	0,0021	0,9839

6. Literature

Achkova, D. and Maher, J. (2016) 'Role of the colony-stimulating factor (CSF)/CSF-1 receptor axis in cancer', *Biochemical Society Transactions*. doi: 10.1042/BST20150245.

Allavena, P. *et al.* (2008) 'The inflammatory micro-environment in tumor progression: The role of tumor-associated macrophages', *Critical Reviews in Oncology/Hematology*. doi: 10.1016/j.critrevonc.2007.07.004.

Alvarez, C. and Sztul, E. S. (1999) 'Brefeldin A (BFA) disrupts the organization of the micuotubule and the actin cytoskeletons', *European Journal of Cell Biology*. doi: 10.1016/S0171-9335(99)80002-8.

American Cancer Society (2017) *Colorectal Cancer Facts&Figures 2017-2019*, *American Cancer Society*. doi: 10.1016/S0140-6736(13)61649-9.

Araghi, M. *et al.* (2019) 'Global trends in colorectal cancer mortality: projections to the year 2035', *International Journal of Cancer*. doi: 10.1002/ijc.32055.

Arnold, M. *et al.* (2017) 'Global patterns and trends in colorectal cancer incidence and mortality', *Gut*. doi: 10.1136/gutjnl-2015-310912.

Bachelerie, Francoise *et al.* (2014) 'International union of pharmacology. LXXXIX. Update on the extended family of chemokine receptors and introducing a new nomenclature for atypical chemokine receptors', *Pharmacological Reviews*. doi: 10.1124/pr.113.007724.

Bachelerie, Françoise *et al.* (2014) 'New nomenclature for atypical chemokine receptors', *Nature Immunology*. doi: 10.1038/ni.2812.

Bacman, D. *et al.* (2007) 'TGF-beta receptor 2 downregulation in tumour-associated stroma worsens prognosis and high-grade tumours show more tumour-associated macrophages and lower TGF-beta1 expression in colon carcinoma: A retrospective study', *BMC Cancer*. doi: 10.1186/1471-2407-7-156.

Baggiolini, M. and Loetscher, P. (2000) 'Chemokines in inflammation and immunity', *Immunology Today*. doi: 10.1016/S0167-5699(00)01672-8.

Bagnardi, V. *et al.* (2015) 'Alcohol consumption and site-specific cancer risk: A comprehensive dose-response meta-analysis', *British Journal of Cancer*. doi: 10.1038/bjc.2014.579.

Balmain, A. *et al.* (1993) 'Is colony-stimulating factor-1 a key mediator of breast cancer invasion and metastasis?', *Molecular Carcinogenesis*. doi: 10.1002/mc.2940070402.

Bartoli, C. *et al.* (2001) 'CCR2A and CCR2B, the two isoforms of the monocytes chemoattractant protein-1 receptor are up-regulated and expressed by different cell subsets in idiopathic inflammatory myopathies', *Acta Neuropathologica*.

Bonapace, L. *et al.* (2014) 'Cessation of CCL2 inhibition accelerates breast cancer metastasis by promoting angiogenesis', *Nature*. doi: 10.1038/nature13862.

Bray, F. (2014) 'Transitions in human development and the global cancer burden.', *World cancer report*. doi: 978-92-832-0430-5.

Bray, F. *et al.* (2018) 'Global cancer statistics 2018: GLOBOCAN estimates of incidence and mortality worldwide for 36 cancers in 185 countries', *CA: A Cancer Journal for Clinicians*. doi: 10.3322/caac.21492.

Bronte, V. *et al.* (2016) 'Recommendations for myeloid-derived suppressor cell nomenclature and characterization standards', *Nature Communications*. doi: 10.1038/ncomms12150.

Callewaere, C. *et al.* (2007) 'Chemokines and chemokine receptors in the brain: Implication in neuroendocrine regulation', *Journal of Molecular Endocrinology*. doi: 10.1677/JME-06-0035.

Chanmee, T. *et al.* (2014) 'Tumor-associated macrophages as major players in the tumor microenvironment', *Cancers*. doi: 10.3390/cancers6031670.

Chao, A. (2000) 'Cigarette Smoking and Colorectal Cancer Mortality in the Cancer Prevention Study II', *Journal of the National Cancer Institute*. doi: 10.1093/jnci/92.23.1888.

Charo, I. F. *et al.* (1994) 'Molecular cloning and functional expression of two monocyte chemoattractant protein 1 receptors reveals alternative splicing of the carboxyl-terminal tails', *Proceedings of the National Academy of Sciences of the United States of America*. doi: 10.1073/pnas.91.7.2752.

Cho, E. *et al.* (2004) 'Alcohol Intake and Colorectal Cancer: A Pooled Analysis of 8 Cohort Studies', *Annals of Internal Medicine*. doi: 10.7326/0003-4819-140-8-200404200-00007.

Chun, E. *et al.* (2015) 'CCL2 Promotes Colorectal Carcinogenesis by Enhancing Polymorphonuclear Myeloid-Derived Suppressor Cell Population and Function', *Cell Reports*. doi: 10.1016/j.celrep.2015.06.024.

Davies, L. C. *et al.* (2013) 'Tissue-resident macrophages', *Nature Immunology*. doi: 10.1038/ni.2705.

Deshmane, S. L. *et al.* (2009) 'Monocyte chemoattractant protein-1 (MCP-1): An overview', *Journal of Interferon and Cytokine Research*. doi: 10.1089/jir.2008.0027.

Dolznig, H. *et al.* (2011) 'Modeling colon adenocarcinomas in vitro: A 3D co-culture system induces cancer-relevant pathways upon tumor cell and stromal fibroblast interaction', *American Journal of Pathology*. doi: 10.1016/j.ajpath.2011.03.015.

Edin, S. *et al.* (2013) 'Phenotypic Skewing of Macrophages In Vitro by Secreted Factors from Colorectal Cancer Cells', *PLoS ONE*. doi: 10.1371/journal.pone.0074982.

Erreni, M., Mantovani, A. and Allavena, P. (2011) 'Tumor-associated macrophages (TAM) and inflammation in colorectal cancer', *Cancer Microenvironment*. doi: 10.1007/s12307-010-0052-5.

Fearon, E. R. and Vogelstein, B. (1990) 'A genetic model for colorectal tumorigenesis', *Cell*. doi: 10.1016/0092-8674(90)90186-I.

Fidler, M. M., Soerjomataram, I. and Bray, F. (2016) 'A global view on cancer incidence and national levels of the human development index', *International Journal of Cancer*. doi: 10.1002/ijc.30382.

Fleming, M. *et al.* (2012) 'Colorectal carcinoma: Pathologic aspects', *Journal of Gastrointestinal Oncology*. doi: 10.3978/j.issn.2078-6891.2012.030.

Francescone, R., Hou, V. and Grivennikov, S. I. (2015) 'Cytokines, IBD, and colitis-associated cancer', *Inflammatory Bowel Diseases*. doi: 10.1097/MIB.0000000000000236.

Galdiero, M. R., Marone, G. and Mantovani, A. (2018) 'Cancer inflammation and cytokines', *Cold Spring Harbor Perspectives in Biology*. doi: 10.1101/cshperspect.a028662.

Geissmann, F. *et al.* (2010) 'Development of monocytes, macrophages, and dendritic cells', *Science*. doi: 10.1126/science.1178331.

Ginhoux, F. *et al.* (2016) 'New insights into the multidimensional concept of macrophage ontogeny, activation and function', *Nature Immunology*. doi: 10.1038/ni.3324.

Giovannucci, E. *et al.* (1994) 'A prospective study of cigarette smoking and risk of colorectal adenoma and colorectal cancer in U.S. Women', *Journal of the National Cancer Institute*. doi: 10.1093/jnci/86.3.192.

Gool, S. W. *et al.* (1996) 'CD80, CD86 and CD40 Provide Accessory Signals in a Multiple-Step T-Cell Activation Model', *Immunological Reviews*. doi: 10.1111/j.1600-065x.1996.tb00920.x.

Gordon, S. and Mantovani, A. (2011) 'Diversity and plasticity of mononuclear phagocytes', *European Journal of Immunology*. doi: 10.1002/eji.201141988.

Gordon, S. and Martinez, F. O. (2010) 'Alternative activation of macrophages: Mechanism and functions', *Immunity*. doi: 10.1016/j.immuni.2010.05.007.

Grivennikov, S. I. (2013) 'Inflammation and colorectal cancer: Colitis-associated neoplasia', *Seminars in Immunopathology*. doi: 10.1007/s00281-012-0352-6.

Grossman, J. G. *et al.* (2018) 'Recruitment of CCR2 + tumor associated macrophage to sites of liver metastasis confers a poor prognosis in human colorectal cancer', *OncoImmunology*. doi: 10.1080/2162402X.2018.1470729.

Hanahan, D. and Weinberg, R. A. (2011) 'Hallmarks of cancer: The next generation', *Cell*. doi: 10.1016/j.cell.2011.02.013.

Herrera, M. *et al.* (2013) 'Functional heterogeneity of cancer-associated fibroblasts from human colon tumors shows specific prognostic gene expression signature', *Clinical Cancer Research*. doi: 10.1158/1078-0432.CCR-13-0694.

Hume, D. A. and MacDonald, K. P. A. (2012) 'Therapeutic applications of macrophage colony-stimulating factor-1 (CSF-1) and antagonists of CSF-1 receptor (CSF-1R) signaling', *Blood*. doi: 10.1182/blood-2011-09-379214.

Irvine, K. M. *et al.* (2009) 'Colony-stimulating factor-1 (CSF-1) delivers a proatherogenic signal to human macrophages', *Journal of Leukocyte Biology*. doi: 10.1189/jlb.0808497.

Janeway, C. A. (1992) 'The T cell receptor as a multicomponent signalling machine: CD4/CD8 coreceptors and CD45 in T cell activation', *Annual Review of Immunology*. doi: 10.1146/annurev.iy.10.040192.003241.

Kalluri, R. and Zeisberg, M. (2006) 'Fibroblasts in cancer', *Nature Reviews Cancer*. doi: 10.1038/nrc1877.

Karin, N. (2018) 'Chemokines and cancer: new immune checkpoints for cancer therapy', *Current Opinion in Immunology*. doi: 10.1016/j.coi.2018.03.004.

Khorana, A. A. *et al.* (2003) 'Vascular endothelial growth factor, CD68, and epidermal growth factor receptor expression and survival in patients with stage II and stage III colon carcinoma: A role for the host response in prognosis', *Cancer*. doi: 10.1002/cncr.11152.

Kikuchi, Y. *et al.* (2008) 'Periostin is expressed in pericryptal fibroblasts and cancer-associated fibroblasts in the colon', *Journal of Histochemistry and Cytochemistry*. doi: 10.1369/jhc.2008.951061.

Kim, E. R. and Chang, D. K. (2014) 'Colorectal cancer in inflammatory bowel disease: The risk, pathogenesis, prevention and diagnosis', *World Journal of Gastroenterology*. doi: 10.3748/wjg.v20.i29.9872.

Kim, Y. *et al.* (2018) 'The distribution of intratumoral macrophages correlates with molecular phenotypes and impacts prognosis in colorectal carcinoma', *Histopathology*. doi: 10.1111/his.13674.

Komohara, Y. *et al.* (2016) 'Tumor-associated macrophages: Potential therapeutic targets for anti-cancer therapy', *Advanced Drug Delivery Reviews*. doi: 10.1016/j.addr.2015.11.009.

Koshida, Y., Kuranami, M. and Watanabe, M. (2006) 'Interaction Between Stromal Fibroblasts and Colorectal Cancer Cells in the Expression of Vascular Endothelial Growth Factor', *Journal of Surgical Research*. doi: 10.1016/j.jss.2006.02.025.

Kramer, N. *et al.* (2013) 'In vitro cell migration and invasion assays', *Mutation Research - Reviews in Mutation Research*. doi: 10.1016/j.mrrev.2012.08.001.

Kruse, J. *et al.* (2013) 'Macrophages promote tumour growth and liver metastasis in an orthotopic syngeneic mouse model of colon cancer', *International Journal of Colorectal Disease*. doi: 10.1007/s00384-013-1703-z.

Kuipers, E. J.; Grady, W. M.; Lieberman, D.; Seufferlein, T.; Sung, J. J.; Boelens, P. G.; Van de Velde, C. J. H. . and T. W. (2015) 'COLORECTAL CANCER', *Nat Rev Dis Primers.*, 1: 15065(doi:10.1038/nrdp.2015.65.).

Kumar, V. *et al.* (2016) 'CD45 Phosphatase Inhibits STAT3 Transcription Factor Activity in Myeloid Cells and Promotes Tumor-Associated Macrophage Differentiation', *Immunity*. doi: 10.1016/j.immuni.2016.01.014.

De la Fuente López, M. *et al.* (2018) 'The relationship between chemokines CCL2, CCL3, and CCL4 with the tumor microenvironment and tumor-associated macrophage markers in colorectal cancer', *Tumour biology : the journal of the International Society for Oncodevelopmental Biology and Medicine*. doi: 10.1177/1010428318810059.

Levine, J. S. and Ahnen, D. J. (2006) 'Clinical practice. Adenomatous polyps of the colon.', *The New England journal of medicine*. doi: 10.1056/NEJMcp063038.

Lim, S. Y. *et al.* (2016) 'Targeting the CCL2-CCR2 signaling axis in cancer metastasis', *Oncotarget*. doi: 10.18632/oncotarget.7376.

Lin, H. *et al.* (2008) 'Discovery of a cytokine and its receptor by functional screening of the extracellular proteome', *Science*. doi: 10.1126/science.1154370.

Lin, X. *et al.* (2019) 'miR-195-5p/NOTCH2-mediated EMT modulates IL-4 secretion in colorectal cancer to affect M2-like TAM polarization', *Journal of Hematology & Oncology*. doi: 10.1186/s13045-019-0708-7.

Lonza, P. and B. (no date) *PBMCs – The One Stop Immune Cell Shop*. Available at: https://bioscience.lonza.com/lonza_bs/FR/en/pbmcs-the-one-stop-immune-cells-shop#accept.

Maecker, H. T. and Trotter, J. (2006) 'Flow cytometry controls, instrument setup, and the determination of positivity', *Cytometry Part A*. doi: 10.1002/cyto.a.20333.

Mantovani, A. *et al.* (2017) 'Tumour-associated macrophages as treatment targets in oncology', *Nature Reviews Clinical Oncology*. doi: 10.1038/nrclinonc.2016.217.

Martinez, F. O. *et al.* (2006) 'Transcriptional Profiling of the Human Monocyte-to-Macrophage Differentiation and Polarization: New Molecules and Patterns of Gene Expression', *The Journal of Immunology*. doi: 10.4049/jimmunol.177.10.7303.

Mroczko, B. *et al.* (2007) 'Serum macrophage-colony stimulating factor levels in colorectal cancer patients correlate with lymph node metastasis and poor prognosis', *Clinica Chimica Acta*. doi: 10.1016/j.cca.2007.02.037.

Mroczko, B., Szmitkowski, M. and Okulczyk, B. (2002) 'Granulocyte-colony stimulating factor (G-CSF) and macrophage-colony stimulating factor (M-CSF) in colorectal cancer patients', *Clinical Chemistry and Laboratory Medicine*. doi: 10.1515/CCLM.2002.056.

Murdoch, C. *et al.* (2008) 'The role of myeloid cells in the promotion of tumour angiogenesis', *Nature Reviews Cancer*. doi: 10.1038/nrc2444.

Murray, P. J. and Wynn, T. A. (2011) 'Protective and pathogenic functions of macrophage subsets', *Nature Reviews Immunology*. doi: 10.1038/nri3073.

Nagasaki, T. *et al.* (2014) 'Interleukin-6 released by colon cancer-associated fibroblasts is critical for tumour angiogenesis: Anti-interleukin-6 receptor antibody suppressed angiogenesis and inhibited tumour-stroma interaction', *British Journal of Cancer*. doi: 10.1038/bjc.2013.748.

Negus, R. P. M. *et al.* (1995) 'The detection and localization of monocyte chemoattractant protein-1 (MCP-1) in human ovarian cancer', *Journal of Clinical Investigation*. doi: 10.1172/JCI117933.

Parsonage, G. *et al.* (2005) 'A stromal address code defined by fibroblasts', *Trends in Immunology*. doi: 10.1016/j.it.2004.11.014.

Pathria, P., Louis, T. L. and Varner, J. A. (2019) 'Targeting Tumor-Associated Macrophages in Cancer', *Trends in Immunology*. doi: 10.1016/j.it.2019.02.003.

PDQ® Screening and Prevention Editorial Board (no date) *PDQ Colorectal Cancer Prevention*, *Bethesda, MD: National Cancer Institute.* Available at: https://www.cancer.gov/types/colorectal/hp/colorectal-prevention-pdq (Accessed: 13 September 2019).

Peddareddigari, V. G., Wang, D. and Dubois, R. N. (2010) 'The tumor microenvironment in colorectal carcinogenesis', in *Cancer Microenvironment*. doi: 10.1007/s12307-010-0038-3.

Peterson, L. W. and Artis, D. (2014) 'Intestinal epithelial cells: Regulators of barrier function and immune homeostasis', *Nature Reviews Immunology*. doi: 10.1038/nri3608.

Pickhardt, P. J. *et al.* (2013) 'Assessment of volumetric growth rates of small colorectal polyps with CT colonography: A longitudinal study of natural history', *The Lancet Oncology*. doi: 10.1016/S1470-2045(13)70216-X.

Pudelko, K. (2016) *Determining the molecular crosstalk of macrophages interacting with colon cancer cells and stromal fibroblasts*. University of Vienna.

Pyonteck, S. M. *et al.* (2013) 'CSF-1R inhibition alters macrophage polarization and blocks glioma progression', *Nature Medicine*. doi: 10.1038/nm.3337.

Quail, D. F. and Joyce, J. A. (2017) 'Molecular pathways: Deciphering mechanisms of resistance to macrophage-targeted therapies', *Clinical Cancer Research*. doi: 10.1158/1078-0432.CCR-16-0133.

Ries, C. H. *et al.* (2014) 'Targeting tumor-associated macrophages with anti-CSF-1R antibody reveals a strategy for cancer therapy', *Cancer Cell*. doi: 10.1016/j.ccr.2014.05.016.

Risio, M. (2010) 'Reprint of: The natural history of adenomas', *Best Practice and Research: Clinical Gastroenterology*. doi: 10.1016/j.bpg.2010.08.002.

Round, J. L. and Mazmanian, S. K. (2009) 'The gut microbiota shapes intestinal immune responses during health and disease', *Nature Reviews Immunology*. doi: 10.1038/nri2515.

Sanders, S. K. *et al.* (2000) 'Functional Differences Between Monocyte Chemotactic Protein-1 Receptor A and Monocyte Chemotactic Protein-1 Receptor B Expressed in a Jurkat T Cell', *The Journal of Immunology*. doi: 10.4049/jimmunol.165.9.4877.

Sapi, E. (2004) 'The Role of CSF-1 in Normal Physiology of Mammary Gland and Breast Cancer: An Update', *Experimental Biology and Medicine*. doi:

10.1177/153537020422900101.

Siegel, R. L., Miller, K. D. and Jemal, A. (2019) 'Cancer statistics of American 2019.', *CA: a cancer journal for clinicians*. doi: 10.3322/caac.21551.

Sierra-Filardi, E. *et al.* (2014) 'CCL2 Shapes Macrophage Polarization by GM-CSF and M-CSF: Identification of CCL2/CCR2-Dependent Gene Expression Profile', *The Journal of Immunology*. doi: 10.4049/jimmunol.1302821.

Smith, P. D. *et al.* (2011) 'Intestinal macrophages and response to microbial encroachment', *Mucosal Immunology*. doi: 10.1038/mi.2010.66.

Stadler, M. *et al.* (2015) 'Increased complexity in carcinomas: Analyzing and modeling the interaction of human cancer cells with their microenvironment', *Seminars in Cancer Biology*. doi: 10.1016/j.semcancer.2015.08.007.

Stadler, M. (2016) *Tumor Cell - Fibroblast Interaction Influences Macrophage Recruitment and Polarization in Colon Cancer*. University of Vienna.

Stewart, S. L. *et al.* (2006) 'A population-based study of colorectal cancer histology in the United States, 1998-2001', *Cancer*. doi: 10.1002/cncr.22010.

Strachan, D. C. *et al.* (2013) 'CSF1R inhibition delays cervical and mammary tumor growth in murine models by attenuating the turnover of tumor-associated macrophages and enhancing infiltration by CD8+ T cells', *OncoImmunology*.

Stryker, S. J. *et al.* (1987) 'Natural history of untreated colonic polyps', *Gastroenterology*. doi: 10.1016/0016-5085(87)90563-4.

Sun, X. *et al.* (2017) 'CCL2-driven inflammation increases mammary gland stromal density and cancer susceptibility in a transgenic mouse model', *Breast Cancer Research*. doi: 10.1186/s13058-016-0796-z.

Svensson, J. *et al.* (2011) 'Macrophages at the Fetal–Maternal Interface Express Markers of Alternative Activation and Are Induced by M-CSF and IL-10', *The Journal of Immunology*. doi: 10.4049/jimmunol.1100130.

Tan, S. Y. *et al.* (2005) 'Prognostic significance of cell infiltrations of immunosurveillance in colorectal cancer', *World Journal of Gastroenterology*. doi: 10.3748/wjg.v11.i8.1210.

Tarin, D. and Croft, C. B. (1969) 'Ultrastructural features of wound healing in mouse skin.', *Journal of anatomy*.

Terzić, J. *et al.* (2010) 'Inflammation and Colon Cancer', *Gastroenterology*. doi: 10.1053/j.gastro.2010.01.058.

Tomasek, J. J. *et al.* (2002) 'Myofibroblasts and mechano: Regulation of connective tissue remodelling', *Nature Reviews Molecular Cell Biology*. doi: 10.1038/nrm809.

Tommelein, J. *et al.* (2015) 'Cancer-Associated Fibroblasts Connect Metastasis-Promoting Communication in Colorectal Cancer', *Frontiers in Oncology*. doi: 10.3389/fonc.2015.00063.

Torres, S. *et al.* (2013) 'Proteome profiling of cancer-associated fibroblasts identifies novel proinflammatory signatures and prognostic markers for colorectal cancer', *Clinical Cancer Research*. doi: 10.1158/1078-0432.CCR-13-1130.

Unger, C. *et al.* (2014) 'Modeling human carcinomas: Physiologically relevant 3D models to improve anti-cancer drug development', *Advanced Drug Delivery Reviews*. doi: 10.1016/j.addr.2014.10.015.

Vinnakota, K. *et al.* (2017) 'M2-like macrophages induce colon cancer cell invasion via

matrix metalloproteinases', *Journal of Cellular Physiology*. doi: 10.1002/jcp.25808.

De Visser, K. E., Eichten, A. and Coussens, L. M. (2006) 'Paradoxical roles of the immune system during cancer development', *Nature Reviews Cancer*. doi: 10.1038/nrc1782.

Winawer, S. J. and Zauber, A. G. (2002) 'The advanced adenoma as the primary target of screening', *Gastrointestinal Endoscopy Clinics of North America*. doi: 10.1016/S1052-5157(03)00053-9.

Wolf, M. J. *et al.* (2012) 'Endothelial CCR2 Signaling Induced by Colon Carcinoma Cells Enables Extravasation via the JAK2-Stat5 and p38MAPK Pathway', *Cancer Cell*. doi: 10.1016/j.ccr.2012.05.023.

Xu, M. *et al.* (2016) 'Role of MCP-1 in alcohol-induced aggressiveness of colorectal cancer cells', *Molecular Carcinogenesis*. doi: 10.1002/mc.22343.

Yaal-Hahoshen, N. *et al.* (2006) 'The chemokine CCL5 as a potential prognostic factor predicting disease progression in stage II breast cancer patients', *Clinical Cancer Research*. doi: 10.1158/1078-0432.CCR-06-0074.

Yan, D. *et al.* (2017) 'Inhibition of colony stimulating factor-1 receptor abrogates microenvironment-mediated therapeutic resistance in gliomas', *Oncogene*. doi: 10.1038/onc.2017.261.

Yu, J. *et al.* (2015) 'Novel recurrently mutated genes and a prognostic mutation signature in colorectal cancer', *Gut*. doi: 10.1136/gutjnl-2013-306620.

Zaynagetdinov, R. *et al.* (2011) 'A Critical Role for Macrophages in Promotion of Urethane-Induced Lung Carcinogenesis', *The Journal of Immunology*. doi: 10.4049/jimmunol.1100558.

Zhang, T. *et al.* (2006) 'Migration of cytotoxic T lymphocytes toward melanoma cells in three-dimensional organotypic culture is dependent on CCL2 and CCR4', *European Journal of Immunology*. doi: 10.1002/eji.200526208.

Zhou, Q. *et al.* (2010) 'The density of macrophages in the invasive front is inversely correlated to liver metastasis in colon cancer', *Journal of Translational Medicine*. doi: 10.1186/1479-5876-8-13.

Zixuan Guo, Tianyu Liu, Kui Jiang, Bangmao Wang, H. C. (2019) 'High-fat diet-induced gut microbiota dysbiosis activate MCP-1/CCR2 pathway and promote intestinal carcinogenesis', *BMJ Journals, Basic gastroenterology, Gut*, (IDDF2019-ABS-0339).